THE PROCEEDINGS OF
THE PHYSICAL SOCIETY

VOL. 49, PART 3 *May* 1, 1937 NO. 272

THE VISCOSITY OF AIR

BY W. N. BOND, M.A., D.SC., F.INST.P.,
Lecturer in Physics in the University of Reading

Received 14 *May* 1936. *Read* 13 *November* 1936

ABSTRACT. The viscosity of dry air at atmospheric pressure was measured by a capillary-tube method, at about 15° C. The ends of a wide-limbed U tube containing paraffin oil, of density 0·87, were connected by a pair of capillary tubes in series, so as to form a closed system. The oil was initially displaced, and in proceeding towards its equilibrium position it forced air through the capillaries. Care was taken to avoid constant and systematic errors, and two U tubes, two sets of capillaries and two methods of drying the air were used. Assuming that the viscosity increases by $4{\cdot}93 \times 10^{-7}$ per °C., the value at 23° C. is $(1834{\cdot}7 \pm 0{\cdot}8) \times 10^{-7}$ c.g.s. units. The paper includes a summary of the general theory of the capillary-tube method and the correction terms involved, as well as a detailed theory of the present experiments.

§ 1. GENERAL THEORY

FOR steady stream-line flow of incompressible fluid of constant viscosity η through an infinitely long straight tube of radius r, when there is zero velocity at the walls of the tube, we have Poiseuille's equation

$$V = \frac{\pi r^4}{8\eta}\left(-\frac{dp}{dl}\right),$$

where V is the volume of fluid passing through in unit time and $(-dp/dl)$ is the pressure gradient causing flow, the hydrostatic pressure gradient having been deducted. It will be assumed that all correction terms are so small that they may be treated as if they were independent of one another.

It was shown by Osborne Reynolds that stable stream-line motion only occurs when

$$\frac{vr\rho}{\eta} \ll 1000,$$

where ρ is the density of the fluid and v is its mean velocity, defined by $\pi r^2 v = V$.

It may happen that the internal radius r varies as we pass along the tube.

Treating each short part of the tube as if it were part of a circular cone of semi-angle α, we have$^{(1)}$

$$V = \frac{\pi r^4}{3\eta} \frac{\cos\alpha\,(2\cos^3\alpha - 3\cos^2\alpha + 1)}{\sin^4\alpha\,(3\cos^2\alpha - 1)} \left(-\frac{dp}{dl}\right)$$

$$= \frac{\pi}{8\eta} \frac{p_1 - p_2}{\int \left(1 - \frac{3}{2}\alpha^2 + \dots\right)\frac{dl}{r^4}},$$

where p_1 and p_2 are the pressures at entrance and exit. The hydrostatic difference in pressure must be deducted, as before.

If the cross-section of the tube be elliptic, it can be shown$^{(2)}$ that r^4 in the above equation has to be replaced by $2r_1^3 r_2^3/(r_1^2 + r_2^2)$, where r_1 and r_2 are the semi-axes of the ellipse. If the mass of liquid required to fill the tube is used to deduce the mean radius, the corresponding value of $1/r^4$ requires to be increased by $k^2/200$ per cent, where k is the small percentage difference between r_1 and r_2.

If, instead of measuring the pressure gradient in the tube, we measure the pressure difference between the fluid in the reservoirs to which the tube is joined, then end corrections have to be applied. It has been shown$^{(3)}$ that, when $vr\rho/\eta < 8$, the total effect of the two ends is to make the effective length of the tube greater than its actual length by an amount $1{\cdot}15r$. For the range of Reynolds' number

$$8 < vr\rho/\eta \ll 1000,$$

the correction$^{(3,4)}$ is chiefly due to the kinetic energy of the fluid, and is made by replacing $p_1 - p_2$ by

$$(p_1 - p_2) - 1{\cdot}08 \frac{V^2\rho}{\pi^2 r^4}, \text{ which equals } (p_1 - p_2) - 1{\cdot}08\, v^2\rho.$$

For a gas which obeys Boyle's law, Poiseuille's equation is replaced by O. E. Meyer's equation

$$p_1 V_1 = p_2 V_2 = \frac{p_1 + p_2}{2} \frac{\pi r^4 (p_1 - p_2)}{8\eta l} \qquad \text{......(1)},$$

where V_1, V_2 are the volumes of gas entering and leaving in unit time, provided$^{(5)}$ that the flow is isothermal and that the forces due to variation in velocity *along* the tube may be neglected. If there is no heat conduction through the walls of the tube, the conditions will not be quite isothermal. We shall have $p/\rho^n = \text{constant}^{(6)}$, where

$$n = 1 + (\gamma - 1)\left(\frac{v}{c}\right)^2,$$

γ denoting the ratio of the principal specific heats of the gas, and c the velocity of sound in the gas. There would also be adiabatic cooling of the gas as it entered the capillary, the fractional decrease in the absolute temperature being equal to

$$\frac{\gamma - 1}{2}\left(\frac{v}{c}\right)^2.$$

These two effects are generally quite small, and conduction will usually decrease them considerably.

It has been found that, in the case of a gas, slip occurs at the walls of the tube. The capillary acts as if its radius were greater than r by an amount$^{(7)}$ $0{\cdot}874\lambda$, where

λ is the mean free path of the gas molecules. Consequently the value deduced for the viscosity requires correction by multiplying by

$$1+4\left(\frac{0\cdot874\lambda}{r}\right).$$

For air at normal atmospheric pressure the factor becomes

$$1+\frac{0\cdot000{,}033\ \text{cm.}}{r}.$$

§ 2. THEORY OF THE PRESENT EXPERIMENTS

In the present experiments two capillary tubes in series were joined to the ends of a wide-limbed **U** tube containing a paraffin oil, the whole forming a closed system shown diagrammatically in figure 1. The two oil-air surfaces were initially at different levels. In proceeding towards its equilibrium position, the oil forced the air through the capillaries. The rate of flow can be deduced from the rate of movement of the oil surfaces, and their difference in level determines the value of the driving pressure, (p_1-p_2). Thus

$$p_1-p_2=hg\,(\sigma-\rho) \qquad \text{......(2)},$$

where h denotes the difference in level and σ the density of the oil in the manometer. The density ρ of the gas has little effect in decreasing the driving pressure, and need only be known approximately.

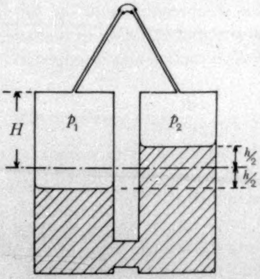

Figure 1.

We require to find expressions for p_1V_1 and p_1+p_2 in order to use equation (1). Let ρ^* be the density of the gas at unit pressure, and let p_0 be the final pressure of the gas when $h=0$. Equating the sum of the masses of the gas in the two sides of the apparatus to the total mass of gas in the final equilibrium condition, we have

$$a\left(H+\frac{h}{2}\right)\rho^*p_1+a\left(H-\frac{h}{2}\right)\rho^*p_2=a.2H\rho^*p_0 \qquad \text{......(3)},$$

where a and H denote the area of cross-section and final length of each air column, figure 1. From equations (2) and (3) we find

$$p_1 = p_0 + \frac{hg\,(\sigma-\rho)}{2}\left(1 - \frac{h}{2H}\right),$$

and

$$\frac{p_1+p_2}{2} = p_0 - \frac{h^2 g\,(\sigma-\rho)}{4H} \qquad \text{......(4).}$$

The mass of air passing through the capillary per second is equal to the rate of decrease with time of the mass on the p_1 side. Hence

$$(p_1\rho^*)\,V_1 = -\frac{d}{dh}\left[a\left(H+\frac{h}{2}\right)\rho^*\left\{p_0 + \frac{hg\,(\sigma-\rho)}{2}\left(1-\frac{h}{2H}\right)\right\}\right]\frac{dh}{dt}.$$

Substituting from this equation and equations (2) and (4) in equation (1), we obtain

$$-\int \frac{1 + \dfrac{Hg\,(\sigma-\rho)}{p_0} - \dfrac{3h^2 g\,(\sigma-\rho)}{4Hp_0}}{1 - \dfrac{h^2 g\,(\sigma-\rho)}{4Hp_0}}\,\frac{dh}{h} = \frac{\pi r^4 g\,(\sigma-\rho)}{4al\eta}\int dt.$$

The term $h^2 g\,(\sigma-\rho)/4Hp_0$ is to be quite small in comparison with unity, and therefore its square may be neglected. With this approximation, the equation becomes

$$\eta = \frac{\pi g\,(\sigma-\rho)}{4a\Sigma\left(\dfrac{l}{r^4}\right)} \times \frac{[t]}{-[\log_e h] + \dfrac{Hg\,(\sigma-\rho)}{p_0}\left[\left(\dfrac{h}{2H}\right)^2 - \log_e \dfrac{h}{2H}\right]} \qquad \text{......(5),}$$

where quantities in square brackets have to be taken between two limits. The terms involving H are due to the compressibility of the gas (air). The corrections still have to be made for ellipticity and variation in diameter of the capillary, for end effects, and for slip. A small correction may also be necessary for the friction of the oil in the manometer.

In evaluating $\int\left(1-\frac{3}{2}\alpha^2+\dots\right)\frac{dl}{r^4}$ for a capillary tube, it will usually be found that the term in α^2 can be neglected. The volume of the tube can be obtained accurately by finding the mass of mercury required to fill the tube. A short column of mercury is then inserted in the tube, and its length, q, is measured at a number of points along the tube. A curve can be drawn showing the value of q at different parts of the tube. Denoting the average value of $1/q$ along the tube by $[1/q]$ and the average value of q^2 along the tube by $[q^2]$, we find

$$\int\frac{dl}{r^4} = \frac{\pi^2 l^3}{(\text{volume of tube})^2}\left[\frac{1}{q}\right]^2 [q^2] \qquad \text{......(6).}$$

§ 3. EXPERIMENTAL DETAILS

Two U tubes were used in these experiments. The first had thick glass walls and an area of section of $a = 18$ cm.^{2} approximately. The value of a varied along the limbs of the tube, and a complicated method of calculation which need not be described here had to be used. The second U was made of drawn brass and is illustrated in figure 2. Long vertical slots, at the back and front of the limbs of the U, were covered with cellophane and pyrex respectively and used as windows. The oil-air surfaces, about 4½ cm. in diameter, were viewed with a microscope that had vertical and horizontal traverses. The microscope was used with a 1-in. or 2-in. objective, and its position was read by vernier to 1/100 mm. The total vertical travel of the microscope was about 10½ cm. Light from a small lamp was collimated by a lens of focal length 100 cm. and aperture 15 cm., shown on the right in figure 2, and passed in a horizontal beam to illuminate the oil surfaces 3 m. from the lens.

A dense medicinal paraffin oil was used in the U tubes. This oil had a viscosity of about 0·55 at 16° C. and a vapour pressure of not more than 0·15 cm. of mercury column at 15° C. Its density, found by comparison with distilled water by means of three specific-gravity bottles, was $0{\cdot}8716 \pm 0{\cdot}00016$ g./cm.^{3} at 15° C. and $0{\cdot}8649 \pm 0{\cdot}0002$ g./cm.^{3} at 25° C. The density is almost the same as that of Apiezon Oil B at the same temperatures$^{(8)}$.

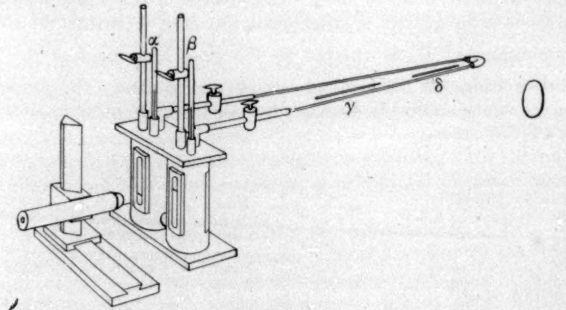

Figure 2.

The value of a for the first U tube was found by measuring the rise in level when known masses of water were inserted. The second tube was calibrated similarly by means of the oil, giving $a = 15{\cdot}526 \pm 0{\cdot}003_5$ cm.^{2} Measurements of the diameter of the tube and of the size of the window recesses gave a value $a = 15{\cdot}51_5 \pm 0{\cdot}01$.

Two capillary tubes in series were used in each experiment, and two pairs of such tubes were used. The tubes were of glass, and each had a radius of about 0·036 cm. and a length of about 150 cm. The value of l for each tube was found to an accuracy of about ±0·005 per cent, and the mass of mercury to fill each tube to an accuracy of about ±0·01 per cent. The value of q was measured at about 20 places in each tube, all parts of each tube being tested. The maximum value attained by α at any point in the four tubes was 0·0004 radian, and hence the term in α^2 is quite negligible. From each $\{q, l\}$ curve about 30 equally spaced ordinates were read, and the corresponding values of $1/q$ and q^2 were used to calculate the average values $[1/q]$ and $[q^2]$. Four checks on the accuracy of this work were obtained. Firstly, one calculation was repeated by a seven-ordinate method, giving a value of $[1/q]^2 . [q^2]$ that differed from the result obtained by the 30-ordinate method by only 0·01 per cent. Secondly, two of the tubes were calibrated more crudely, and the calculations were carried out by the 7-ordinate method, giving results that only differed from the more precise ones by 0·1 per cent. Thirdly, the mean diameter of each of the four tubes was measured at each end with a travelling microscope, and each result was compared with the value deduced from the mercury weighing together with the $\{q, l\}$ curve. The average of all eight diameters as measured with the microscope was greater than the average of the eight as measured by the mercury column by (0·15 ± 0·13) per cent, or (0·000,11 ± 0·000,09) cm.; thus the general accuracy of the measurements was checked. At any one of the eight places the discrepancy between the two methods of measuring the diameter was about ± 0·3 per cent or ± 0·0002 cm. If all of the discrepancy be attributed to inaccuracy in the $\{q, l\}$ curve, none of the error being attributed to the microscope measurements of the diameter, it would follow that the value of $[1/q]^2 . [q^2]$ of equation (6) had been found to an accuracy of about ± 0·03 per cent. Fourthly, the accuracy of the determinations of $\int \frac{dl}{r^4}$ is checked by the close agreement of the viscosity measurements made with the first and second pairs of tubes. The corrections for ellipticity were quite small. The data for the four tubes are given in table 1.

Table 1

Capillary	$\frac{\pi^2 l^3}{(\text{volume of tube})^2}$ × 10⁻⁷	$\int \frac{dl}{r^4} \times 10^{-7}$	End corrections $\times 10^{-7}$	Ellipticity corrections $\times 10^{-7}$	Corrected $\Sigma \frac{l}{r^4} \times 10^{-7}$
1	8·460	8·507	0·002	0·002	8·511
2	11·767	11·903	0·003	0·007	11·913
1 + 2	—	—	—	—	20·424 cm.$^{-3}$
3	10·153	10·521	0·003	0·001	10·525
4	5·664	5·692	0·002	0·001	5·695
3 + 4	—	—	—	—	16·220 cm.$^{-3}$

The maximum Reynolds' number $v r \rho / \eta$ in any of the present experiments was about 10. Consequently, there was no risk of turbulence. Moreover, the end correction was only kinetic for the highest rates of flow used. For the lower rates, at which $v r \rho / \eta < 8$, the end correction was 0·025 per cent. The correction was so small that it could be treated as a constant percentage, even for the highest rates of flow used.

The maximum value of $(v/c)^2$ was about $1 \cdot 7 \times 10^{-6}$, and hence the temperature of the air was not appreciably influenced by expansion and friction. The terms involving H in equation (5), which correct the measurements of rate of flow for the effect of compressibility of the air, had an average value of about 0·3 per cent; the connecting-tubes with taps cause the effective top of each wide air-column to be slightly above the top of the U tube. The maximum possible value of $h/2$ is H. When $h/2$ has the value $H/\sqrt{2}$, the two terms involving H change at equal and opposite rates, and the correction for compressibility is zero. It was not convenient, however, to restrict the experiment to the range in which $h/2$ is nearly equal to $H/\sqrt{2}$. The correction for slip was 0·09 per cent.

In the first apparatus the tube forming the bottom of the U was rather long and narrow: owing to the rather large viscosity of the manometer oil, a correction of −0·35 per cent had to be applied to the apparent viscosity of the air. In the second apparatus the connecting tube was wider and much shorter, and consequently the correction was only −0·03 per cent.

In commencing any experiment, air was drawn into the apparatus through one of the tubes shown at the top of figure 2. The air was always dried before being passed into the apparatus. In some experiments the air had been bubbled through and stored over fairly strong sulphuric acid. In the other experiments the air was drawn from a glass tower packed with soda lime. The pressure of the air in the apparatus was initially atmospheric on one side, and slightly less on the other side. The various parts of the apparatus were tested for air leakage before or after each experiment. This is essential, because changes in atmospheric pressure would cause any leaks to vary in a complicated way.

The apparatus was not placed in a thermostat, but in a room in which the temperature only changed very slowly. The temperature was read at various times during each experiment by means of four thermometers α, β, γ and δ, figure 2. The zeros of the thermometers were tested on two occasions, and the thermometers were compared with one another and with a standard. The determinations of temperature cannot have been in error by more than 0·1° C., which corresponds to a change of 0·027 per cent in the viscosity of air.

In a typical experiment the value of h decreased from 10 to 3 cm. in about 15 min. The microscope was adjusted into position, and then the time of passage of the meniscus was recorded with a calibrated stop-watch, fitted with a "split" seconds hand. In this way a series of 8 or 10 timings could be made, by stopping only one part of the hand. Incidentally, the effect of the starting error of the watch is eliminated. Readings were taken on the two oil-air surfaces alternately throughout the experiment. The position occupied by meniscus B at the instant at which meniscus A was being timed can subsequently be deduced from the preceding and succeeding observations of meniscus B by means of logarithmic interpolation. Directly an experiment had been completed a second experiment was performed with the flow in the reverse direction. This procedure avoids any slight error due to the microscope not travelling exactly horizontally.

§ 4. EXPERIMENTAL RESULTS

The results of the experiments are given in table 2. For purposes of comparison with the results of other workers, the value of η at 23° C. has been estimated, on the assumption that the viscosity increases by $4{\cdot}93 \times 10^{-7}$ per °C. rise in temperature(9).

Tables 3 and 4 show that changes of U tube, capillary, and drying agent had no significant effect.

Table 2

Date	Number of experiments performed	Reference no.		Drying agent	Temperature (°C.)	$\eta \times 10^7$	η at 23° C. $\times 10^7$
		U tube	Capillary				
8 April	2	1	1+2	H_2SO_4	$13{\cdot}6_5$	1790·9	1837·0
13 April	4	1	1+2	H_2SO_4	$13{\cdot}8_4$	1788·8	1833·9
27 April	2	2	1+2	H_2SO_4	$16{\cdot}9_0$	1803·6	1833·6
1 May	2	2	3+4	Soda lime	$14{\cdot}2_0$	1792·8	1836·2
4 May	2	2	3+4	Soda lime	$15{\cdot}7_2$	1798·5	1834·4
4 May	2	2	3+4	H_2SO_4	$15{\cdot}9_0$	1798·8	1833·8

Table 3

U tube	Capillaries	$\eta \times 10^7$ at 23° C.	Number of experiments
1	1+2	1834·9	6
2	1+2	1833·6	2
2	3+4	1834·8	6

Table 4

Drying agent	$\eta \times 10^7$ at 23° C.	Number of experiments
H_2SO_4	1834·4	10
Soda lime	1835·3	4

The probable error of the arithmetic mean of the above results, deduced from the residuals, is ±0·019 per cent. Allowing for uncertainties of ±0·018 per cent in the value of σ, of ±0·023 per cent in the values of a for each U tube, of ±0·03 per cent in the value of $\Sigma\,(l/r^4)$ for each pair of capillaries, and of ±0·027 per cent for an uncertainty of ±0·1° C. in the average of all the temperatures, the final probable error becomes ±0·046 per cent, giving $(1834{\cdot}7 \pm 0{\cdot}8) \times 10^{-7}$ c.g.s. units as the value of η at 23° C.

I was rather surprised to find that my results disagreed with the value adopted by Millikan but agreed well with the result obtained recently by Kellström(10), who used a rotating-cylinder method.

In conclusion, it may be remarked that the amount of vapour that will come from the dense paraffin oil, and diffuse about 8 cm. in 10 min., is almost certain to be very small. Its effect on the viscosity of the air will probably be quite insignificant.

§ 5. ACKNOWLEDGEMENTS

I have much pleasure in thanking Prof. J. A. Crowther, in whose laboratories the work was carried out, for his interest in the experiments. My thanks are also due to the Research Board of this University for making a grant for the purchase of apparatus. Mr J. S. Burgess, the laboratory steward, has helped me considerably by constructing apparatus.

REFERENCES

(1) Bond, W. N. *Proc. phys. Soc.* **34**, 188 (1922).
(2) Lamb, H. *Hydrodynamics*, 3rd ed., p. 545.
(3) Bond, W. N. *Proc. phys. Soc.* **34**, 142 (1922).
(4) Schiller, L. *Z. angew. Math. Mech.* **2**, 96 (1922).
(5) Poynting and Thomson. *Properties of Matter*, 6th ed., p. 210.
(6) Bond, W. N. *An Introduction to Fluid Motion*, p. 88.
(7) Millikan, R. A. *The Electron*, 1st ed., p. 113.
(8) Beeck, O. *Rev. sci. Instrum.* **6**, 400 (1935).
(9) Millikan, R. A. *Ann. Phys.*, Lpz., **41**, 759 (1913).
(10) Kellström, G. *Nature*, Lond., **136**, 682 (1935).
Note added September 28. Kellström has since confirmed his results (*Phys. Rev.* **50**, 190, 1936).

IONOSPHERIC CONDITIONS DURING THE SOLAR ECLIPSE OF 19 JUNE 1936

By R. NAISMITH, A.M.I.E.E.

Radio Department, National Physical Laboratory

Communicated by Dr R. L. Smith-Rose 13 *January* 1937. *Read* 12 *February* 1937.

ABSTRACT. The radio observations made in south-eastern England during the five days centred on the eclipse of 19 June 1936 are described. The eclipse was sufficient to increase the minimum equivalent height of the F region from 300 to over 600 kilometres and to decrease the ionization of the same region by about 50 per cent although only 56 per cent of the sun's disk was obscured at the maximum phase. The effect on these two elements reached a maximum at the same time and occurred 30 min. after the eclipse reached its maximum. A large magnetic disturbance occurred during the period of observation. The radio observations are therefore discussed in relation also to the changes which occurred in the magnetic elements during the effect of the eclipse on the ionosphere. The results of a number of field-strength measurements made on signals traversing the path of the eclipse are given and interpreted in relation to the ionospheric measurements made at vertical incidence. The coincidence of the eclipse with sunrise over south-eastern England suggests that the minimum of ionization thereby created made this the control region so far as the long-distance transmissions are concerned. This explains the close correlations which have been found to occur. It is shown that a reduction in field-strength was associated with the time during which the eclipse effect occurred in the path of the signals.

---

§ 1. INTRODUCTION

A SERIES of ionospheric measurements were made at the Radio Research Station of the National Physical Laboratory at Slough, in latitude 51° 29½′ N. and longitude 0° 34′ W., in connexion with the solar eclipse of 19 June 1936. They were carried out in accordance with a programme arranged by a subcommission of the Union Radio Scientifique Internationale, under the Presidency of Prof. E. V. Appleton, and form a part of an extended series of observations carried out on an international scale. This programme was supplemented by a number of field-strength measurements made by the Radio Branch of the British Post Office. The Slough series were confined to measurements of the ionization-density and the equivalent height of the different ionospheric regions returning radio energy at normal incidence. The measurements made by the Post Office supplied data over a more extended area concerning the variation in the amount of radio energy arriving from different directions.

It should be mentioned at the outset that extremely unfavourable conditions existed over south-eastern England on the morning of the eclipse. In the first place, the optical eclipse reached a total magnitude of only 0·56 and began before sunrise.

The difference between a total and a partial solar eclipse is, of course, less important in relation to radio observations than in relation to the corresponding astronomical ones. (In all that follows the term "eclipse" means the "optical eclipse".) In addition, one of the most intense thunderstorms of the year passed overhead during the observations. The system of recording(1) adopted at Slough, however, permitted good observations to be made in spite of the very high atmospheric noise-level thereby created. Whilst the measurements were being made it was obvious that an important magnetic disturbance was in progress; this was later found to be one of the largest for many months. The magnetic character figure for the day, derived according to the formula $(HR_H + VR_V)/10{,}000$, where R_H and R_V are the absolute range in gauss of H and V respectively during the day, was 1224, while the average for the month was only 392·5.

In spite of these unfavourable conditions it has been possible to interpret the results obtained in terms of established theories, although some modification of these interpretations may be necessary when all the results become available under the complete international programme.

A solar eclipse has, in recent years, been regarded as an opportunity for establishing the nature of the agency producing the normal ionization in the upper atmosphere. This normal ionizing agency for regions E and F_1 has been found to travel with a velocity closely approximating to that of light and has therefore been identified with the ultraviolet light from the sun. Similarly for region F_2 it has been concluded that ultraviolet light is responsible for at least part of the ionization, though it is suggested that corpuscles may also contribute(2). A study of the ionosphere during the solar eclipse of 1935 suggested(3) that the electron-dissipative process in region F_2 was by attachment to neutral gas particles and in region E by a process of recombination of the positive and negative charges.

It had been suggested that the two outstanding problems for study during an eclipse were (*a*) the causes of ionization in the F_2 region and (*b*) abnormal region-E echoes.

The observations described in this paper were therefore directed towards a study of these two problems.

§ 2. IONOSPHERIC MEASUREMENTS

Observations on the height and density of the different regions of the ionosphere returning energy at vertical incidence were made half-hourly from 17 to 21 June 1936. During the period of the eclipse they were repeated as rapidly as possible. One complete observation was made on all the frequencies on which echoes were observed in less than 9 mins., so that twelve complete $\{P', f\}$ curves are available for inspection for the $1\frac{3}{4}$ hours during which conditions in the ionosphere were rapidly changing. From this whole series of observations, two series of curves were drawn. One series shows the average values for the 2 days before and the 2 days after the morning of the eclipse, while the other illustrates the different conditions existing on the morning of the eclipse.

(*a*) ***Minimum equivalent height of the F region.*** The first two curves, plotted in figure 1, show the minimum equivalent heights at which reflection took place from the *F* region. It should be noted that at the times in the morning to which these curves refer, it is not normally possible to distinguish between the F_1 and F_2 regions, owing to the low angle of the sun's rays at this hour. This normal condition prevailed during the observations described in this paper. The relatively small difference between the effective heights shown by the two curves throughout the first $4\frac{1}{4}$ hours presents a striking contrast to the conditions during the succeeding 2 hours.

The results shown in this graph are therefore interpreted as a clear indication of an eclipse effect which resulted in an increase of the minimum equivalent height of region *F* to almost double the value appropriate at that hour. The time relation suggests that the agency producing this great change in the equivalent height of the region travels with a velocity approaching that of light. The greatest height was recorded at 0445 G.M.T. or approximately 30 min. after the time at which the eclipse reached its maximum phase on the ground. Since the time of maximum phase at a height of approximately 300 km. would not be greatly different from that on the ground, this difference in time cannot be explained in this way.

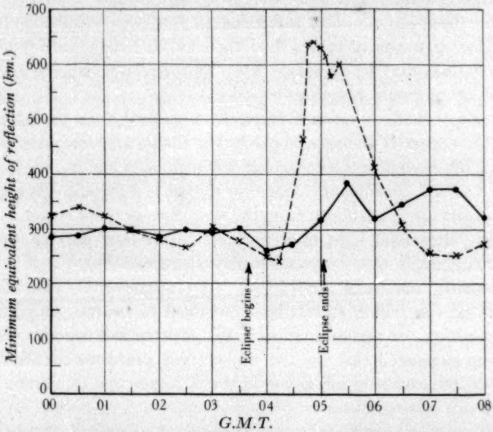

Figure 1. Minimum equivalent height of the F_2 region. ●—● mean for 17, 18, 20, 21 June; ×---× values for 19 June.

(*b*) *Critical frequency of the F region.* It will be seen from figure 3 that considerable magnetic activity was present throughout the whole period. Now, one of the great difficulties associated with the interpretation of the results obtained during the present eclipse will be to separate any effect due to the eclipse from that which can be associated with the magnetic variations which continued throughout the morning of the eclipse.

The changes which occurred in the ionization-density of region F_2 are plotted in figure 2. The quantity measured is the lowest frequency for the ordinary-wave component which just succeeds in penetrating the region. Now it has been shown by Appleton(4, 5) that this critical frequency is proportional to the square root of the ionization in the region in question. In order to show how the ionization varies, the measured values of the critical frequency have been squared. One curve shows the average conditions on the control days and the other curve shows the conditions existing on the morning of the eclipse. It is clear from this graph that the time of minimum ionization on the morning of the eclipse was 0445 G.M.T. The delay may have been due to the combination of sunrise and eclipse effects or it may have been due in part to a very reduced recombination or attachment coefficient. It is probable that both effects are present. A similar discrepancy was observed at Washington(3) during the solar eclipse of 3 February 1935, although the delay was only $9\frac{1}{2}$ min. in the case of region F_2 and 20 min. in the case of region F_1. These values were, however, calculated for a height of 250 km., so that the delay times are not strictly comparable.

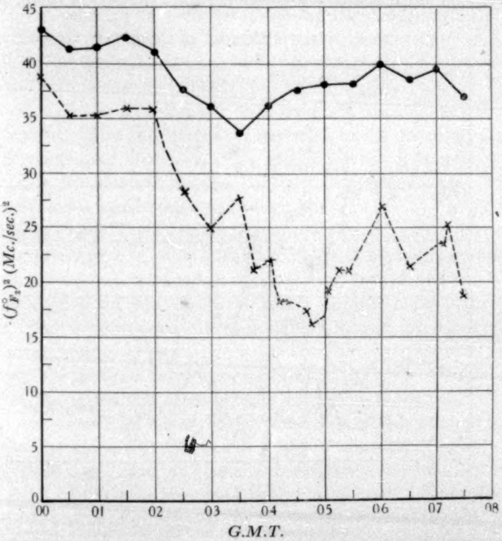

Figure 2. Critical frequencies for the ordinary ray in region F_2. ●—● mean curve for 17, 18, 20–25 June; ×---× values for 19 June.

In figure 2 the reduction of ionization on the morning of the eclipse is clearly shown and it is observed to begin about 45 min. before the height begins to alter.

At the minimum the ionization was actually 56 per cent below the normal value, although it must be recorded that the general level of the ionization was about 15 per cent below the normal values on the morning of the eclipse. In this connexion it should be noted that the percentage of the sun's disk which was obscured at the maximum phase of the eclipse was also 56 per cent.

§ 3. COMPARISON WITH MAGNETIC CONDITIONS

To demonstrate the effect of the eclipse on the ionization more clearly, the departures from the normal curve for region F_2 are plotted in figure 3(*a*). On the same graph the values of the horizontal component of the magnetic force are plotted. Here it can be seen that a close correspondence between the curves exists over the eclipse period. The marked minimum at 0445 G.M.T. in both curves is repeated in the vertical-intensity and declination traces shown in figure 3(*b*). Indeed, the marked correspondence, even in detail, between these two elements, one a force and the other an angle, during the period of the eclipse contrasts with their otherwise generally opposite trends.

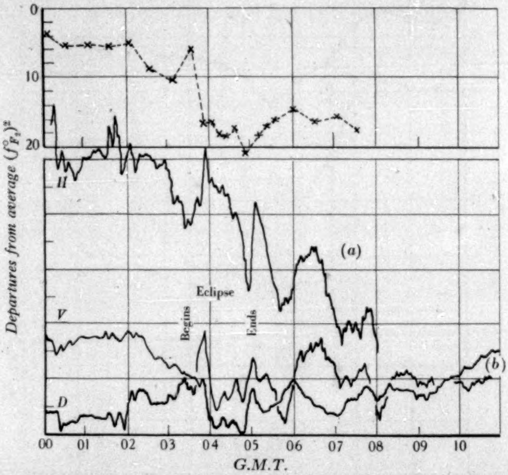

Figure 3. Departures of $(f^{\circ}_{F_2})^2$ from the mean values compared with (*a*) variations in the horizontal magnetic force and (*b*) the vertical magnetic force and the declination plotted for the morning of the eclipse. ×---× departures of $(f^{\circ}_{F_2})^2$ from average value; *H*, horizontal value of magnetic force; *V*, vertical component of magnetic force; *D*, declination; Scale intervals = 26·1γ for *H*, 24·5γ for *V* and 6′·1 for *D*.

Now, it has been shown above that, superimposed on the general effect on the F_2 region of a magnetic disturbance which was in progress throughout the day of the eclipse, there was a marked effect due to the eclipse itself. This eclipse effect resulted in a marked increase in the minimum equivalent height accompanied by a marked decrease in the maximum ionization-content of region F_2. Appleton and Ingram have shown that this same two-element change in this region accompanies a magnetic disturbance(6, 7). It seems reasonable therefore to investigate the changes in the magnetic elements over the period occupied by the eclipse effect on the ionosphere, to see if any special perturbation can be attributed to the eclipse.

From this investigation it is concluded that there is an indication that the effect of the eclipse of the sun can be observed in the magnetic elements.

Now, Prof. Chapman(8) has discussed the effect of a solar eclipse on the earth's magnetic field in relation to data provided by radio observations. In addition, variations in the magnetic elements themselves have been studied(9) during a number of solar eclipses, but there is still no general agreement on the existence of an eclipse effect upon the earth's magnetic field.

In contrast it should be remarked that Dr L. A. Bauer(9) was firmly convinced that a small eclipse effect had been demonstrated in several instances, while Dr C. Nordmann(10) concluded that "during the eclipse of 30 August 1905 there was superposed upon the general magnetic disturbance which took place at that time a special perturbation attributable to the eclipse".

The words of Chree(11) written on this subject nearly a quarter of a century ago are still applicable and are quoted to justify the publication of these comments: "At the present stage of our knowledge, the best course seems to be to describe the phenomena with an unprejudiced mind, in the hope that when sufficient eclipse data have accumulated some common feature or features may become apparent."

If we now consider the *E* region, we find that at the hour of the eclipse the critical frequency for this region was already so low that it was impossible to measure any reduction in its value. This region has already been closely studied during previous eclipses so that attention was concentrated on the abnormalities only in this region. First among these was a notable absence during the early hours of the morning of the type of echo which has been previously designated "*E* persistence".* These echoes appeared on the mornings of the control days, and the mean curve for these is shown in figure 4. It should be observed that on the morning of the eclipse these echoes began to appear at 0100 G.M.T. From 0130 to 0400 G.M.T. no sign of them could be seen. After that period the frequency on which they could be observed increased steadily and afterwards decreased as shown in the graph. The absence of this type of echo at a time when the corpuscular eclipse might be expected to occur must be recorded, although from experience of these echoes from region *E*, particularly in relation to their sudden appearance and disappearance, it is impossible to be certain of any conclusion. The observations which are shown in the dotted curve in figure 4 refer to the lowest frequency on which reflection from the *F* region of the ionosphere was obtained. During the night these values correspond very closely with f_E°, but in the morning they increase more rapidly than f_E°. The maximum in this curve of abnormal region-*E* echoes occurred at the same time as the minimum of ionization in region F_2 and the minimum in the magnetic elements, already referred to.

---

* This term has been used to denote the persistence of region *E* echoes at frequencies beyond those corresponding to the normal penetrating value for the appropriate time of the day.

Now there is no clear indication of the amount of ionization existing when these echoes are observed, but it is known that this must be high(12). It is clear from figure 4 that during the period of the eclipse there was certainly no diminution of ionization in this region, but there is rather strong evidence that it actually increased. There is here a clear indication that these abnormal region-*E* echoes are not caused by increased ultraviolet light from the sun.

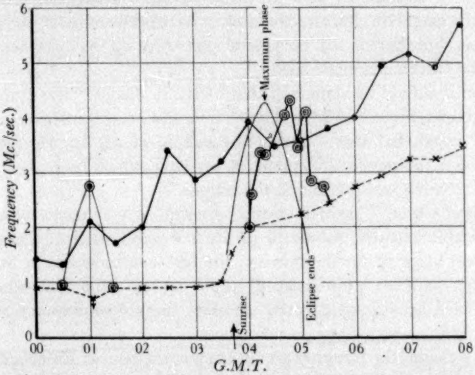

Figure 4. Measurements of the highest frequency on which echoes were obtained from the *E* region and of the lowest frequency on which echoes were obtained from the *F* region on the morning of the eclipse. ●—● highest frequency on which region *E* echoes were observed, mean of 17, 18, 20 and 21 June; ◎---◎ ditto for 19 June; ×---× lowest frequency on which echoes from region *F* were observed on 19 June.

§4. OBLIQUE-INCIDENCE MEASUREMENTS OF FIELD-STRENGTH

These measurements were made from 17 to 21 June. The four mornings, excluding the morning of the eclipse, have been averaged to form a basis of comparison from which departures on the morning of the eclipse could be assessed.

The observations were made on the following transmissions: (*a*) Rocky Point 5130 metres, 72° 56′ W., 40° 56′ N.; (*b*) Lawrenceville 30·4 metres, 74° W., 40° N.; (*c*) Nagoya 33·41 and 19·08 metres, 137° E., 35° N.; (*d*) Fiskville 28·73 metres, 143° E., 37° S.

In figure 5 are shown the two curves for the low-frequency signal traversing the transatlantic path from Rocky Point to Cupar, lat. 56° 19′ N., long. 2° 57′ W. It is almost certain that this frequency of 60 kc./sec. travelled via the lowest part of the normal *E* region. It is far removed from the critical penetration value, so that changes in ionization would not be observed. It is evident that approximately the same energy was received on the night of the eclipse as on the other nights.

Next consider a high-frequency transmission on 9·87 Mc./sec., figure 6, from Lawrenceville to Baldock, lat. 51° 57′ N., long. 0° 11′ W., which follows roughly the same path. In this case it is almost certain that the energy travelled via the F_2 region of the ionosphere. There is a marked fade-out of energy shortly after 0400 G.M.T. At vertical incidence at this time the critical frequency for region F_2 was 4·25 Mc./sec. If we assume a simple cosine law to hold in relating the highest frequency on which echoes can be observed with $f^{\circ}_{F_2}$ we have

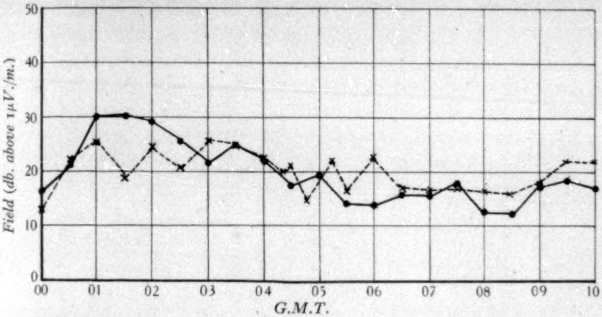

Figure 5. Field-strength measurements made at Cupar, lat. 56° 19′ N., long. 2° 57′ W., on transmissions from Rocky Point, lat. 40° 56′ N., long. 72° 56′ W., on a wave-length of 5130 metres (58·5 kc./sec.). ●—● mean curve for 17, 18, 20 and 21 June; ×---× values for 19 June.

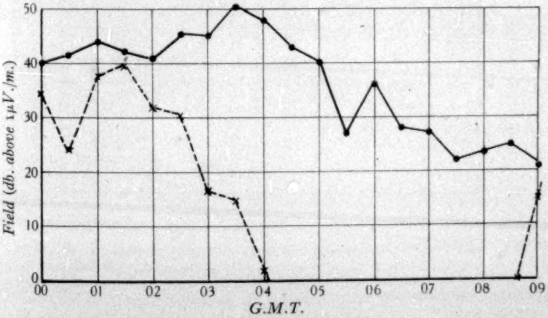

Figure 6. Field-strength measurements made at Baldock, lat. 51° 57′ N., long. 0° 11′ W., on transmissions from Lawrenceville, lat. 40° N., long. 74° W., on a wave-length of 30·4 metres (9·87 Mc./sec.). ●—● mean curve for 17, 18, 20 and 21 June; ×---× values for 19 June.

$$\theta_0 = 64\tfrac{1}{2}^{\circ},$$

where θ_0 is the angle of incidence at the layer.

The minimum equivalent height of reflection measured at vertical incidence at 0400 was 300 km. and the distance from the transmitter to the receiver was roughly 5,500 km. Now if we consider that the energy travels by three successive reflections between the earth and the F_2 region, we can calculate the angle of incidence at the layer, and in this way we find that $\theta_0 = 66°$.

This close agreement between the values of the angles of incidence at the layer as calculated from two different measurements, namely the critical frequency and the equivalent height of reflection, is strong evidence that the fade-out observed on the transmission from Lawrenceville was a genuine case of electron-limitation. This linking of vertical-incidence measurement with oblique-incidence measurement is also extremely convincing and shows that, as one would expect from the path of the signals, the conditions at the receiving site control the situation. On this occasion we had the unique situation of the eclipse effect superimposed on a mimimum of ionization or, as it may otherwise be regarded, a delayed sunrise.

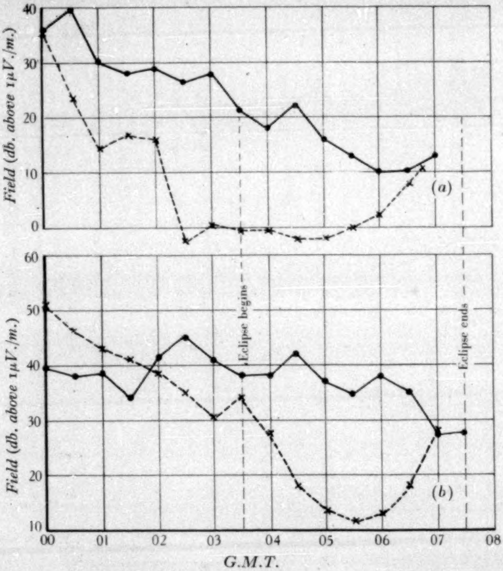

Figure 7. (*a*) Field-strength measurements made at Baldock on transmissions from Nagoya, lat. 35° N., long. 137° E., on a wave-length of 19·1 metres (15·72 Mc./sec.). ●—● mean curve 17, 18, 20 and 21 June; ×---× values for 19 June. (*b*) As figure 7(*a*) but on a wave-length of 33·4 metres (8·98 Mc./sec.). ●—● mean curve 17, 18, 20 and 21 June; ×---× values for 19 June.

This agreement can be tested further if we consider the measurements made at Baldock on the transmissions from Japan and shown in figure 7. The higher frequency of 15·72 Mc./sec. appears to be critical about 0200 G.M.T. when $f^{\circ}_{F_2}$ was 6·0 Mc./sec. After performing the same calculations as before we obtain a value of

$67\frac{1}{2}°$ for the angle of incidence at the layer, and if we determine this quantity from the measurement of equivalent height which was also 300 km. we obtain a value of 68° which is again a very satisfactory agreement. In this case five reflections have been assumed.

The lower frequency of 8·98 Mc./sec. from the same station shows a marked reduction of energy received over the period 0330 G.M.T. till the end of the observation at 0700 G.M.T. In figure 7(*b*) this is shown in relation to the time of the eclipse over the path of the transmission, and the comparison shows that these periods coincide. This reduction in energy may be attributed to the removal, as a result of the decreased ultraviolet light from the sun, of certain of the multiply reflected rays of higher order traversing the path. It should be noted that the return of the energy to normal occurs on both frequencies at about 0700 G.M.T.

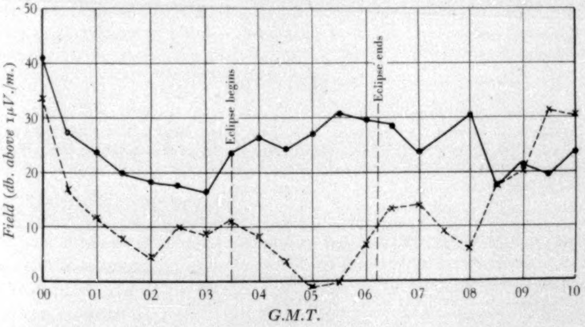

Figure 8. Field-strength measurements made at Baldock on transmissions from Fiskville, lat. 37° S., long. 143° E., on a wave-length of 28·7 metres (10·45 Mc./sec.). ●—● mean curve 17, 18, 20 and 21 June; ×---× values for 19 June.

The energy from the Fiskville transmitting station in Australia on a frequency of 10·45 Mc./sec. is plotted in figure 8, where it is shown that on the morning of the eclipse the energy showed a marked departure from the usual trend over the period 0330 to 0630 G.M.T. This is very similar to figure 7(*b*) except that it reaches its normal value half an hour earlier. If we consider the path of the Australian transmission in relation to the eclipse belt we find that the eclipse was actually over half an hour earlier on this route.

From these five graphs we conclude that the energy-level on the morning of the eclipse was about 10 db. lower than normal and that energy traversing the path of the eclipse was definitely reduced during the period of the eclipse. This can be interpreted in terms of accepted theory. In one case electron-limitation caused the energy to disappear before the beginning of the eclipse. This interpretation of electron-limitation was doubly checked and found to be in agreement with measurements made at vertical incidence. It should be noted that the sunrise and eclipse condition at the receiving site probably represents the minimum ionization in the path the energy travels in the various cases considered. Also, the time and magnitude of the eclipse have been considered only in relation to the surface of the earth. For the regions concerned a small correction would be necessary if high accuracy were required.

§ 5. ACKNOWLEDGEMENTS

In conclusion, the author wishes to thank Prof. E. V. Appleton for helpful discussion during the writing of this paper. He is indebted to Colonel A. G. Lee for arranging for the measurements of field-strength to be made by the British Post Office and to Dr H. Spencer Jones for the Abinger magnetic data discussed in the paper.

The work was undertaken as part of the programme of the Radio Research Board and is published by permission of the Department of Scientific and Industrial Research.

REFERENCES

(1) [Polar Year paper. *Proc. roy. Soc.*]
(2) Appleton, E. V. and Chapman, S. *Proc. Inst. Radio Engrs*, N.Y., **23**, 649 (1935).
(3) Kirby, S. S., Gilliland, T. R. and Judson, E. B. *Bur. Stand. J. Res.*, Wash., **16**, 213 (1936).
(4) Appleton, E. V. *Nature*, Lond., **127**, 197 (1931).
(5) Appleton, E. V. and Naismith, R. *Proc. roy. Soc.* **137**, 36 (1932).
(6) Appleton, E. V. and Ingram, L. J. *Nature*, Lond., **136**, 548 (1935).
(7) International Union of Geodesy and Geophysics, Dept. 1936 Report.
(8) Chapman, S. *Terr. Mag. atmos. Elect.* **38** 175 (1933).
(9) Bauer, L. A. *Terr. Mag. atmos. Elect.* **25**, 81 (1920).
(10) Nordmann, C. *Terr. Mag. atmos. Elect.* **12**, 25 (1907).
(11) Chree, C. *Quart. J. R. met. Soc.* **39**, 232 (1913).
(12) Appleton, E. V. and Naismith, R. *Proc. roy. Soc.* A, **150**, 707 (1935).

NOTE ON THE RADIATION BETWEEN TWO COAXIAL RADIATING CYLINDERS

By H. BUCKLEY, M.Sc., F.Inst.P.,
National Physical Laboratory

Received 12 *August* 1936. *Read in title* 12 *February* 1937

ABSTRACT. The paper discusses the problem of the radiation transfer from an electrically heated inner cylinder to a surrounding coaxial cylinder. Expressions are derived for the total radiation, emitted and reflected, from unit area of each of the cylindrical surfaces between which multiple reflection of radiation occurs. It is then shown how, from these expressions, the relation of the true temperatures to the apparent temperatures of the surfaces (obtained by means of a total-radiation pyrometer or by means of a disappearing-filament optical pyrometer) can be determined.

§ 1. INTRODUCTION

The problem of the determination of the effect of multiple reflections is of practical importance in radiometric measurement of the temperatures of bodies heated by radiation from surrounding or partly surrounding bodies. A particular case mentioned to the author by Dr Ezer Griffiths concerned two coaxial cylinders, of which the outer one was of material whose thermal conductivity was to be deduced from temperature-measurements of its inner and outer surfaces when it was in a steady state under the influence of radiation from the electrically heated inner cylinder.

The problem of the heat-transfer from the inner cylinder in this case has been considered by Merkel(1), Gröber(2), ten Bosch(3), Clausing(4) and Saunders(5).

Clausing's work was in connexion with the anodes and cathodes of thermionic valves and with indirectly heated filaments. Saunders also discussed the effect of displacement of the inner cylinder on the amount of the heat-transfer, when the reflecting power of the outer cylinder was small.

All the above-mentioned authors dealt with the amount of the heat-transfer alone. None of them dealt with the quantity of radiation emitted per unit area from each of the surfaces in the steady state, nor did they deal with the possibility of deducing the true temperatures of the surfaces from radiometric observation of the surfaces between which the heat-transfer occurs. If the inner and outer cylinders are absolutely black bodies, observation by means of a total radiation pyrometer or an optical pyrometer through a small hole in the outer cylinder will determine their temperatures directly. If, however, the two cylinders are not black bodies, the apparent temperatures derived in this way may differ very considerably from the true temperatures, and in consequence may lead, unless corrected, to very serious errors in the determination of the thermal conductivity of the outer cylinder.

It is the purpose of this note to determine the total radiation from each of the two surfaces in this case and to show how their true temperatures may be obtained.

§ 2. RADIATION BETWEEN INFINITE COAXIAL CYLINDERS

Consider an infinitely long solid cylinder of radius a, coaxial with an infinitely long hollow cylinder of internal radius b and external radius c. This system is further assumed to be surrounded by a non-radiating enclosure at an infinite distance. The inner cylinder A is heated by means of an electric current, and the various surfaces finally attain a steady state. Let the steady temperatures corresponding to this steady state be T_a, T_b and T_c respectively. Let it be further assumed that the surfaces of the cylinders are completely diffusing and have total emissivities of ϵ_a, ϵ_b and ϵ_c respectively which are all independent of wave-length, so that the surfaces are grey radiators. Their reflection factors will therefore be $(1-\epsilon_a)$, $(1-\epsilon_b)$ and $(1-\epsilon_c)$.

The surfaces A and B of the cylinders will emit radiation in virtue of their temperature alone equal to $\epsilon_a \sigma T_a^4$ and $\epsilon_b \sigma T_b^4$ per unit area and will reflect and absorb portions of the radiations falling on them from other parts of themselves or from other bodies. In the case of the outer surface of the outer cylinder no other radiation falls on the surface, so that the total radiation from it is $\epsilon_c \sigma T_c^4$ per unit area.

Thus the total radiation from any point on surface A will consist of the radiation emitted by A in virtue of its temperature, namely $\epsilon_a \sigma T_a^4$, together with the reflected fraction $(1-\epsilon_a)$ of the radiation received from the surrounding surface B. If the total radiation per unit area from surface A is denoted by ϕ_a, we have

$$\phi_a = \epsilon_a \sigma T_a^4 + (1-\epsilon_a)\,\phi_b \qquad \text{......(1)},$$

where ϕ_b is the total radiation per unit area from surface B. Similarly, the total radiation per unit area from surface B will consist of its temperature radiation $\epsilon_b \sigma T_b^4$ together with the fraction $(1-\epsilon_b)$ of the radiation received from the rest of the surface B and from the surface A.

Now the radiation received at any point P on surface B from the surface A is equal to the radiation from the projected area of A on surface B, the projected area on surface B being assumed to emit the same amount of radiation per unit area as the surface A. The projected area can be regarded as a series of elementary strips parallel to the common axis of the two cylinders. Now the radiation per unit area received at point P on surface B from an infinitely long elementary strip of width $b\,d\theta$ can be shown to be

$$\frac{\phi}{4}\sin\frac{\theta}{2}\,d\theta,$$

where θ is the angle which the normal to the elementary strip makes with the normal at the point P.

Thus the radiation per unit area received at point P from the projection of surface A on surface B is given by

$$2\int_{2\cos^{-1}(a/b)}^{\pi} \frac{\phi}{4}\sin\frac{\theta}{2}\,d\theta = \frac{a}{b}\,\phi.$$

Similarly, the radiation per unit area received at point P from the portion of surface B not in the projection of surface A, is given by

$$2\int_0^{2\cos^{-1}(a/b)} \frac{\phi}{4}\sin\frac{\theta}{2}\,d\theta=\frac{b-a}{b}\,\phi.$$

Hence the total radiation per unit area from any point on surface B is given by

$$\phi_b=\epsilon_b\sigma T_b^4+(1-\epsilon_b)\left\{\frac{b-a}{b}\,\phi_b+\frac{a}{b}\,\phi_a\right\} \qquad \text{......(2).}$$

Equations (1) and (2) are two simultaneous equations in ϕ_a and ϕ_b. The solutions are

$$\phi_a=\sigma T_a^4-\frac{\epsilon_b b\,(1-\epsilon_a)\,(\sigma T_a^4-\sigma T_b^4)}{\epsilon_a a+\epsilon_b b-\epsilon_a\epsilon_b a},$$

$$\phi_b=\sigma T_b^4+\frac{\epsilon_a a\,(1-\epsilon_b)\,(\sigma T_a^4-\sigma T_b^4)}{\epsilon_a a+\epsilon_b b-\epsilon_a\epsilon_b a}.$$

Thus the total radiation from surface A is less than the full radiation corresponding to its temperature, and that from surface B is greater than the corresponding quantity. In each case the total radiation is a mixture of radiations of two qualities, corresponding to colour temperatures T_a and T_b respectively.

As we have assumed that the system of cylinders is situated at an infinite distance from non-radiating surroundings, the radiation from surface C of the outer cylinder will be unaffected by the surroundings and will be $\epsilon_c\sigma T_c^4$ per unit area, where ϵ_c will equal ϵ_b if emissivity is independent of temperature. This radiation will of course represent the heat transferred from the inner cylinder, which also equals the electrical energy required to maintain the inner cylinder at the steady temperature T_a.

Since radiation-emission involves loss of heat, radiation-absorption involves gain of heat, and reflection of radiation involves neither loss nor gain, the loss of heat per unit area from surface A is given by

$$H_a=\epsilon_a\sigma T_a^4-\epsilon_a\phi_b.$$

The total heat-loss per unit length from surface A is therefore

$$Q=2\pi H_a=2\pi a\,(\epsilon_a\sigma T_a^4-\epsilon_a\phi_b).$$

On substitution of the value of ϕ_b given above this reduces to

$$Q=\frac{2\pi\epsilon_a\epsilon_b ab\,(\sigma T_a^4-\sigma T_b^4)}{\epsilon_a a+\epsilon_b b-\epsilon_a\epsilon_b a}$$

$$=\frac{\epsilon_b S_a\epsilon_a\sigma T_a^4-\alpha\epsilon_a S_b\epsilon_b\sigma T_b^4}{\epsilon_b+\alpha\epsilon_a R_b},$$

where S_a and S_b are the areas of unit lengths of the surfaces A and B, $\alpha=a/b$, the fraction of the radiation from B received by A, and R_b is the reflection factor of surface B. This expression for the total heat-transfer between the two cylinders is the same as that which has been obtained by previous workers on the subject. It might be noted that these previous derivations of the result were rather complicated as they involved the summation of an infinite number of successive reflections or the introduction of fictitious surfaces.

§ 3. DETERMINATION OF THE TRUE TEMPERATURES OF THE SURFACES *A* AND *B* OF THE CYLINDERS

Now ϕ_a and ϕ_b can be measured, for example, by observation with a pyrometer through a small hole in the outer cylinder. If the observations are made with a total-radiation pyrometer, the apparent temperatures $\mathscr{T}_a$ and $\mathscr{T}_b$ determined are those for which $\sigma\mathscr{T}_a^4=\phi_a$ and $\sigma\mathscr{T}_b^4=\phi_b$.

From equation (1) $\qquad \epsilon_a\sigma T_a^4=(\phi_a-\phi_b)+\epsilon_a\phi_b,$

so that

$$T_a^4=\frac{\mathscr{T}_a^4-\mathscr{T}_b^4}{\epsilon_a}+\mathscr{T}_b^4.$$

Similarly from equation (2)

$$T_b^4=\mathscr{T}_b^4-\frac{a\,(1-\epsilon_b)}{b\epsilon_b}\,(\mathscr{T}_a^4-\mathscr{T}_b^4).$$

These equations enable T_a and T_b to be deduced from observations of $\mathscr{T}_a$ and $\mathscr{T}_b$.

If the observations are made by means of an optical pyrometer with a monochromatic screen, the calculations given above become more general and the restriction that the emissivities be independent of wave-length need no longer apply. Equations (1) and (2) still hold for each wave-length interval in the steady state, so that they become

$$\phi_{a\lambda}=\epsilon_{a\lambda}C_1\lambda^{-5}\exp\left(-C_2/\lambda T_a\right)+(1-\epsilon_{a\lambda})\,\phi_{b\lambda} \qquad \ldots\ldots(3),$$

$$\phi_{b\lambda}=\epsilon_{b\lambda}C_1\lambda^{-5}\exp\left(-C_2/\lambda T_b\right)+(1-\epsilon_{b\lambda})\left\{\frac{b-a}{b}\,\phi_{b\lambda}+\frac{a}{b}\,\phi_{a\lambda}\right\} \qquad \ldots\ldots(4).$$

The apparent temperatures $\mathscr{T}_a$ and $\mathscr{T}_b$ observed with the optical pyrometer are such that

$$\phi_{a\lambda}=C_1\lambda^{-5}\exp\left(-C_2/\lambda\mathscr{T}_a\right),$$
$$\phi_{b\lambda}=C_1\lambda^{-5}\exp\left(-C_2/\lambda\mathscr{T}_b\right).$$

From equation (3) it can be shown that

$$\exp\left(-C_2/\lambda T_a\right)=\frac{\exp\left(-C_2/\lambda\mathscr{T}_a\right)-\exp\left(-C_2/\lambda\mathscr{T}_b\right)}{\epsilon_{a\lambda}}+\exp\left(-C_2/\lambda\mathscr{T}_b\right),$$

and from equation (4) that

$$\exp\left(-C_2/\lambda T_b\right)=\exp\left(-C_2/\lambda\mathscr{T}_b\right)-\frac{a\,(1-\epsilon_{b\lambda})}{b\epsilon_{b\lambda}}\left\{\exp\left(-C_2/\lambda\mathscr{T}_a\right)-\exp\left(-C_2/\lambda\mathscr{T}_b\right)\right\}.$$

The table gives the observed temperature corresponding to a true temperature T_b of 1400° K. for different values of ϵ_b when $\epsilon_a=1$, $T_a=\mathscr{T}_b=1600°$ and $a/b=1/2$.

	$T_a=\mathscr{T}_b=1600°$ K. $T_b=1400°$ K.		ϵ_a or $\epsilon_{a\lambda}=1$ $\lambda=0{\cdot}62$	
ϵ_b or $\epsilon_{b\lambda}$	$\mathscr{T}_b$ by radiation pyrometer (° K.)	Correction to $\mathscr{T}_b$ (° K.)	$\mathscr{T}_b$ by optical pyrometer (° K.)	Correction to $\mathscr{T}_b$ (° K.)
0·1	1569	−169	1581	−181
0·25	1529	−129	1553	−153
0·50	1476	−176	1508	−108
0·75	1434	−34	1460	−60
0·90	1413	−13	1427	−27
1·00	1400	0	1400	0

REFERENCES

(1) Merkel. *Die Grundlagen der Wärmeübertragung*, p. 168 (1927). Dresden and Leipzig: Th. Steinkopff.

(2) Gröber. *Einführung in die Lehre von der Wärmeübertragung*, p. 131 (1926). Berlin: J. Springer.

(3) ten Bosch. *Die Wärmeübertragung*, p. 26 (1927). Berlin: J. Springer.

(4) Clausing. *Rev. Opt.* **10**, 353 (1931).

(5) Saunders. *Proc. phys. Soc.* **41**, 569 (1928–9).

THE MAGNETIC PROPERTIES OF MANGANESE AMALGAMS

By L. F. BATES, D.Sc., Professor of Physics,
University College, Nottingham,

AND

L. C. TAI, B.Sc. (Nanking), Ph.D. (London).

Received 27 *October* 1936. *Read in title* 12 *February* 1937

ABSTRACT. The variation with temperature of the magnetic susceptibilities of a series of manganese amalgams of known concentration has been determined over a range from 15° to 350° C. The amalgams show pronounced temperature hysteresis of their magnetic properties, and it is found that the manganese becomes more paramagnetic as the temperature rises, until, in the case of the more concentrated amalgams, a steady state is reached. The phenomena are briefly discussed in the light of the recent theories of alloys.

§ 1. INTRODUCTION

In an account of some measurements of the magnetic susceptibilities of mercury amalgams(1) the writers recently described the behaviour of amalgams containing small quantities of manganese. It was pointed out that in very dilute solution manganese possesses an atomic susceptibility of $13,700 \times 10^{-6}$ e.m.u./g., a high value which was in accord with the experimental values for manganese dissolved in copper, silver and gold. The atomic susceptibility so found depended on the concentration of the manganese, and the value quoted above refers to solutions containing less than 1 part of manganese in 1000 parts of mercury, where it is thought that manganese does not form complex molecular groups, like Mn_2Hg_5, which are considered to exist in higher concentrations(2). Now, in order to determine the atomic moment of the manganese atom in dilute solution we must know whether the values of the atomic susceptibility for a series of temperatures obey a Curie-Weiss law, and the measurements described below were primarily undertaken with this end in view.

§ 2. EXPERIMENTAL PROCEDURE

The amalgams in the previous investigation were prepared by electrolysis, washed and dried, without being heated. It was now necessary to ensure that all traces of water were completely removed, since in order to prevent oxidation at higher temperatures the amalgams had to be placed in evacuated sealed tubes. Freshly prepared amalgam was placed as quickly as possible in the bulb *A*, figure 1, which was evacuated through *B*. The amalgam was then heated to about 100° C. and finally poured into the tube *C* which was then sealed at *D*. A glass hook was provided at *D* and the tube and its contents suspended together with an evacuated compensating tube from one arm of a sensitive balance, and the susceptibility was measured by the Gouy method as previously described. If the tube containing the amalgam is of uniform cross-section α, and the lower end of the amalgam is in a uniform field H while the upper end is in a field H_0, the additional magnetic force $m_T.g$ on the column is given by

$$m_T.g=\tfrac{1}{2}.(k_{\text{Am}})_T.\alpha.(H^2-H_0^2),$$

where $(k_{\text{Am}})_T$ is the volume susceptibility of the amalgam at the temperature T. In deriving this expression it is assumed that effects due to the magnetic properties of the air are entirely eliminated by the use of the compensating tube. If the tube is now opened and the amalgam replaced by pure mercury of susceptibility $(k_{\text{Hg}})_R$ at room temperature R, the additional force $m_R'.g$ is given by

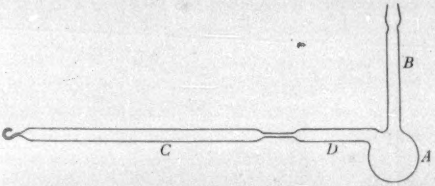

Figure 1. Apparatus for preparation of dry amalgam.

$$m_R'.g=\tfrac{1}{2}.(k_{\text{Hg}})_R.\alpha.(H^2-H_0^2),$$

whence
$$(k_{\text{Am}})\,T=\frac{m_T}{m_R'}\,(k_{\text{Hg}})_R=m_T.Q,$$

and, assuming that at any given temperature the density of the amalgam is identical with that of pure mercury at the same temperature,

$$(\chi_{\text{Am}})_T=\frac{m_T.Q}{\rho_T},$$

where χ_{Am} refers to the mass susceptibility of the amalgam and ρ_T is the density of the mercury at that temperature.

The results may possibly be made a little more precise by comparing the magnetic pull m_T with the magnetic pull m_T' for pure mercury at the temperature T, and some experiments on these lines were actually made. A set of results showing how the mass susceptibility of pure mercury varies with temperature is given in table 1, where the values merely rise from $-0{\cdot}168$ at 15° C. to $-0{\cdot}167\times10^{-6}$ at 350° C.

Table 1

T (° K.)	290·3	364·2	448·3	521·2	570·5	618·0
$-\chi\times10^6$	0·1680	0·1684	0·1677	0·1670	0·1668	0·1670

In all, three such sets of results were obtained with different samples of mercury; they agree very well from room temperature up to about 250° C., but at higher temperatures two of the sets show increases to $-0{\cdot}164\times10^{-6}$ at 350° C.; the differences may have been due to the formation of small cavities of vapour between the liquid mercury and the walls of the containers, or to the presence of very small amounts of impurity. However, even if the higher value of the susceptibility at 350° C. is taken as correct, it has very little influence on the amalgam results described here; we prefer to take the lower value in view of the following results.

§ 3. RESULTS

The main experiments were made with amalgams I, II and III respectively containing 0·0016, 0·016 and 0·03 g. of manganese in 100 g. of mercury. In all cases very definite hysteresis phenomena were recorded. The variation with temperature of the mass susceptibility of amalgam I is shown at I in figure 2. Starting at room temperature the mass susceptibility rose regularly from $-0{\cdot}1645\times10^{-6}$ to about $-0{\cdot}155\times10^{-6}$ at about 200° C. after which there was a more definite increase, and eventually a steady state was reached at about 350° C. Each of the experimental points was obtained after the amalgam had been maintained at a chosen temperature for about 45 min.; the arrows indicate the course of the observations and the points marked with open circles were obtained on the same day. The following day the point marked with a cross was obtained before the temperature was raised, and the points marked with filled circles were obtained after the specimen had been raised to 350° C., the value at the highest temperature being recorded after the amalgam had been maintained at 350° for about 1 hour. The filled circles clearly lie below the open circles and this feature is attributed to the difference in the times taken in heating and cooling the amalgam on the different days. The point marked with

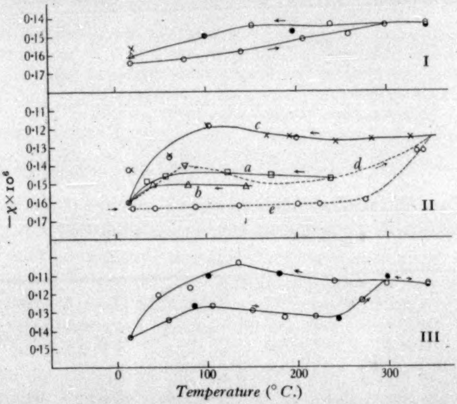

Figure 2. Graphs showing susceptibility of manganese amalgams as a function of temperature. I, 0·0016 g. manganese in 100 g. mercury; II, 0·016 g. manganese in 100 g. mercury; III, 0·030 g. manganese in 100 g. mercury.

an upright triangle was obtained a day later. It is clear that the initial and final values of the susceptibility at room temperature do not coincide and it is considered that this too may be occasioned by the rate at which the cooling was carried out. Further support for this view was obtained from some experiments made on an amalgam IV, containing 0·008 g. of manganese in 100 g. mercury. This was kept at 350° C. for 1 hour and then quenched to room temperature; values of the mass susceptibility found at various mean intervals of time after the quenching are given in table 2.

Table 2. Variation of mass susceptibility of amalgam IV with time after quenching

t (min.)	32	75	123	195
$-\chi_{\mathrm{Am}} \times 10^6$	0·1427	0·1480	0·1501	0·1550

A series of curves obtained with amalgam II are shown at II in figure 2. Curve *a* was obtained by first raising the temperature to 250° C. and maintaining it at 239·4° C. for 1 hour and then observing the susceptibility at chosen temperatures at each of which it was maintained for 45 min. Curve *b* was similarly obtained after the amalgam had been heated to 155° C. and maintained at 146° C. Curve *c* through the points marked with a cross was likewise obtained when the amalgam was initially raised to 345° C. It is seen that whereas the starting and final values at room temperature taken on successive days were the same for curves *a* and *b*, this was not the case in *c*, when the amalgam had been heated to 350°. There appears to be some instability, or at any rate uncertainty, about successive values obtained at room temperature after high-temperature treatment, and it may be that the amalgam near the pole pieces is no longer homogeneous, but it is difficult to see how this state can arise. The broken curve *d* shows approximately the variation of susceptibility as the specimen is heated from room temperature to 350° C. The specimen was now cooled for a short time in carbon dioxide snow and the series of values shown by curve *e* was obtained while the temperature was raised to 345° C. and then lowered to room temperature. The hysteresis in this case is very striking.

The behaviour of the most concentrated amalgam, III, is shown at III in figure 2, where the arrows indicate the direction in which the temperature was changed during the course of the observations, the filled-circle values being obtained on the day following that on which the open-circle values were found. In the case of this amalgam the initial increase in susceptibility is followed by a steady decrease until a rapid rise in susceptibility occurs at about 250° C., as with the other amalgams described above, and a final steady value is reached. Temperature hysteresis is again strongly marked, and the time factor is still involved but to a lesser extent;

Table 3. Variation of mass susceptibility of amalgam III with time after quenching

t (min.)	43	94	150	245	345	$\rightarrow\infty$
$-\chi_{\mathrm{Am}} \times 10^6$	0·1344	0·1389	0·1408	0·1432	0·1435	0·1435

in table 3 are given the values of the susceptibility at room temperature observed at various mean times *t* following the quenching of the amalgam from 350° C. to room temperature.

§ 4. DISCUSSION OF RESULTS

The present measurements provide a fresh example of the temperature hysteresis associated with the magnetic properties of manganese. It is well known that manganese forms ferro-magnetic compounds with antimony, arsenic, bismuth, nitrogen and phosphorus and that in many cases, particularly with the arsenide, the ferromagnetic Curie point found when the temperature of the compound is gradually raised is some 15 or 20° C. higher than that found when the paramagnetic substance is slowly cooled(3).

The curves of figure 2 suggest that in these weak amalgams the manganese atom becomes increasingly paramagnetic as the temperature is raised, until when the kinetic energy of the mercury atoms becomes sufficiently great a maximum value is attained. This suggests that the manganese atom or ion becomes increasingly free of its neighbouring mercury atoms as the temperature is raised, attaining a maximum freedom at temperatures above 300° C. On the cooling of a hot amalgam the manganese remains free, and accordingly the paramagnetic susceptibility increases with fall in temperature as it normally does in paramagnetic substances. Finally, a stage is reached when the manganese becomes less free and there is a decrease in the paramagnetism. It is interesting that cooling to low temperatures produces such a marked and persistent diminution in the freedom of the manganese as that shown at II in figure 2.

At first sight it might appear that the behaviour of manganese in amalgams invites discussion on the lines of the theoretical studies of Bragg and Williams(4) and of Bethe(5). Bragg and Williams discuss atomic arrangements in alloys on the supposition that each sort of atoms form on their own a kind of superlattice which repeats itself throughout the specimen, the two lattices existing meshed with each other. This arrangement they call "superlattice order"; Bethe terms it "long-distance order". In Bethe's work it is assumed that the energy associated with the atomic arrangement in the alloy is uniquely fixed by the order of neighbouring atoms, by "local order", and not by a superlattice order. Clearly, in the case of these dilute fluid amalgams the possibility of the existence of long-distance order must be remote, although the general behaviour of amalgams with increasing concentrations shows that there is a tendency to solidify which may possibly be interpreted as due to the establishment of such long-distance order. As the mass susceptibility of manganese in the more concentrated amalgams falls with increase in concentration, it would then follow that long-distance order leads to the suppression of the pronounced paramagnetism of manganese; on this basis the loss of paramagnetism by freezing the amalgam could be explained. Now, the picture of local order given by Bethe was worked out in detail for alloys containing equal numbers of two kinds of atoms, while in the case of these amalgams there is an overwhelming preponderance of atoms of one kind.

The idea of local order is, however, implied in the explanation of the magnetic behaviour which we have given above. For it would appear that each manganese atom or possibly pair of atoms in an amalgam is surrounded by a group of mercury atoms forming a kind of complex molecule. The formation of such complex arrangements must, of course, depend upon the manganese concentration and the temperature. Once a particular set of complex arrangements have been broken down by increase in the kinetic energy of their constituents, they will only be re-formed with some difficulty as the temperature is lowered; in other words, temperature hysteresis will be observed and time will be required for their re-formation at any given temperature. The peculiar shape of the curve III of figure 2 is no doubt due to the successive breaking-down of two different sets of complex arrangements.

Since the completion of the work described in this communication the publication of Hume-Rothery's report on the structure of metals and alloys(6) has directed our attention to the important study of intermetallic compounds formed in mercury, carried out by Russell and his collaborators(7). Using purely chemical methods of examination which did not involve the removal of the compounds from the mercury, they showed that compounds such as Zn_7Mn, Zn_4Mn, Zn_3Mn, Sn_3Mn, Sn_2Mn, $SnMn$ and $SnMn_2$, into which mercury does not enter as a constituent, can be formed. We feel that the magnetic method of examination which we have so far used only for the examination of the single metal manganese dissolved in mercury might also provide useful information in the case of the more complicated binary and ternary compounds studied by Russell, particularly from the examination of compounds containing manganese at temperatures above 100° C.

§ 5. ACKNOWLEDGEMENTS

The above work was in the main carried out at University College, London, and we tender our best thanks to Prof. E. N. da C. Andrade for the many facilities afforded us, to the Government Grants Committee of the Royal Society for the magnet used in the measurements, and to Prof. Lovatt-Evans for the loan of a Bosch and Lomb colorimeter.

Note added 12 *February* 1937

Recent work in Nottingham with iron amalgams suggested that a small quantity of a highly paramagnetic compound, or possibly metallic manganese, might be found at the surface of a manganese amalgam; this has been verified. It has been found that when a manganese amalgam is violently shaken and then allowed to stand, the intensely magnetic constituent very quickly rushes to the surface. In the experiments described in the present paper this constituent would remain outside the magnetic field and play no part in the measurements. The composition of the amalgam was always found as described in an earlier paper(1) by analysing a sample from that portion near the pole pieces where $H \, . \, dH/dx$ was at a maximum during the magnetic measurements; the portion mainly responsible for the experimental value of the susceptibility. It is difficult to see how the existence of the highly magnetic constituent outside the field can account for the hysteresis phenomena described, unless it is broken up at high temperatures and dispersed throughout the body of the amalgam; this would not, however, explain why the high value of the susceptibility observed at high temperatures persists on cooling.

REFERENCES

(1) Bates, L. F. and Tai, L. C. *Proc. phys. Soc.* **48**, 795 (1936).
(2) Royce, H. D. and Kahlenberg, L. *Trans. Amer. Electrochem. Soc.* **59**, 791 (1931).
(3) Bates, L. F. *Phil. Mag.* **16**, 657 (1933); *Proc. roy. Soc.* A, **117**, 680 (1928).
(4) Bragg, W. H. and Williams, E. J. *Proc. roy. Soc.* A, **145**, 699 (1934); **151**, 540 (1935); **152**, 231 (1935).
(5) Bethe, H. *Proc. roy. Soc.* A, **150**, 552 (1935).
(6) Hume-Rothery, W. "The Structure of Metals and Alloys," *Rep. Inst. Metals*, No. 1 (1936).
(7) Russell, A. S. *J. chem. Soc.* pp. 841, 852, 857, 2340 (1932); p. 1750 (1934); *Nature*, Lond., **133**, 217 (1934); **138**, 161 (1936).

WOOD-WATER RELATIONSHIPS, PART III. MOLECULAR SORPTION OF WATER BY SITKA SPRUCE WOOD

By WILFRED W. BARKAS, M.Sc., Forest Products Research Laboratory, Princes Risborough, Aylesbury, Bucks.

Received 15 *December* 1936. *Read in title* 26 *February* 1937

ABSTRACT. The apparent molecular sorption of water by Sitka spruce flour is shown to remain constant at about 23 per cent of the dry weight of the wood over a period of 83 days when a sucrose solution is used as the indicator, but with sodium chloride solutions a gradual fall in the apparent sorption occurs which reaches a value of about 5 per cent after 14 days. This fall is here put down to the slow sorption of the salt and not to a low value of the true molecular sorption. It is also suggested that the low value of the molecular sorption derived by Stamm and Loughborough from considerations of the heat of wetting of wood is due to their assumption that molecular sorption is complete at about 30 per cent relative vapour pressure, when the capillary sorption commences.

In the first paper on this subject(1), which will be referred to in what follows as *paper* 1, the molecular sorption w_a was determined from the change in concentration of an evacuated sucrose solution on being mixed with dry evacuated flour of Sitka spruce wood. The value of the molecular sorption measured in this way would be an apparent and not an absolute one if sorption of sucrose also occurred, because the change in concentration of the solution would be smaller than that represented by the simple extraction of water. Further, the sorption must be in vapour-pressure equilibrium with the solution used, so that each different concentration provides a point on a {moisture-content, vapour pressure} isothermal in w_a which on extrapolation to saturated vapour pressure gives an approximate saturation value w_s equal to 23 per cent of the dry weight of the wood flour. This is considerably higher than the values given by other workers, e.g. Pidgeon and Maass(2) or Stamm and Loughborough(3).

In a recent publication Stamm(4) has offered some criticisms of the method which are based on the author's original note to *Nature*(5). Some of these had already been dealt with in paper 1, which was then in the press, but one point remained which, it was thought, required further consideration. Stamm kindly communicated these criticisms informally, and thus made it possible to consider them before his work appeared.

Stamm had found in similar experiments with sodium chloride solutions that the initial change in concentration was not an equilibrium value but decreased slowly until after several days it corresponded to a value of w_a of approximately

6 per cent, which he considered to be the correct one. He thought that the high initial value might be due to the more rapid diffusion of the water as compared with that of the larger salt molecules, and suggested that the same effect would be found in sucrose solutions, though the fall in apparent sorption might be slower since the sucrose molecules are larger still.

Although in paper 1 evidence was given that the sucrose molecules were small enough to enter the capillaries and that therefore the change in concentration was not due to filtration, Stamm's findings on the still smaller molecules of sodium chloride are obviously important, and I am grateful to him for drawing my attention to them. The present paper describes experiments to test whether for sucrose the apparent value of the sorption is an equilibrium value or not.

First of all Stamm's findings for sodium chloride solution were confirmed by experiments carried out exactly as described in paper 1, the change of refractive index of salt solutions with concentration being obtained from the *International Critical Tables*. A 7 per cent concentration* of sodium chloride was used, as this exerts approximately the same relative vapour pressure as an 18 per cent solution of sucrose, and should therefore give the same initial value of 0·20 for w_a. The changes in refractive index were not so great as for sucrose, so that the accuracy was somewhat less. The sorption bottles were kept in a thermostat at 23° C. and only opened when a sample was removed to measure the concentration. Successive samples could be taken later from the same bottles in order to calculate any further sorption changes, provided allowance was made for the smaller amount of solution present. This calculation is cumbersome but quite straightforward, and need not be given here. Table I gives the results obtained. If these values of w_a are plotted against time they show, except for one reading, a regular decrease from the assumed initial value of 0·20 to an apparently constant value between 0·04 and 0·05 after long periods, thus supporting Stamm's results.

Table I. Change in w_a with time for sodium chloride solutions

Initial concentration, 6·91 per cent; relative vapour pressure 0·981

Reference	$\frac{\text{Weight of solution}}{\text{weight of wood}}$	Time (days)	w_a
120/9A			
1st sample	17·4	7	0·134
2nd sample	—	14	0·087(?)
120/11			
1st sample	16·0	9	0·130
2nd sample	—	13	0·058
120/12			
1st sample	16·7	13·5	0·041
2nd sample	—	19	0·041

Measurements were next made on 18 per cent sucrose solutions. In the original experiments the sorption times had purposely been limited to one or two days, owing to the tendency for mould to grow in the solutions. Since the sorption times were now to be increased, the whole experiment had to be performed under sterile conditions, which was achieved through the co-operation of the Mycology Section of the Laboratory. The wood flour and the solution were autoclaved and the whole apparatus assembled and evacuated as quickly as possible after being sterilized with a 0·1 per cent solution of mercuric chloride and rinsed with sterile water. The flour was dried *in vacuo* for several weeks and then flooded with the solution as before.

---

* Gram of solute per 100 grams of solution.

As it was found impossible to keep the reference solution sterile in the double cell of the interferometer, the refractive index was measured against that of distilled water. For this purpose the interferometer had to be modified to allow of large angles of tilt of the compensating glass which somewhat reduced the sensitivity of the instrument, but it remained sufficiently accurate for the purpose in hand.

After the wood flour had been flooded with solution, the stock solution was measured in the interferometer, first against water and then against a sample of solution taken from the first sorption bottle. This sample was then itself measured against water. On calibrating the interferometer for both ranges of tilt, it was found that values of the change in concentration measured in these two ways were in good agreement. The remainder of the stock solution was held *in vacuo* till the end of the experiment, when a repetition of this cycle of measurements showed that it had in fact remained sterile. This would have been in doubt if the measurements against water had not been made.

Successive samples were also taken from these sorption bottles, but the results were irregular and were discarded, as it seemed that the solutions had become contaminated after being once opened. Table 2 gives the results for first samples only, measured both against water and against the stock solution.

Table 2. Change in w_a with time for sucrose solutions

Initial concentration 0·183; relative vapour pressure 0·984

Reference	Weight of solution / weight of wood	Time (days)	w_a by comparison with	
			water	stock solution
136/1	12·40	4	0·182	0·206
136/12	11·55	83	0·191	0·205

The values obtained by comparison with the stock solution are in agreement with that obtained previously at this concentration, which suggests that the heat treatment in the autoclave does not affect the molecular sorption. The less accurate values obtained against water, though rather low, are also consistent. Both readings show no change in sorption over a period of 83 days, which is about six times as long as was required by the sorption from sodium chloride solutions to reach its minimum value.

If the fall in apparent sorption in the case of the sodium chloride solutions is in fact due to slow *diffusion* of the salt molecules, then the diffusion of sucrose should take place in a longer time proportional to the diffusion rates of the two solutes. The diffusion coefficients of salt and sucrose are in a ratio of approximately 2·4 to 1, and the higher concentration of sucrose would tend to make the ratio of the diffusion-rates smaller than this, so evidently diffusion alone will not account for the apparent stability of w_a in sucrose solutions. Since paper 1 showed that the sucrose molecule is not large enough to be filtered out at the orifices of the colloidal capillaries, the explanation would appear to be that the salt is slowly sorbed on to the wood (possibly by partially displacing water molecules) whereas the sucrose is not. This is in agreement with the polar nature of the salt molecule.

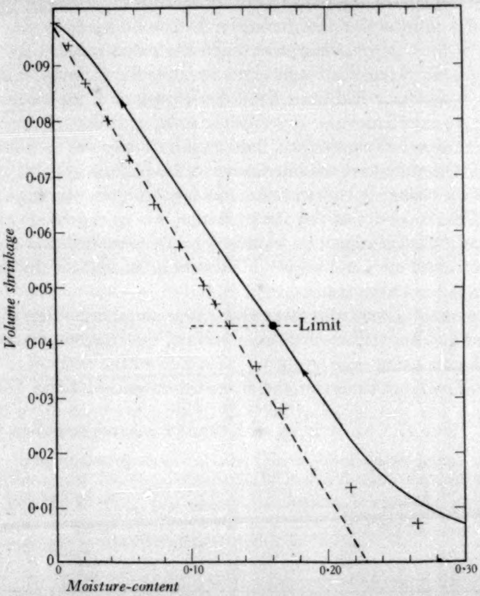

Figure 1. --- $(m-c)$.

Independent evidence is now available from consideration of the shrinkage of wood[(6)] to prove that the values of w_a obtained in paper 1 are substantially correct. At the lower moisture-contents where the water is held entirely by molecular forces, the volume of the wood-water aggregate is that of the components less the sorption-compression c which they suffer. If, therefore, the shrinkage is plotted against $(m-c)$, where m is the moisture content, a straight line results as long as m is principally molecular and equal to w_a, but as soon as the capillary sorption becomes apparent, m becomes greater than w_a and the points diverge towards the higher moisture-contents. In the figure it is seen that the straight line holds from dryness to points corresponding to about 16 per cent moisture content. If this line is extrapolated to zero shrinkage (i.e. to saturated vapour pressure) its intersection corresponds to a moisture content of 26 per cent, which compares favourably with the approximate value of 23 per cent obtained from the sorption measurements. As has been pointed out(6) the values of c are obtained under conditions which would measure compression due to both molecular and capillary forces and that the points corresponding to moisture contents below 6 per cent (where by common consent the sorption is entirely molecular), considered alone, tend to lie on a slightly steeper line, giving a value of approximately 0·25 for w_s. This is admittedly straining the limits of accuracy to be expected from the data, and undoubtedly the sorption-compression due to capillary forces is very small; but it does support the opinion of Stamm and Loughborough(3) that capillary sorption begins to be apparent at a moisture content of about 6 per cent. The author does not agree, however, that molecular sorption is complete at this moisture-content.

Stamm and Loughborough reach their conclusions from their observation that for a moisture-content below 6 per cent the change with moisture-content of the heat of wetting and the entropy are unaffected by temperature. They state (p. 129) that "According to these conceptions the inflection point in the moisture-content, relative-vapour-pressure curves corresponds approximately to the transition point between the surface-bound water and the water held by van der Waals forces...this point occurs at a relative vapour pressure of about 0·30 for all temperatures...and should represent the limiting capillary (radius) in which capillary condensation can take place." Elsewhere (p. 128) they admit the possibility of "a slight overlap" between these two types of sorption. It seems to the author that the molecular sorption is unlikely to be saturated when the vapour pressure is only 30 per cent saturated, and that it would be expected on the other hand to continue on the external surfaces—and on the interior walls of those larger capillaries which had not yet been filled with water—until the saturated vapour pressure was reached.

If this view is correct, there is no discrepancy between the various values for w_a which have been proposed, since they refer only to particular vapour pressures. In this connexion, by taking the isothermal for white spruce published by Filby and Maass(7) it will be found possible to construct a plausible isothermal for the molecular sorption which follows their curve up to the point of inflection, runs very close to it as far as 65 per cent relative vapour pressure (corresponding to the desorption moisture-content of 15 per cent) and, after including the author's experimental values of w_a near saturation(1), reaches a saturation value at a moisture-content between 23 per cent and 25 per cent. A hypothetical curve of this type suggests that the hysteresis loop in w_a is of approximately constant width except where it begins to close near zero and at saturated vapour pressure.

The capillary sorption at any vapour pressure is the difference between the total and molecular sorptions, and at the higher vapour pressures is composed of water partly in the colloidal and partly in the anatomical capillaries. The greater width of the hysteresis loop for total sorption, which increases up to vapour pressures indistinguishable from saturation, is to be accounted for in terms of capillary sorption in the anatomical structure(8).

I wish to thank the Mycology section of the Laboratory for their suggestions and assistance in evolving a technique for performing these experiments under sterile conditions. Without their help this paper could not have been written. I am also indebted to the Director of this Laboratory, Mr W. A. Robertson, for permission to publish the paper.

REFERENCES

(1) Barkas, W. W. *Proc. phys. Soc.* **48**, 1 (1936).
(2) Pidgeon, L. M. and Maass, O. *J. Amer. chem. Soc.* **52**, 1053 (1930).
(3) Stamm, A. J. and Loughborough, W. K. *J. phys. Chem.* **39**, 121 (1935).
(4) Stamm, A. J. "Colloid Chemistry of Cellulosic Materials." *Misc. Publ. U.S. Dep. Agric.* No. 240 (1936).
(5) Barkas, W. W. *Nature*, Lond., **130**, 699 (1932).
(6) Barkas, W. W. *Forest Products Research Laboratory*. Project 8, *Progress Report*, No. 1 (1936).
(7) Filby, E. and Maass, O. *Canad. J. Res.* **7**, 1 (1935).
(8) Barkas, W. W. *Proc. phys. Soc.* **48**, 576 (1936).

THE PHASE BOUNDARIES IN BINARY ALLOYS, PART 1: THE EQUILIBRIUM BETWEEN LIQUID AND SOLID PHASES

BY H. JONES, H. H. Wills Physical Laboratory, University of Bristol

Communicated by Prof. A. M. Tyndall, F.R.S., 16 *December* 1936.
Read in title 12 *March* 1937

ABSTRACT. The thermodynamic theory of the melting-point and freezing-point curves, in the α solid-solution region, of binary alloys is briefly considered. It is shown that the van 't Hoff relation should be applicable to these alloys, and its validity, for sufficiently dilute solutions is verified by comparison with experiment. It is shown from experiment that the change in the latent heat when small quantities of nickel, zinc, gallium or germanium are dissolved in copper is proportional to the electron : atom ratio. Similar results are obtained for cadmium, indium or tin dissolved in silver. A qualitative theory is proposed to account for these effects.

§ 1. INTRODUCTION

It has long been known that in binary alloys in which the atoms are of approximately the same size, the phase boundaries in the solid state are determined by the ratio (1) of the number of valency electrons to that of atoms, and an outline of a theory to account for this has already been given (2, 3, 4, 5). The recent work of Hume-Rothery and his collaborators (6) suggests that the electron : atom ratio is also of importance in determining the melting and freezing-point curves of simple alloys.

In part I of this paper the thermodynamic theory of the liquidus and solidus lines of alloys is considered afresh, and an attempt is made to separate the role played by the electron : atom ratio from the effect of the atomic concentration of solute atoms. We shall deduce from the experiments that, in solutions in copper of elements belonging to the same row of the periodic table, the change in the energy-difference between the liquid and the solid phases at the same composition is proportional to the electron : atom ratio. In § 4 a simple explanation of this result is suggested.

§ 2. THE GENERAL CONDITIONS OF EQUILIBRIUM BETWEEN TWO PHASES

Let F_1 and F_2 be the free energies per atom of two alloy phases which are in equilibrium with each other. Let x_1 denote the composition of one phase (i.e. the atomic fraction of one element in the alloy) and x_2 that of the other. F_1 is a function of the specific volume of the phase V_1, the common temperature T, and x_1; F_2 is a function of V_2, T and x_2. The condition for equilibrium is expressed by the two equations ⁽³⁾

$$\frac{\partial F_1}{\partial x_1}=\frac{\partial F_2}{dx_2}=\frac{F_1(x_1)-F_2(x_2)}{x_1-x_2} \qquad \text{......(1).}$$

If we regard the volumes as constant, these two equations will determine for given T the values of x_1 and x_2. Thus the solution of equations (1) determines the boundaries in the phase diagram of the mixed-crystal region between the two pure phases 1 and 2. Thus if 1 stands for a solid solution and 2 for the liquid phase, equations (1) determine the liquidus and solidus curves. It has been shown that the free energy per atom may be written ⁽³⁾

$$F_1(x_1)=kT\{x_1\log x_1+(1-x_1)\log(1-x_1)\}$$
$$+U_1(x_1)-T\int_0^T\frac{C_v^{(1)}}{T}\,dT+\int_0^T C_v^{(1)}\,dT \qquad \text{......(2),}$$

where $C_v^{(1)}$ denotes the specific heat at constant volume of phase 1 assuming the alloy to be totally disordered. $U_1(x_1)$ denotes the internal energy of the alloy as a function of its composition at the absolute zero of temperature measured with respect to the energy of the individual atoms. If for convenience we write

$$f_1(x_1,T)=U_1(x_1)-T\int_0^T\frac{C_v^{(1)}}{T}\,dT+\int_0^T C_v^{(1)}\,dT \qquad \text{......(3),}$$

then f is the whole of the free energy except for the disorder term. We obtain from equations (1)

$$\log\frac{x_2(1-x_1)}{x_1(1-x_2)}=\frac{1}{kT}\left(\frac{\partial f_1}{\partial x_1}-\frac{\partial f_2}{\partial x_2}\right)$$
$$\log\left(\frac{1-x_1}{1-x_2}\right)=\frac{1}{kT}\left(f_1(x_1T)-f_2(x_2T)-x_1\frac{\partial f_1}{\partial x_1}+x_2\frac{\partial f_2}{\partial x_2}\right) \qquad \text{......(4).}$$

§ 3. EQUILIBRIUM BETWEEN LIQUID AND SOLID PHASES

We consider the equilibrium between a solid solution and the liquid phase. Let T_{C} be the melting point of the pure solvent metal. We have the condition

$$f_l(0,T_0)=f_s(0,T_0) \qquad \text{......(5),}$$

where the subscripts l and s refer to the liquid and solid phases. From equation (3) we obtain easily for any temperature T

$$f_l(0,T)-f_s(0,T)=(T_0-T)\frac{\lambda}{T_0}+\int_{T_0}^T(C_v^{(l)}-C_v^{(s)})\,dT-T\int_{T_0}^T\frac{C_v^{(l)}-C_v^{(s)}}{T}\,dT \qquad \text{......(6),}$$

where λ is the latent heat of fusion of the pure solvent. The second and third terms on the right together yield a term of the order of magnitude

$$\tfrac{1}{2}(C_v^{(l)}-C_v^{(s)})(T-T_0)^2/T_0,$$

which for temperatures near to T_0 is negligible in comparison with the first term. We make the following approximation:

$$f_l(x_l, T) - f_s(x_s, T) - f_l(0, T) + f_s(0, T) = U_l(x_l) - U_s(x_s) - U_l(0) + U_s(0),$$

and hence obtain from equations (4) and (6) the two equations which determine the liquidus and solidus lines in the region of solid solution, viz.

$$\frac{\lambda}{T_0}(T - T_0) + kT \log \frac{1 - x_s}{1 - x_l} = \left\{ U_l(x_l) - U_s(x_s) - U_l(0) + U_s(0) - x_l \frac{dU_l}{dx_l} + x_s \frac{dU_s}{dx_s} \right\} \quad \ldots\ldots(7\cdot 1),$$

$$kT \log \frac{x_s(1 - x_l)}{x_l(1 - x_s)} = \frac{dU_l}{dx_l} - \frac{dU_s}{dx_s} \quad \ldots\ldots(7\cdot 2).$$

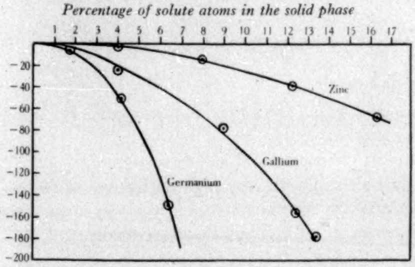

Figure 1.

If $U_l(x_l)$ and $U_s(x_s)$ are developed as power series in x_l and x_s we see that for small concentrations the right-hand side of equation (7·1) is quadratic in x_l and x_s. For small concentrations, x_l, x_s, therefore, the well-known formula of van t' Hoff is obtained from equation (7·1), viz.

$$x_l - x_s = \frac{\lambda}{k}\left(\frac{1}{T} - \frac{1}{T_0}\right) \quad \ldots\ldots(8).$$

In certain metallic alloys this law is found to agree well with experiment⁽⁷⁾. On the other hand for solutions of a number of metals in copper and silver Hume-Rothery and his collaborators do not find good agreement⁽⁶⁾. In figure 1 we have plotted the values of the left-hand side of equation (7·1) against x_s for solutions of zinc, gallium and germanium in copper, using the data given in table 1. The value of the latent heat of copper assumed is 3·18 kcal. per gram-atom, which is also the best value obtained by direct observation⁽⁸⁾. We see that, as the theory predicts, the curves for small concentrations are approximately parabolas. It appears therefore that the breakdown of the van t' Hoff law for the alloys examined by Hume-Rothery is only apparent; the concentrations used when equation (8) was applied were not small enough.

§ 3·1. From the observed liquidus and solidus curves it is possible to calculate the difference in internal energy between the liquid and the solid phase at the same concentration and at zero temperature. This may be done as follows. Let x_l and x_s be the concentrations at temperature T which are in equilibrium, and let

$$\bar{x} = \tfrac{1}{2}(x_s + x_l).$$

Expanding $U_l(x_l)$ and $U_s(x_s)$ as Taylor's series about the value of the concentration $\bar{x}$ we obtain for the right-hand side of equation (7·1), which we shall denote by P for brevity,

$$P = (U_l - U_s)_{\bar{x}} - (U_l - U_s)_0 - \bar{x}\frac{d}{d\bar{x}}(U_l - U_s) - \tfrac{1}{2}(x_l^2 - \bar{x}^2)\frac{d^2 U_l}{d\bar{x}^2} + \tfrac{1}{2}(x_s^2 - \bar{x}^2)\frac{d^2 U_s}{d\bar{x}^2} + \text{etc.}$$

For the right-hand side of equation (7·2), which we denote by Q, we obtain

$$Q = \frac{d}{d\bar{x}}(U_l - U_s) + (x_l - \bar{x})\frac{d^2 U_l}{d\bar{x}^2} - (x_s - \bar{x})\frac{d^2 U_s}{d\bar{x}^2} + \text{etc.}$$

and therefore we find that

$$P + \bar{x}Q = (U_l - U_s)_{\bar{x}} - (U_l - U_s)_0 - \tfrac{1}{8}(x_l - x_s)^2 \frac{d^2}{d\bar{x}^2}(U_l - U_s) + \text{etc.}$$

We may safely neglect the second and higher powers of $(x_l - x_s)$, especially in view of the fact that they are multiplied by high derivatives of $(U_l - U_s)$. It has been verified *a posteriori* that the error introduced in this way is quite negligible for small values of the concentrations. We obtain therefore finally

$$(U_l - U_s)_{\bar{x}} = \frac{\lambda T}{T_0} + kT\left\{\log\frac{1 - x_s}{1 - x_l} + \tfrac{1}{2}(x_s + x_l)\log\frac{x_s(1 - x_l)}{x_l(1 - x_s)}\right\} \qquad \text{......(9).}$$

From equation (9), using experimental values of x_s, x_l, λ, we can calculate $(U_l - U_s)$ for small concentrations of nickel, zinc, gallium and germanium individually dissolved in copper. To do this we require the concentrations of the liquid and solid phases which are in equilibrium at a given temperature. These were obtained by plotting the liquidus and solidus curves from experimental data and reading off the values of x_l and x_s for a number of temperatures. The results are summarized in the table. Instead of $(U_l - U_s)_{\bar{x}}$ we give $\Delta U = (U_s - U_l)_{\bar{x}} - (U_s - U_l)_0$, so that in all cases ΔU tends to zero as $\bar{x}$ becomes zero. ΔU may be regarded as the decrease in the latent heat of fusion due to the addition of a fraction $\bar{x}$ of some other element in solution.

The data for copper-zinc are taken from the work of Ruer and Kremers(9), those for copper-gallium are from the work of F. Weibke(10), those for copper-germanium from the work of Hume-Rothery, Mabbott and Channel-Evans(6), and those for copper-nickel from the work of N. S. Kurnakow(11). The melting point of pure copper is 1356° K. We note that in the case of nickel dissolved in copper the latent heat is increased; this is to be expected since the latent heat of pure nickel is greater than that of pure copper.

Table 1

T (° K.)	x_s	x_l	$\bar{x}$	ΔU (cal./g.-atom)
		Zinc dissolved in copper		
1333	0·041	0·060	0·050	55
1313	0·081	0·111	0·096	101
1293	0·122	0·158	0·140	147
1273	0·163	0·204	0·183	192
		Gallium dissolved in copper		
1323	0·040	0·058	0·049	76
1273	0·090	0·130	0·110	191
1223	0·124	0·176	0·150	305
1203	0·134	0·194	0·164	352
		Germanium dissolved in copper		
1323	0·017	0·044	0·0305	84
1273	0·042	0·094	0·068	199
1223	0·0645	0·124	0·094	310
		Nickel dissolved in copper		
1423	0·205	0·126	0·165	−155
1453	0·330	0·190	0·260	−229
1503	0·495	0·300	0·397	−342

Figure 2 shows ΔU plotted against $\bar{x}$. We see from figure 2 that ΔU is very closely proportional to the valency-electron concentration, i.e. if v denotes the valency of the solute atoms, $\Delta U \propto (v-1)\,\bar{x}$. Using the data given by Hume-Rothery for solutions of cadmium, indium and tin in silver we find according to

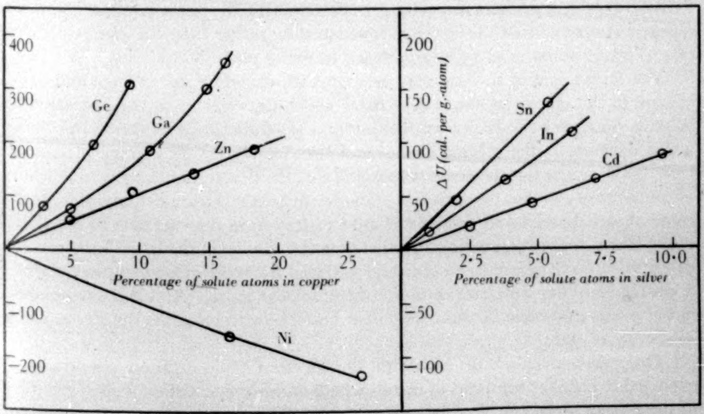

(*a*) (*b*)

Figure 2. The change in the latent heat ΔU as a function of the concentration of solute atoms. (*a*) For nickel, zinc, gallium and germanium dissolved in copper. (*b*) For cadmium, indium and tin dissolved in silver.

equation (9) that $\Delta U = 0{\cdot}9\,(v-1)\,\bar{x}$ kcal. per gram-atom; see figure 2 (*b*). For palladium dissolved in silver, just as for nickel in copper, ΔU is negative. A precise calculation for this alloy cannot be made, for the liquidus and solidus lines are not known with sufficient accuracy.

§ 4. THE VARIATION OF THE INTERNAL ENERGY OF A PHASE WITH COMPOSITION

We have seen in the previous sections that the first requirement of a theory of the phase boundaries in binary alloys is a knowledge of the internal energy of the various phases as a function of the composition. The modern theory of metals provides a means by which the change of internal energy with composition can be calculated. It is now well established that the energy spectrum of the valency electrons in a metal is a band having a width equal to a few electron-volts. The calculation of the internal energy of a metal compared with the energy of the widely separated individual atoms which compose it is made in two steps. Firstly the energy of the lowest level of the valency electrons should be found by some method such as that of Wigner and Seitz; secondly the whole energy of the band of electrons referred to this lowest level must be calculated. This latter part of the energy we call the Fermi energy. The energy of the lowest level is sensitive to changes in atomic volume, but is not so sensitive to changes in crystal structure for a given atomic volume.* On the other hand the Fermi energy is sensitive to changes in structure even when the atomic volume remains unchanged. It is for this reason that the Fermi energy is of primary importance in determining the phase boundaries in many types of alloys and that the electron-concentration rather than the atom-concentration of solute atoms is of such importance in fixing phase boundaries.

The latent heat of melting may be regarded, therefore, as arising from (*a*) the change in the energy of the lowest state, which depends upon the distortion and volume change of the lattice on melting and (*b*) the change in the Fermi energy which depends on the volume change and also, largely, on the change of structure. Our results can be interpreted if we assume that the first term is largely independent of composition, so that the variation of the latent heat when small quantities of other elements are dissolved in copper will arise mainly from the variation of the change of the Fermi energy on melting. In that case the change in the latent heat would be determined by the electron : atom ratio as found by experiment for solute atoms of approximately the same size as those of the solvent metal. An exact calculation is not at present possible because we do not know how to calculate the Fermi energy in the liquid state.

The proportionality of ΔU with the electron concentration would not be expected to hold for solutions of metals whose atoms are of different size from those of the solvent metals, for instance tin in copper. The reason is that in the solid state there must in such cases be an additional energy which arises directly from the internal strain produced in the lattice. Formula (9) shows that ΔU for tin in copper is considerably greater than for germanium in copper, and this is in agreement with the above consideration.

---

* Fuchs has shown(12) that the difference in energy of the lowest level between the body-centred and face-centred cubic structures having the atomic volume of copper is 4×10^{-4} electron-volts per atom.

REFERENCES

(1) Hume-Rothery. *The Metallic State* (Oxford, 1931).
(2) Jones. *Proc. roy. Soc.* A, **144**, 225 (1934).
(3) Mott and Jones. *The Theory of the Properties of Metals and Alloys* (Clarendon Press, 1936).
(4) Dehlinger. *Z. Phys.* **94**, 231 (1935).
(5) Konobejewski. *Ann. Phys.*, Lpz., **26**, 97 (1936).
(6) Hume-Rothery, Mabbott and Channel-Evans. *Philos. Trans.* **233**, 44 (1934).
(7) Jeffery. *Trans. Faraday Soc.* **36**, 86 (1930).
(8) Umino. *Sci. Rep. Tôhoku Univ.* **15**, 597 (1915).
(9) Ruer and Kremers. *Z. anorg. Chem.* **184**, 196 (1929).
(10) Weibke. *Z. anorg. Chem.* **220**, 293 (1934).
(11) Kurnakow. *Z. anorg. Chem.* **54**, 153 (1907).
(12) Fuchs. *Proc. roy. Soc.* A, **151**, 585 (1935).

THE PHASE BOUNDARIES IN BINARY ALLOYS, PART 2: THE THEORY OF THE α, β PHASE BOUNDARIES

By H. JONES, H. H. Wills Physical Laboratory, University of Bristol

Communicated by Prof. A. M. Tyndall, 16 December 1936. Read 12 March 1937

ABSTRACT. A quantitative theory of the phase boundaries in alloys between the face-centred and the body-centred cubic structures is given. The theory is applied in detail to alloys in which copper is the major constituent. The width of the $(\alpha+\beta)$ mixed-crystal region is obtained with fair approximation; it is found that the width of this region decreases with increasing valency of the solute element, a result which is in accordance with experiment. The variation with temperature of the limits of the α and β regions is obtained also, and again agreement with observations is fairly satisfactory.

§ 1. INTRODUCTION

Our aim in this part of the paper is to determine theoretically the boundaries limiting the α (face-centred) and the β (body-centred) phases for solutions of such metals as zinc, gallium, germanium, etc., in copper. The method is general and could equally well be applied to any alloys which form these two phases. It is a more quantitative development of the theory previously given by the author to account for the Hume-Rothery rule.

As we have seen in part 1 it is essential for this purpose to know the energies of the two phases as functions of the concentration of the solute atoms. In § 4 of part 1 we have already discussed the factors which contribute to the internal energy of a phase, and have seen that for the present purpose the Fermi energy of the valency electrons is of particular importance. The only other factor contributing to the internal energy which is likely to affect the phase formation in alloys is the energy arising from the repulsive forces between the ions of the lattice. These forces, according to Fuchs(1), are responsible for the fact that copper forms a face-centred lattice, and, as he has shown, they have an important effect on the elastic properties of the noble metals.

If we assume that the energy associated with the repulsive forces between two ions may be written in the form $w=ae^{-r/b}$, where r is the distance between the ions, the constants a and b can be determined from the observed elastic constants(2). The difference in energy between the face-centred and body-centred structures with the same atomic volume, due to ion repulsion, could then be estimated. However, calculation shows that a and b depend somewhat sensitively upon the elastic constants (the difference between two nearly equal quantities is involved) and it was not found possible to obtain in this way reliable comparisons between the contributions to the energy in the different phases.

In the following sections the phase boundaries are determined on the assumption that they arise entirely through the difference in the Fermi energy of the two phases. The good agreement with experiment may be interpreted as confirming the conclusion, which follows from the mere existence of the Hume-Rothery electronic rules, that the repulsive forces between the ions is not of major importance in this connexion for copper alloys.

§ 2. THE CALCULATION OF THE FERMI ENERGY FOR THE FACE-CENTRED AND BODY-CENTRED CUBIC STRUCTURES

According to a well-known theorem of Bloch the wave function of an electron in a metal crystal has the form of a modulated plane wave, $ue^{2\pi i(k,r)}$, where the amplitude u is a function with the same periodicity as the lattice potential. The wave vector k is a measure of the electron's momentum and is used to specify its state of motion. A point in the space of the vector k corresponds to a particular state of the electron and is associated with a certain energy. Our first problem is to find the energy of an electron as a function of position in this k space. Brillouin zones are closed regions in this space, across the boundaries of which the energy changes discontinuously.

We shall consider the energy of the states which lie along a line from the origin of k space perpendicular to some plane across which the energy changes discontinuously by an amount ΔE. We choose axes so that the perpendicular from the origin coincides with the k_z axis, and denote the point where this line cuts the plane of energy-discontinuity by $(00k_0)$. It has been shown(2) that in the neighbourhood of $(00k_0)$ for $k_z \leqslant k_0$ the energy E is given by

$$E = \frac{h^2}{2m}\{k_x^2 + k_y^2 + \alpha(k_z - k_0)^2\} - \tfrac{1}{2}\Delta E \qquad \ldots\ldots(1),$$

where α is the oscillator strength of zero frequency of the state at $(00k_0)$ and is connected to the energy gap by the approximate formula

$$\alpha = 1 - 4E_0/\Delta E \qquad \ldots\ldots(1\cdot 1),$$

E_0 being the energy of a free electron at the point $(00k_0)$; thus $E_0 = h^2k_0^2/2m$. Near the origin the energy must depend upon k in approximately the same way as for free electrons. We are interested, of course, only in those metals for which the valency electrons in the individual atoms are in s states. We shall assume therefore that for all points along the line from the origin to $(00k_0)$, and in the neighbourhood of this line, the energy is given by

$$E = \frac{h^2}{2m}\left[k_x^2 + k_y^2 + k_0^2 + (k_0 - k_z)^2 - 2k_0\sqrt{\left\{(k_0 - k_z)^2 + \frac{k_0^2}{(\alpha - 1)^2}\right\}}\,\right] \quad \ldots(2).$$

For points near k_0 this reduces to equation (1), and near the origin it gives the form for free electrons.

Our next step in the calculation of the Fermi energy is to consider the Brillouin zone to be divided into prisms, the faces of the zone forming the bases and the origin the vertex. Within each prism, except in the neighbourhood of the corners, formula (2) may be applied, the axes being suitably chosen for each prism. The energies obtained in this way should be satisfactory for occupied states when there are not more than about 1·5 electrons per atom.

The number of states per unit energy range $N(E)$ is given by the formula

$$N(E)=2\int\frac{dS}{|\operatorname{grad} E|} \qquad \text{......(3)},$$

where the integration is over the surface in k space for which the energy has the value E. $N(E)\,dE$ gives per cm.^{3} of metal the number of states, including the factor 2 which occurs on account of electron spin, which lie in the energy-range E to $(E+dE)$. Since the energy, according to equation (2), as a function of k has axial symmetry about the k_z axis we may write equation (2)

$$E=\frac{h^2}{2m}\{k_r^2+f(k_z)\},$$

where $f(k_z)$ is given at once by comparison with (2), and $k_r=\sqrt{(k_x^2+k_y^2)}$. If θ denotes the angle between the normal to a surface of constant energy and the k_z axis, then we may write $\sin\theta\, dS=2\pi k_r\, dk_z$ and

$$\sin\theta\,|\operatorname{grad} E|=\frac{\partial E}{\partial k_r}=\frac{h^2}{m}k_r.$$

Thus in a region in which the energy has axial symmetry about the k_z axis we obtain

$$N(E)=\frac{4\pi m}{h^2}(k_{z(\max)}-k_{z(\min)}) \qquad \text{......(4)}.$$

This formula gives the contribution to $N(E)$ from that part of the whole energy surface E which may, with sufficient approximation, be regarded as having axial symmetry about some axis which we take to be the k_z axis. $k_{z(\max)}$ is then the maximum value of k_z on this part of the surface and $k_{z(\min)}$ the minimum value. We can apply formulae (2) and (4) to calculate the number of states per unit energy-range in the interior of the first Brillouin zone if we make the approximation of replacing the prisms, into which the zone is divided, by cones having the same solid angle as the prisms. This approximation should not introduce an appreciable error in most cases. From (2) we have

$$\frac{k_{z(\max)}}{k_0}=1-\left\{\frac{2mE}{h^2k_0^2}+1-2\left(\frac{2mE}{h^2k_0^2}+\frac{1}{(\alpha-1)^2}\right)^{\frac{1}{2}}\right\}^{\frac{1}{2}} \qquad \text{......(5)}.$$

In a cone of solid angle ω the height k_z measured from the vertex is related to the radius of the base as follows:

$$k_x^2+k_y^2=k_z^2\{(1-\omega/2\pi)^{-2}-1\}.$$

Thus according to equation (2) the value of $k_{z(\min)}$ is given by the equation

$$E=\frac{h^2}{2m}\left[k_z^2{}_{(\min)}\left(1-\frac{\omega}{2\pi}\right)^{-2}+2k_0\left\{(k_0-k_{z(\min)})-\sqrt{\left((k_0-k_{z(\min)})^2+\frac{k_0^2}{(\alpha-1)^2}\right)}\right\}\right] \qquad \text{......(6)}.$$

We use these equations to calculate $N(E)$ for the body-centred and face-centred cubic structures. For the body-centred structure the first Brillouin zone has 12 faces, therefore $\omega = \frac{1}{3}\pi$ and $k_0 = 1/2^{5/6}\,\Omega^{1/3}$, where Ω cm.³ is the atomic volume. Thus taking a value less than k_0 for $k_{z(\min)}$ we can find the corresponding value of E from equation (6) and therefore $k_{z(\max)}$ from equation (5) and therefore finally $N(E)$ by equation (4). To obtain the whole value of $N(E)$ the expression given by equation (4) needs to be multiplied by $4\pi/\omega$, i.e. in this case by 12. Curve (*b*) in figure 1 has been obtained in this way. When the surface of the Fermi distribution has touched the boundary of the zone, $k_{z(\max)}$ always remains equal to k_0 and the density of states is given by

$$N(E) = \frac{4\pi}{\omega} \cdot \frac{4\pi m}{h^2}\,(k_0 - k_{z(\min)}) \qquad \text{......(7).}$$

The peak in the $\{N(E), E\}$ curve corresponds to the energy surface which just touches the zone boundary.

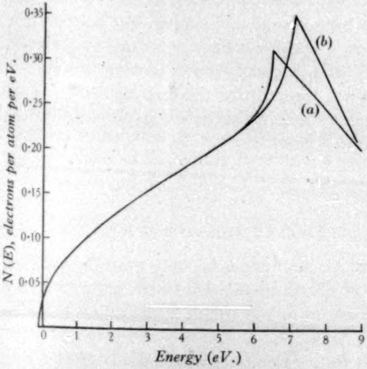

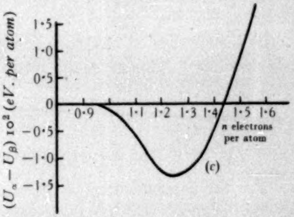

Figure 1 (*a*) and (*b*). Curves showing the number of states per unit energy range as a function of the energy. (*a*) For the face-centred cubic structure, (*b*) for the body-centred cubic structure.

Figure 1 (*c*). The difference between the Fermi energies of the face-centred and body-centred structures as a function of the number of electrons per atom.

Since we are, at present, interested only in the states within the first Brillouin zone which are occupied when the zone is about half filled with electrons, for the face-centred cubic structure, we shall consider only the effect of the octahedral planes of the zone on the density of states. We take therefore $\omega = \frac{1}{2}\pi$, and $k_0 = 3^{1/2}/4^{5/6}\,\Omega^{1/3}$, where Ω is the atomic volume as before. Curve (*a*), figure 1, shows $N(E)$ for the face-centred cubic structure having the same atomic volume as the body-centred structure (*b*) and having the same value of the energy-discontinuity.

We obtain the value of α for copper from the magnitude of the energy gap as determined by the optical properties. This value $\Delta E = 4{\cdot}1$ electron-volts(2). Since the atomic volume is $11{\cdot}76 . 10^{-24}$ cm.^{3} we find, for the face-centred cubic structure, that the free electron energy E_0 corresponding to the point k_0 is $8{\cdot}64$ electron-volts and therefore, according to equation (1.1), $\alpha = -7{\cdot}41$. For the body-centred cubic structure, assuming the same energy gap, we find $E_0 = 9{\cdot}14$ electron-volts and $\alpha = -7{\cdot}89$.

When the number of states per unit energy range $N(E)$ is known, we can obtain the Fermi energy $U(n)$ immediately as a function of the number of electrons per atom. We have

$$\left.\begin{aligned} n &= \int_0^{\zeta} N(E)\, dE \\ U &= \int_0^{\zeta} EN(E)\, dE \end{aligned}\right\} \qquad \ldots\ldots(8),$$

where ζ is the energy of the surface bounding the occupied states. Eliminating ζ between these equations gives $U(n)$. Figure 1 (*c*) shows the difference between the Fermi energies of the face-centred and body-centred cubic structures, which have atomic volumes that are the same and are equal to that of copper, as a function of n, the number of valency electrons per atom. The curve has been obtained by numerical integration, according to equation (8), of the data given in curves (*a*) and (*b*), figure 1. For pure copper, for which $n = 1$, we find that the limiting surface of the Fermi distribution of electrons occurs almost exactly at the energy for which $N(E)$ is a maximum. This gives the result $\zeta = 6{\cdot}6$ volts.

§ 3. THE DETERMINATION OF THE α, β PHASE BOUNDARIES

For the determination of the α, β phase boundaries we only need the variation of the Fermi energy with n for values of n somewhat greater than unity. For this range it is possible, as we shall now show, to obtain simple approximate formulae for the Fermi energies in the α and β phases.

According to equations (6) and (7) for an electron : atom ratio n greater than $1{\cdot}25$, the density of states for either phase may be written

$$N(E) = \frac{4\pi}{\omega} \cdot \frac{4\pi m}{h^2} \left\{ k_0 - \left(1 - \frac{\omega}{2\pi}\right) \sqrt{\frac{2mE}{h^2}} \right\} \qquad \ldots\ldots(9),$$

where ω and k_0 are given their values appropriate to either phase. This formula is only approximate since the term in curly brackets of formula (6) has been neglected. The error introduced, however, is so small as to be of no consequence for our purpose; see figures 1 (*a*) and 1 (*b*).

It can be seen from figure 1 that for a certain energy E_1 the number of states enclosed by this energy surface will be the same in both the α and the β phases. Let the number of states per atom bounded by the surface E_1 be n_0. Numerical integration shows that in the case considered $E_1 = 7{\cdot}23$ electron-volts and $n_0 = 1{\cdot}23$ electrons per atom. Formula (9) may still further be simplified if we write $E = E_1 + \epsilon$

and expand the square root for small values of ϵ. We may then write

$$\left.\begin{aligned} N_\alpha(E) &= N_1 - a\epsilon \\ N_\beta(E) &= N_2 - b\epsilon \end{aligned}\right\} \quad \text{......(10),}$$

where

$$a = 3\frac{4\pi m}{h^2}\sqrt{\frac{2m}{h^2 E_1}},$$

$$b = 5\frac{4\pi m}{h^2}\sqrt{\frac{2m}{h^2 E_1}},$$

and N_1 and N_2 are the values of $N(E)$ when the energy is E_1 in the α and β phases respectively. The numerical values of these quantities are as follows:

$N_1 = 0{\cdot}280$, $N_2 = 0{\cdot}346$ electrons per atom per volt; $a = 0{\cdot}0454$, $b = 0{\cdot}0757$ electrons per atom per (volt)^2.

Equations (8) and (10) determine the Fermi energies of the two phases as functions of the number of electrons per atom. We find

$$\left.\begin{aligned} U_\alpha(n) &= U_\alpha + E_1(n-n_0) - \frac{N_1^3}{3a^2} + \frac{N_1(n-n_0)}{a} + \frac{N_1^3}{3a^2}\left\{1 - \frac{2a(n-n_0)}{N_1^2}\right\}^{\frac{3}{2}} \\ U_\beta(n) &= U_\beta + E_1(n-n_0) - \frac{N_2^3}{3b^2} + \frac{N_2}{b}(n-n_0) + \frac{N_2^3}{3b^2}\left\{1 - \frac{2b(n-n_0)}{N_2^2}\right\}^{\frac{3}{2}} \end{aligned}\right\} \text{......(11).}$$

U_α and U_β are the energies of the α and β phases when there are n_0 electrons per atom in each. If v denotes the valency of the solute atoms and x denotes their concentration in the phase, the number of electrons per atom n is given by

$$n = (v-1)x + 1.$$

We introduce a variable ξ such that

$$\xi = (n-n_0) = (v-1)x + 1 - n_0 \quad \text{......(12).}$$

The equations which determine the limits of the α and β phase boundaries at the absolute zero may be written

$$\left.\begin{aligned} \frac{dU_\alpha(\xi_\alpha)}{d\xi_\alpha} &= \frac{dU_\beta(\xi_\beta)}{d\xi_\beta} \\ U_\alpha(\xi_\alpha) - \xi_\alpha\frac{dU_\alpha(\xi_\alpha)}{d\xi_\alpha} &= U_\beta(\xi_\beta) - \xi_\beta\frac{dU_\beta(\xi_\beta)}{d\xi_\beta} \end{aligned}\right\} \quad \text{......(13);}$$

compare equation (4) of part 1. From equations (11) and (12) we obtain easily, by substituting in (13), the following values for ξ_α and ξ_β:

$$\xi_\alpha = N_1 z - \tfrac{1}{2}az^2,$$

$$\xi_\beta = N_2 z - \tfrac{1}{2}bz^2,$$

where z is the root of the equation

$$z^3 - 3\left(\frac{N_2 - N_1}{b-a}\right)z^2 + \frac{6(U_\beta - U_\alpha)}{b-a} = 0 \quad \text{......(14).}$$

From figure 1 (*c*) we find that for $n = n_0 = 1{\cdot}23$, $U_\beta - U_\alpha = 0{\cdot}0135$ electron-volt, and with the numerical values already given we find, for the solution of equation (14),

$z=0{\cdot}675$ and therefore $\xi_\alpha=0{\cdot}179$ and $\xi_\beta=0{\cdot}217$. Thus since $\xi_\alpha=(n_\alpha-n_0)$ and $\xi_\beta=(n_\beta-n_0)$ we find, for the corresponding values of the electron concentrations, $n_\alpha=1{\cdot}409$ and $n_\beta=1{\cdot}447$.

§ 4. THE VARIATION OF THE α, β PHASE BOUNDARIES WITH TEMPERATURE

To determine ξ_α and ξ_β when $T>0$ we first expand the energies $U_\alpha(\xi_\alpha)$ and $U_\beta(\xi_\beta)$ about the values $\xi_\alpha(0)$ and $\xi_\beta(0)$ which correspond to $T=0$. We write

$$\xi_\alpha(T)=\xi_\alpha(0)+p,$$
$$\xi_\beta(T)=\xi_\beta(0)+q,$$

and treating p and q as small quantities we obtain

$$\frac{dU_\alpha}{dx_\alpha}-\frac{dU_\beta}{dx_\beta}=(v-1)\left\{\frac{q}{N_2-bz_0}-\frac{p}{N_1-az_0}\right\},$$

$$U_\alpha-x_\alpha\frac{dU_\alpha}{dx_\alpha}-U_\beta+x_\beta\frac{dU_\beta}{dx_\beta}=(v-1)\left\{\frac{x_\alpha^{(0)}\,p}{N_1-az_0}-\frac{x_\beta^{(0)}\,q}{N_2-bz_0}\right\},$$

where $x_\alpha^{(0)}$ and $x_\beta^{(0)}$ are the values of the concentrations x_α and x_β at $T=0$. Similarly we have

$$\log\frac{x_\alpha(1-x_\beta)}{x_\beta(1-x_\alpha)}=\log\frac{x_\alpha^{(0)}(1-x_\beta^{(0)})}{x_\beta^{(0)}(1-x_\alpha^{(0)})}+\frac{1}{(v-1)}\left\{\frac{p}{x_\alpha^{(0)}(1-x_\alpha^{(0)})}-\frac{q}{x_\beta^{(0)}(1-x_\beta^{(0)})}\right\},$$

$$\log\frac{1-x_\beta}{1-x_\alpha}=\log\frac{1-x_\beta^{(0)}}{1-x_\alpha^{(0)}}+\frac{1}{(v-1)}\left\{\frac{p}{1-x_\alpha^{(0)}}-\frac{q}{1-x_\beta^{(0)}}\right\}.$$

We have already said that when applying equations (4) of part 1 we assume that the specific heat within a single phase does not change appreciably with composition (cf. § 3). For the present purpose of finding the variation of the α, β limits with temperature we shall assume also that $f_\alpha(x_\alpha T)-f_\beta(x_\beta T)$ may be replaced with sufficient approximation in equation (4) by $U_\alpha(x_\alpha)-U_\beta(x_\beta)$. This approximation will of course be better for low than for high temperatures. The equations for p and q as functions of T are therefore as follows:

$$\left\{\frac{1}{(v-1)(1-x_\alpha^{(0)})}+\frac{(v-1)\,x_\alpha^{(0)}}{kT(N_1-az_0)}\right\}p-\left\{\frac{1}{(v-1)(1-x_\beta^{(0)})}-\frac{(v-1)\,x_\beta^{(0)}}{kT(N_2-bz_0)}\right\}q$$
$$=\log\left(\frac{1-x_\alpha^{(0)}}{1-x_\beta^{(0)}}\right),$$

$$\left\{\frac{1}{(v-1)(1-x_\alpha^{(0)})\,x_\alpha^{(0)}}-\frac{(v-1)}{kT(N_1-az_0)}\right\}p-\left\{\frac{1}{(v-1)(1-x_\beta^{(0)})\,x_\beta^{(0)}}-\frac{(v-1)}{kT(N_2-bz_0)}\right\}q$$
$$=\log\frac{x_\beta^{(0)}(1-x_\alpha^{(0)})}{x_\alpha^{(0)}(1-x_\beta^{(0)})}.$$

The values of the coefficients in these equations have all been given, and therefore p and q can be found as functions of T. Figure 2 shows the results obtained in this way.

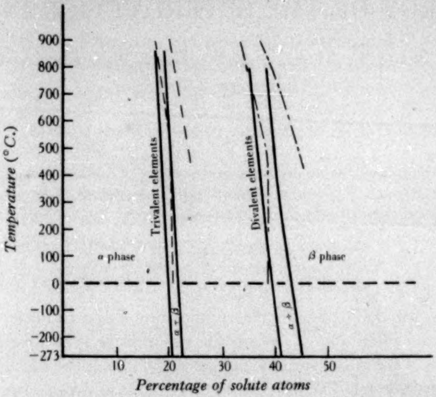

Fig. 2. Phase diagram showing the α, β boundaries. — Theoretical curve for copper. --- Observed lines for aluminium in copper. -·- Observed lines for zinc in copper.

REFERENCES

(1) Fuchs. *Proc. roy. Soc.* **151**, 585 (1935).
(2) Mott and Jones. *The Theory of the Properties of Metals and Alloys*, pp. 83, 118, 147. Clarendon Press (1936).

THE ENERGY OF THE SUPERLATTICE IN β BRASS

BY N. F. MOTT, M.A., F.R.S., H. H. Wills Physical Laboratory,
University of Bristol

Communicated by Prof. A. M. Tyndall, 16 *December* 1936. *Read* 12 *March* 1937

ABSTRACT. An estimate, based on the electron theory of metals, is made of the energy of the superlattice in β brass. The results obtained agree, as regards their order of magnitude, with those for the energy absorbed in the transition from the ordered to the disordered state.

---

§ 1. ELECTROSTATIC ENERGY OF THE SUPERLATTICE

THE body-centred alloy having the composition CuZn (β brass) forms a superlattice below about 460° C. When the superlattice is complete, the atoms at the centres of the cubes are, say, copper and those at the corners zinc, and the alloy is said to be ordered. The purpose of this note is to deduce from the theory of metals an estimate of the energy required to destroy the superlattice, and hence of the heat absorbed in the transition from the ordered to the disordered state.

The copper ion is larger than the zinc ion;* in the ordered state no two copper ions are in contact, but in the disordered state there will be N pairs of copper ions in a crystal containing N atoms (i.e. $\frac{1}{2}N$ copper and $\frac{1}{2}N$ zinc atoms). The repulsive exchange interaction between the ions will therefore hinder the formation of the disordered state. Since, however, Jones(10) has shown that the phase diagram of these alloys is not appreciably influenced by the exchange repulsion between the ions, we should not expect the ion-ion interaction to be very important. An estimate of it will be made in § 2.

We believe the most important force favouring the formation of the superlattice to be polar in origin. Each copper atom contributes one electron and each zinc atom two electrons to the number of conduction electrons in the alloy. If the charge-density due to the conduction electrons in the alloy were uniform, then the atomic polyhedron† surrounding each zinc ion would contain a positive charge $+\frac{1}{2}e$, and that surrounding each copper ion a charge $-\frac{1}{2}e$. The energy attending the formation of the superlattice would then be about twenty times greater than that observed. We must deduce that the conduction electrons tend to cluster about the zinc ions; the charge-density is greater in their neighbourhood than in that of the copper ions.

This clustering has already been estimated for *dilute* solutions of zinc in copper by the present author in a paper(2) on the electric resistance of dilute solid solutions. It was assumed that when a zinc atom is added to copper the field round the copper

* The radii given by Grimm and Wolff(1) are, 0·96 A. for Cu^+ and 0·74 A. for Zn^{++}.
† This is defined below.

is altered in such a way that the electrostatic potential near the zinc atom is greater than that near a copper atom by an amount

$$\Phi = \frac{e}{r} \exp(-qr) \qquad \text{......(1)},$$

Φ is then the difference between the potential in the actual lattice and that in a lattice of pure copper. The increase in the resistivity of copper due to the addition of zinc is then due to the perturbing potential Φ. That due to 1 atomic per cent of zinc was shown to be

$$\Delta\rho = \frac{1}{100} \frac{2\pi e^2}{mv^3} \left\{ \log\left(1 + \frac{1}{y}\right) - \frac{1}{1+y} \right\} \qquad \text{......(2)},$$

where $y = q^2 \hbar^2 / 4m^2 v^2$.

In these equations v is the maximum velocity of the electrons in metallic copper; this may be calculated(3) to be $1{\cdot}57 \times 10^8$ cm./sec. From the observed(4) value of $\Delta\rho$, viz. 0·335 $\mu\Omega$./cm., we may calculate the screening-constant q and obtain

$$1/q = 0{\cdot}37 \text{ A.}$$

Formula (2) depends on the assumption that the effective number of free electrons in metallic copper is one per atom; this may introduce some error into our estimate of q.

In the paper quoted, the Thomas-Fermi method was applied to the electrons in a metal and it was shown that the extra potential Φ satisfied the equation

$$\nabla^2 \Phi = q^2 \Phi \qquad \text{......(3)},$$

and a theoretical expression(3) of the right order of magnitude was found for q. Since, however, the electron-density in metals is not great enough for the Thomas-Fermi method to be very accurate, in this paper we shall use the experimental value of q given above.

We now consider the CuZn alloy in either the ordered or the disordered state. Following Wigner and Seitz(3) we divide up the lattice into polyhedra all of the same size, one surrounding each atom. These we call the atomic polyhedra. Then the polyhedron surrounding a zinc atom will be positively charged and that surrounding a copper atom negatively charged. We denote by $\pm\,\Delta Q$ the charge on either polyhedron.

As Wigner and Seitz have shown, the polyhedra are very symmetrical, and to estimate the field outside them we may replace them by spheres of the same volume. It follows that the total energy of these charges in the disordered state is zero, but in the ordered state it is, per *atom*

$$-\frac{1}{2} \frac{\alpha}{a} (\Delta Q)^2 \qquad \text{......(4)},$$

where a is the lattice constant(5) (2·949 A.)* for CuZn, and α is the Madelung number for the body-centred structure, so that

$$\alpha = 2{\cdot}0354\ldots.$$

---

* For an alloy containing 50·1 per cent Cu.

We have now to obtain ΔQ. We may consider the copper-zinc lattice as a periodic lattice of which each ion has a charge $\frac{3}{2}e$, together with an additional charge $\pm\frac{1}{2}e$ on each copper or zinc ion. The potential due to these additional charges and to the clustering of the conduction electrons that they produce is the extra potential Φ which satisfies equation (3). In the ordered lattice Φ satisfies the boundary conditions

$$\begin{aligned}\Phi &\fallingdotseq \pm\tfrac{1}{2}e/r \qquad (r\to 0)\\ &=0 \text{ at the boundary of each polyhedron.}\end{aligned}$$

As before we replace each polyhedron by a sphere of radius r_0 such that $(4\pi/3)\,r_0^3$ is the atomic volume. The solution of equation (3) is then

$$\Phi=\pm\tfrac{1}{2}e\left[\frac{\exp\{-q\,(r-r_0)\}-\exp\{q\,(r-r_0)\}}{\exp(qr_0)-\exp(-qr_0)}\right].$$

We obtain the extra charge on each polyhedron from Gauss's theorem

$$\begin{aligned}\Delta Q&=\frac{1}{4\pi}\int\frac{\partial\Phi}{\partial n}\,dS\\ &=\pm e\,\frac{qr_0}{\exp(qr_0)-\exp(-qr_0)}.\end{aligned}$$

With r_0 equal to 1·46 A., and the above value of q, this gives us

$$\Delta Q=\pm 0{\cdot}075\,e,$$

and for the binding energy of the ordered state

$$W=-0{\cdot}027 \text{ eV. per atom.}$$

In view of our assumption that the screening constant q is the same for CuZn as for copper no significance can be attached to the exact value obtained, but the order of magnitude should be correct.

§ 2. EXCHANGE INTERACTION BETWEEN THE IONS

We assume that the energy per ion pair in copper is given by

$$w\,(r)=\lambda e^{-r/\sigma},$$

where r is the interatomic distance.

We then deduce λ and σ from the observed elastic constants of copper at low temperatures, namely*

$$\begin{aligned}c_{11}-c_{12}&=5{\cdot}21\times 10^{11}\text{ dyne/cm}^2\\ c_{44}&=8{\cdot}14\times 10^{11}\text{ dyne/cm}^2\end{aligned}$$

From these we subtract estimates of the terms due to the interaction between the ions and the valence electrons as calculated by Fuchs (6), namely 0·57 for $c_{11}-c_{12}$ and 1·89 for c_{44}. The value assumed for c_{44} differs slightly from that assumed by Fuchs because we have taken the ratio between the two quantities equal to that observed by

---

* For the definitions of these quantities, see for instance reference (3), p. 148.

Bender⁽⁷⁾ for sodium. We thus have for that part of the interaction which is due to the exchange repulsion between the ions

$$c_{11}-c_{12}=4\cdot64\times10^{11}\text{ dyne/cm}^2$$
$$c_{44}=6\cdot25\times10^{11}\text{ dyne/cm}^2$$

λ and σ were then deduced from formulae due to Fuchs.* We obtained

$$w(r)=3\cdot22\times10^{-2}\exp\left\{-\frac{r}{0\cdot138\times10^{-8}}+18\cdot53\right\}\text{ eV.}$$

Taking for r the observed interatomic distance (2·09 A) for CuZn, this gives

$$w(r)=0\cdot0127\text{ eV.}$$

As we have seen, this is equal to the energy of the superlattice per atom.

Finally, therefore, for the energy per atom of the superlattice we have

Electrostatic energy	0·027 eV.
Energy due to exchange repulsion between ions	0·013 eV.
Total energy (calculated)	0·040 eV.

It is difficult to obtain an accurate estimate of the observed energy absorbed during the order-disorder change. According to the theory of Bragg and Williams⁽⁸⁾ the entropy change per atom is

$$\int dQ/T=k\log_e 2.$$

Assuming that the entropy change above the critical temperature T_c can be neglected, the left-hand side is somewhat greater than

$$\frac{1}{T_c}\int dQ.$$

Thus the heat evolved per atom is less than

$$kT_c\log_e 2.$$

If $T_c=730°$ K., this gives

Total energy (observed) $<0\cdot043$ eV. per atom.

§ 3. VARIATION OF DEGREE OF ORDER WITH TEMPERATURE

Finally we must enquire whether the assumptions made by Bethe⁽⁹⁾ in calculating the degree of order at any given temperature are correct. Bethe assumes that the work done when a copper atom and a zinc atom change places depends only on the atoms in the lattice which are nearest neighbours to this pair.

For an ionic lattice such as NaCl Bethe's assumption would not be correct; if a kation and an anion were interchanged a dipole would be formed, and the extra potential due to it would fall off only as r^{-2}. These long-range forces cannot however exist in a conductor; in β brass, if a pair of copper and zinc atoms change places the conduction electrons will rearrange themselves round the dipole so formed in such a way as to screen it.

---

* Cf. reference (3), chapter IV, equation (22).

According to equation (3) the potential round a dipole of strength μ will be

$$\frac{\mu \cos \theta}{r^2} e^{-qr}.$$

The term e^{-qr} falls off so rapidly that it is probably correct to assume that the interaction between all but nearest neighbours can be neglected.

On the other hand it is probably not true that the interaction energy between a copper atom and a zinc atom is independent of the degree of order of their neighbours. We have derived the excess charge ΔQ on each atomic polyhedron on the assumption that a copper atom is completely surrounded by zinc atoms and *vice versa*. If, on the other hand, a copper atom is completely surrounded by copper atoms, the charge on its atomic polyhedron will not differ appreciably from zero, because the field due to the copper-zinc boundary falls off as e^{-qr}, so that the atom will not know that it is not in a block of metallic copper. In the intermediate case of a copper or zinc atom in the disordered lattice, with nearest neighbours of both kinds, we should expect the excess charge to be numerically smaller than in the ordered state.

The interaction between neighbouring atoms will therefore decrease as the disorder increases.

In the transition from order to disorder the energy absorbed in the later stages, compared with that absorbed in the earlier stages, is thus less than Bethe's theory indicates. It follows that if the degree of order S is plotted against temperature, S will drop to zero more sharply than in Bethe's theory. This may well be the explanation of the observed fact that the specific-heat bump associated with the transition in β brass is much sharper* than the theory leads one to expect.

---

* Cf. reference (3), figures 14 and 15.

REFERENCES

(1) Grimm and Wolff. *Handb. Phys.* **24** (2), 933 (1933).
(2) Mott. *Proc. Camb. phil. Soc.* **32**, 282 (1936).
(3) Mott and Jones. *The Theory of the Properties of Metals and Alloys* (1936).
(4) Linde. *Ann. Phys.*, Lpz., **10**, 52 (1931).
(5) Owen and Pickup. *Proc. roy. Soc.* A, **140**, 179 (1933).
(6) Fuchs. *Proc. roy. Soc.* A, **153**, 622 (1936).
(7) Bender. *Naturwissenschaften* (in the Press).
(8) Bragg and Williams. *Proc. roy. Soc.* A, **145**, 699 (1934).
(9) Bethe, *Proc. roy. Soc.* A, **150**, 552 (1935).
(10) Jones, page 243 of this volume.

DISCUSSION

Mr BUCKNALL. Although the constitution of a very large number of alloy systems has been determined[*] and metallurgists generally realize the significance of equilibrium diagrams, no one yet understands them in the sense of being able to predict the constitution of unexplored systems of alloys. At present the metallurgist who conducts an argument regarding alloy-constitution must constantly refer to original papers, or perform prodigious feats of memory, and therefore he looks forward eagerly to the time when a sound generalized theory of alloys will have been developed by the application of wave-mechanical considerations to alloys. It is recognized that simplifications are essential in the development of such a theory, but there is a real danger that over-simplification may lead to an unfavorable reception of the generalizations advanced. The sentence with which part 1 of Mr Jones's paper[†] opens would be regarded by many as a dangerous half-truth, as it is only in the alloys of silver and copper that the electron-concentration principle of solid solubility is clearly apparent; as I have pointed out[‡], the solutions of the other metals in aluminium, magnesium, nickel, cobalt and iron do not accord with this rule. Again, elements of the same valency and not greatly differing atomic volume, such as silver and copper, do not always show complete solid miscibility, so that some factor other than electron-concentration is clearly important.

With regard to deviations from the ordinary laws of solution, it is interesting to note that while copper alloys generally exhibit these effects according to Hume-Rothery,[§] recent German work on the solid solubility of tin in copper has shown the normal relation between concentration and temperature. The interstitial type of solid solution, for instance that of carbon in γ iron, warrants immediate attention by workers in this field.

[*] See M. Hansen, *Der Aufbau der Zweistofflegierungen.*

[†] Page 243 of this volume.

[‡] *Metal Industry*, **48**, 305 (1936).

[§] Haase and Pawlek, *Z. Metallkunde*, **18**, 73 (1936).

THE DIVISION OF PRIMARY ELECTRON CURRENT BETWEEN GRID AND ANODE OF A TRIODE

By D. M. MYERS

Communicated by I. O. Griffith, 24 *July* 1936. *Read in title* 26 *February* 1937

ABSTRACT. The paper describes a method of determining the distribution, between the grid and anode, of the current emitted by the cathode of a cylindrical triode. Measurements of the temperature of the anode are used to verify that this distribution depends on the ratio of the potentials applied to the anode and grid, and not on their absolute values. A direct method is then described in which the grid and anode currents are measured in conditions such that there is no flow of secondary current; by this means, the distribution of primary current from the cathode, and the value of any secondary current flowing between the anode and grid, can be deduced in any conditions of operation. Curves are obtained by the former method, showing the variation with impact energy of the secondary-emission ratio for both nickel and molybdenum anodes.

The effect of the anode-potential : grid-potential ratio on the distribution of primary current is determined for a particular triode, and an empirical relation is shown to hold for a considerable range of potential-ratios. This relation is of the same form for any cylindrical triode, but no general relation, applicable to any cylindrical triode, has yet been found.

§ 1. INTRODUCTION

If a thermionic tube has two collecting electrodes, the current emitted from the cathode will be shared between them in some manner depending on their potentials. Direct measurement of the current stream to each does not necessarily give the distribution of the electrons emitted by the cathode, because in general a secondary stream emitted by the electrode of lower potential will be collected by the other cold electrode.

The problem of calculating the partition of the stream is too complex to solve analytically, although it has been stated(1) that it can be shown theoretically that the stream divides in a ratio which depends on the ratio of the potentials of the two electrodes and not on the absolute magnitude of these potentials. The object of the present work is to test this conclusion and to determine experimentally the manner in which the partition of the stream depends on the ratio of the two potentials.

The distribution of current can be examined by direct measurement if no appreciable secondary current flows between the electrodes, or alternatively by some method where the magnitude of the secondary current can be determined. The former condition obtains when the potential applied to at least one of the collecting electrodes is small, or when both collecting electrodes have the same potential.

In the case where a secondary current exists, two methods for determining its magnitude are described here. One of these depends on direct measurement of the currents but relies on extrapolation of a curve, so that it gives only an approximation. The other method requires direct measurement of the currents, combined with measurement of the temperature of one of the collecting electrodes. This method was used to verify that the partition of the current emitted by the cathode is a function only of the ratio of the applied potentials; moreover, this function was obtained experimentally over a limited range of the said ratio. The experiments using this method will be described first.

The temperature-rise of the anode was measured in terms of the e.m.f. produced by a thermocouple attached to it: the magnitude of this e.m.f. is termed the *temperature reading*. When the anode is subject to electronic bombardment its temperature is thereby raised above the temperature produced by radiation from the cathode. The additional thermocouple e.m.f. resulting from electronic bombardment is termed the *deflection*.

So far as the writer has been able to discover, the temperature-rise of the anode has not previously been used for inferring the magnitude of the primary electron stream incident on it. This part of the work is thus believed to be new, and the results give new information about the partition of the primary electron stream in a triode—a problem about which very little seems to be known.

§2. EXPERIMENTAL METHOD

A special triode valve was made, having a pure tungsten filament of V form, a thermojunction attached to the anode, and a grid furnished with a large radiating fin. The electromotive force of the thermocouple and the potential drop across the filament were measured by a potentiometer.

The temperature-rise of the anode is due to radiation from the filament, radiation from the grid and direct electronic bombardment. Since only the temperature-rise from bombardment is of interest, it is necessary to measure the other two components separately.

Thus a curve must be obtained relating the temperature-rise of the anode to the power dissipated in it. This calibration curve having been obtained, the total power received by the anode in any given circumstance of operation can be found from the observed temperature-rise. If the power received by heat-radiation, deduced from other calibrations, is subtracted from the total, the residuum is due to electronic bombardment. The primary stream to the anode can be deduced from this when the anode-potential is known. The main difficulty of the method is to obtain an accurate knowledge of the power received from heat-radiation: the calibration for this has to be built up from many steps, which will now be described in succession.

§3. POWER RECEIVED BY THE ANODE FROM HEAT RADIATED FROM THE CATHODE

A considerable fraction of the power received by the anode is due to radiation of heat from the cathode. In all measurements the tube is operated with a constant potential-difference across the filament, and hence to the first order the heat received from the cathode by the anode is independent of the current evaporated from the cathode and its distribution between the two electrodes. Figure 1 shows the observed relation between the e.m.f. of the thermocouple on the anode and the power input to the cathode in the condition when $V_a = V_g = 0$, and thus when the cathode is not evaporating a current. The graph in figure 1 is curved: partly because the radiation from the cathode is approximately proportional to the fourth power of its temperature and partly because the e.m.f. is not strictly proportional to temperature. Since the balance reading of the potentiometer used to indicate the thermocouple e.m.f. is a measure of the anode temperature, this reading will in future be called *the temperature reading*. If the cathode temperature were uniquely determined by the filament p.d., which is kept constant, then the relevant temperature reading when $V_a = V_g = 0$ could be taken as the effective zero temperature reading in all operating conditions. In practice this is substantially the case but not quite accurately so, because the evaporation of current by the cathode ipso facto causes the latter's temperature to fall. But this effect is partly counteracted, since a fall of temperature causes a corresponding decrease in resistance and hence an increase of power input at a constant filament p.d. Hence the effective zero temperature reading has to be corrected slightly, according to the value of the total current evaporated from the cathode. The method of making this small correction is as follows. Let χ_f be the work function of the cathode and J the current emitted by it at temperature T_f, and let R be its resistance, where $R = R_0(1 + \alpha T_f) \doteqdot \alpha R_0 T_f$. If the filament p.d. is V_f, then

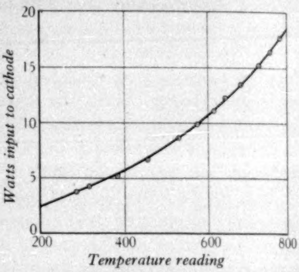

Figure 1. Calibration curve with zero heating of anode by electronic bombardment and by radiation from the grid zero.

$$W_f = \frac{V_f^2}{\alpha R_0 T_f} = kT_f^4 + \chi_f J,$$

where k is some constant, and W_f is the power input to the filament.

In operation W_f is approximately 20 W.: J does not exceed 30 mA., and hence if $\chi_f = 4{\cdot}5$ volts, $\chi_f J / W_f$ is never greater than $0{\cdot}67$ per cent.

The anode temperature T_A is a function of T_f, and hence the quantity which governs T_A is not W_f but kT_f^4, while

$$kT_f^4 \equiv W_1 = W_f - \chi_f J$$

$$= \frac{V_f^2}{\alpha R_0 T_f} - \chi_f J.$$

Now $$\frac{dW_1}{dT_f} = 4kT_f^3$$

and $$\frac{dW_1}{dJ} = -\frac{V_f^2}{\alpha R_0 T_f^2}\frac{dT_f}{dJ} - \chi_f,$$

and
$$\frac{dW_1}{dJ}=\frac{dW_1}{dT_f}\cdot\frac{dT_f}{dJ}=-4kT_f^3\left(\frac{dW_1}{dJ}+\chi_f\right)\frac{R_0\alpha T_f^2}{V_f^2}$$
$$=-4\left(\frac{dW_1}{dJ}+\chi_f\right),\text{ since }kT_f^4\gg\chi_f J.$$
$$\therefore\quad\frac{dW_1}{dJ}=-\frac{4}{5}\chi_f.$$

Let R_a stand for the temperature reading of the anode. Then
$$\frac{dR_a}{dJ}=\frac{dR_a}{dW_1}\cdot\frac{dW_1}{dJ}=-\frac{4}{5}\frac{\chi_f}{g}.$$

Hence
$$\Delta R_a=-\frac{4}{5}\frac{\chi_f}{g}J \qquad \text{......(1)},$$
where g is the gradient of the calibration curve, typified by figure 1.

To make clear the use of this correction, consider the following numerical example. Suppose that for some assigned value of V_f, the temperature reading is 700 when $V_a=V_g=0$ and that it is 720 when $J=10$ mA. Then the heating due to bombardment by 10 mA. is not determined by the quantity (720 − 700) but by
$$720-\left(700-\frac{4}{5}\frac{\chi_f}{g}J\right)=720-(700-0{\cdot}94)$$
$$\doteqdot 21,$$
if we assume that $\chi_f=4{\cdot}5$ and $g=38{\cdot}4$ mW./div., which is the relevant value of g in figure 1, when $R_a=700$.

§ 4. METHOD OF CORRECTING FOR VOLTAGE DROP ALONG THE FILAMENT

Since the filamentary cathode is not an equipotential surface, the p.d. between anode and filament depends on the point of the filament considered. If i is the current evaporated from some specified short length dx of filament, where the p.d. is v, then the work W done on the anode is given by
$$W=\int_0^l iv\,dx,$$
where the integration is along the length l of the filament. If J is the total anode current,
$$I=\int_0^l i\,dx.$$
W cannot be evaluated until i, equal to $f(x)$, and v, equal to $\phi(x)$ are known. If the emission is temperature limited, i is independent of x and then $W=I\left(V_a-\tfrac{1}{2}V_f\right)$. If the current is space-charge-limited and if the anode is long, then $i=kv^{\frac{3}{2}}$ and
$$v=V_a-\frac{x}{l}V_f.\text{*}$$

---

* Since the total current emitted was of the order of 30 mA. and the filament current 2 A., the voltage drop along the filament remains substantially linear and independent of emission.

Hence it can readily be shown, and is well known, that

$$I=\frac{2kl}{5V_f}\{V_a^{\frac{5}{2}}-(V_a-V_f)^{\frac{5}{2}}\}$$

and

$$W=k\int_0^l v^{\frac{5}{2}}\,dx=\frac{5}{7}IV_a\frac{1-(1-V_f/V_a)^{\frac{7}{2}}}{1-(1-V_f/V_a)^{\frac{5}{2}}}.$$

Hence V_a', the effective anode-potential, is given by

$$V_a'=\frac{5V_a}{7}\frac{1-(1-V_f/V_a)^{\frac{7}{2}}}{1-(1-V_f/V_a)^{\frac{5}{2}}}. \qquad \text{......(2).}$$

In these measurements V_f was 9 V.: hence it may be calculated, for example, that $V_a'=7{\cdot}1$ when $V_a=10$, and $V_a'=21$ when $V_a=25$. If and when temperature saturation occurs, $V_a'=V_a-4{\cdot}5$.

It should be understood that in future any numerical values quoted for anode potential are values of V_a' and not of V_a.

§ 5. EFFECT OF THE WORK FUNCTION OF THE RECEIVING ELECTRODES

If an electrode at effective potential V' receives an electron current I, then the work done on it is $W=J(V'+\chi)$, where χ is the work function of the surface. Similarly, if the same electrode emits a current I_s by secondary emission, the net work W will be given by

$$W=I(V'+\chi)-I_s\chi.$$

§ 6. THE RELATION BETWEEN THE TEMPERATURE OF AND THE TOTAL POWER INPUT TO THE ANODE

It is now necessary to obtain the calibration curve relating temperature reading with a known input power to the anode. This can be obtained by bombarding the anode, in the condition when $V_g=0$: for then there is no secondary emission from the anode and no additional heat radiated from the grid as a result of grid bombardment. Figure 2 is an experimental curve relating additional temperature reading, corrected for filament cooling, as described in § 3, with power received by the anode from bombardment. The input power is deduced from the relation

$$W=I(V'+\chi_a),$$

where I is the measured anode current, χ_a is the work function of the anode surface (taken as 4·5 volts), and V_a' has been defined previously. Hereinafter the additional temperature reading, as defined above, will be termed the *deflection*.

It must now be understood that figure 2 relates the deflection to the power received by the anode, otherwise than by radiation from the filament, whether this power is received solely by bombardment (the condition under which the curve is obtained) or partly by heat radiated from the grid (the condition that must occur in the operating condition where positive potentials are applied to both the anode and the grid so that the grid is being heated by primary bombardment from the cathode and possibly by secondary bombardment from the anode).

§7. THE RELATION BETWEEN DEFLECTION AND THE HEAT RADIATED FROM THE GRID

It is now necessary to obtain a calibration curve relating deflection with the power given to the grid by bombardment* in the condition when $V_a=0$, and hence when there is no anode-bombardment. Such a calibration curve is shown in figure 3. It will now be assumed that when the grid receives a certain power W_g from any source, then a constant fraction pW_g is radiated to the anode; this is equivalent to assuming that all radiation from the grid occurs at substantially the same temperature, namely the temperature of the grid wires. It must be understood that the ordinates in figure 3 have been adjusted for work function and effective grid voltage, in the manner previously described for the anode. Moreover, the deflection has been corrected for filament cooling.

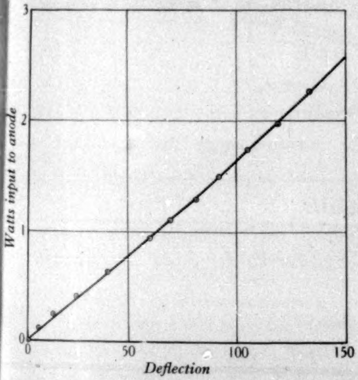

Figure 2. Calibration curve relating additional temperature-rise of anode, due to electronic bombardment, with watts input to anode. The heat-radiation from the grid is zero.

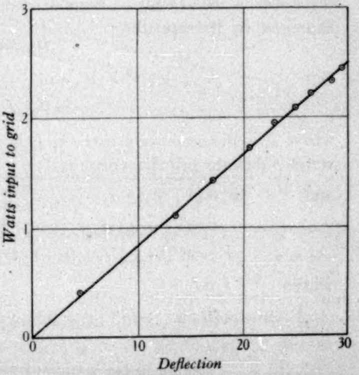

Figure 3. Calibration curve relating additional temperature-rise of anode, due to radiation from grid, with watts input to grid. The anode-bombardment is zero.

The factor p is derived from figures 2 and 3 as follows. When the grid input is W_g' the anode receives energy at the rate pW_g' and there results a deflection D_a' such that $D_a'=f(pW_g')$. Let the same deflection be obtained when the anode receives power W_a' from bombardment alone, so that $V_g=0$, as in figure 2. Then $D_a'=f(W_a')$.

Hence
$$p=\frac{W_a'}{W_g'}.$$

Since both figures 2 and 3 are substantially linear over the range covered by figure 3, it follows that p is equal to the ratio of the initial gradients of these two curves.

---

* Provision was made for leads to be taken from each of the two support wires of the grid, in order to supply heat to the grid directly instead of by bombardment. This method was not actually used, as it was found that there was considerable risk of damage to the pinch of the triode.

§8. THE METHOD OF DEDUCING THE PRIMARY ANODE CURRENT ${}_pI_a$

The previous sections have explained how the power input due to bombardment of the anode can be deduced when the power input to the grid is known. But if neither V_g nor V_a is zero and if V_g is not equal to V_a, the grid input cannot be deduced from the measured value of grid current because the grid is either receiving or emitting an unknown number of secondary electrons. Nevertheless, it is possible to obtain an expression, from which the primary anode current ${}_pI_a$ can be deduced from the measured temperature deflection and currents and the known correcting factors. The derivation of this expression will now be given. The conditions where V_g is greater than V_a and where V_g is less than V_a will be considered separately.

(*a*) *Grid-potential greater than anode-potential.* Let W_a be the power received by the anode as the result of bombardment: then the total power W it receives is expressed by the equation

$$W = W_a + pW_g \qquad \text{......(3).}$$

But

$$\begin{aligned} W_a &= (V_a' + \chi_a)\,{}_pI_a - \chi_a I_s \\ &= V_a'\,{}_pI_a + \chi_a I_a \qquad \text{......(4),} \end{aligned}$$

where I_s is the secondary current, I_a is the measured anode current, and the subscript p denotes primary currents,

and

$$\begin{aligned} W_g &= (V_g' + \chi_g)\,{}_pI_g + (V_g' - V_a' + \chi_g)\,I_s \\ &\equiv (nV_a' + \chi_g)\,{}_pI_g + \{(n-1)\,V_a' + \chi_g\}\,I_s, \quad \text{where} \quad V_g' = nV_a', \\ &= (nV_a' + \chi_g)\,J - \{(n-1)\,V_a' + \chi_g\}\,I_a - V_a'\,{}_pI_a \qquad \text{......(5),} \end{aligned}$$

where $J = I_a + I_g$.

From equations (3) and (4) it follows that

$${}_pI_a = \frac{W_a - \chi_a I_a}{V_a'} = \frac{W - pW_g - \chi_a I_a}{V_a'},$$

whence, in combination with (5), it follows that

$${}_pI_a = \frac{W - p\,(nV_a' + \chi_g)\,J + \{p\,(n-1)\,V_a' - (\chi_a - p\chi_g)\}\,I_a}{(1-p)\,V_a'} \qquad \text{......(6).}$$

Since W is known, by means of figure 2, from the measured temperature deflection, ${}_pI_a$ can now be deduced.

(*b*) *Grid-potential less than anode-potential.*

$$\begin{aligned} W_g &= (V_g' + \chi_g)\,{}_pI_g - \chi_g I_s \\ &= V_g'\,{}_pI_g + \chi_g I_g \qquad \text{......(7),} \end{aligned}$$

and

$$W_a = (V_a' + \chi_a)\,{}_pI_a + (V_a' - V_g' + \chi_a)\,I_s \qquad \text{......(8).}$$

Whence, proceeding as in section (*a*), we deduce that

$${}_pI_a = \frac{W - p\,(nV_a' + \chi_g)\,J + \{(n-1)\,V_a' - (\chi_a - p\chi_g)\}\,I_a}{n\,(1-p)\,V_a'} \qquad \text{......(9).}$$

§ 9. THE EFFECT OF THE RATIO V_g/V_a

When the two potentials are approximately equal, only a certain proportion of the secondary electrons emitted by the electrode of lower potential will be collected by the other. This is partly due to discontinuity of the grid, and probably partly due to space charge at the surface of the emitting electrode. In order to measure total emitted secondary current from one electrode it is necessary that the whole of this current should be collected by the other.

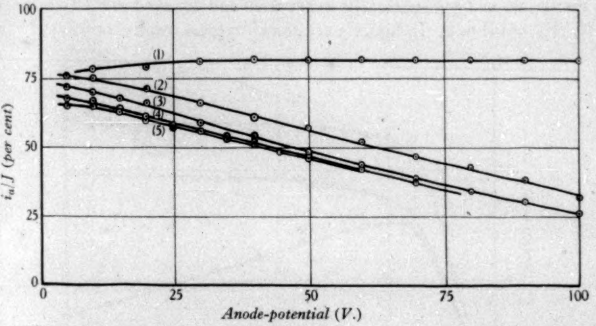

Figure 4. Curves relating I_a/J with V_a when V_g/V_a is maintained constant at five stated values. Curve (1), $V_g/V_a=1\cdot0$; (2), $V_g/V_a=1\cdot5$; (3), $V_g/V_a=2\cdot0$; (4), $V_g/V_a=3\cdot0$; (5), $V_g/V_a=4\cdot0$.

The family of curves in figure 4 shows the observed relation between I_a/J and V_a, in the triode constructed for these measurements, for the values of n, defined as V_g/V_a, specified in the figure. When $n=1$ there is no secondary electron flow and I_a/J is independent of V_a. If n is greater than 1 the anode emits a secondary current, and then I_a/J is a function of V_a. The figure shows that if n exceeds about 2·5, then the members of the family differ only slightly from one another: thus, provided n exceeds about 2·5, the grid collects all the secondary electrons which can be emitted from the anode. Considerations of grid heating have in fact made it desirable to make n equal to 2 in measurements of secondary emission from the anode: the appropriate choice of n must depend on the particular triode in use.

§ 10. EXPERIMENTAL RESULTS

The first series of results was obtained from two special triodes made to the following specification by the British Thomson-Houston Co. Ltd.

Filament. Plain tungsten wire 0·005 in. in diameter, disposed in **V**-form and of total length 3·25 in.

Grid. Helix of molybdenum wire, 0·008 in. in diameter, wound with 10 turns per inch on a mandrel 0·25 in. in diameter: length of helix, 1·75 in.; 2 nickel support wires, 0·030 in. in diameter. The grid was also furnished with a blackened metal radiator, fixed to it at the end remote from the pinch.

Anode: *Triode A*. Nickel anode, ⅝ in. in diameter, 1¾ in. long. *Triode B*. Molybdenum anode, ⅞ in. in diameter, 1¾ in. long. The anode of either valve had a substantial metal strip welded along a generator of the cylinder; to the middle of this strip was attached a thermojunction.

Thermojunction. Copper, 0·004 in. in diameter, eureka, 0·0032 in. in diameter.

The procedure was to record the temperature reading and the relevant currents when the anode- and grid-potentials were varied and adjusted in such a manner as to keep V_g'/V_a' equal to 2. In figure 5 are shown typical results for valve A. In this, curve 1 relates the total emission J to V_a: curve 2 relates the measured anode current I_a to V_a: curve 3 relates V_a to the values of ${}_pI_a$ deduced from the temperature readings. Figures 1, 2, 3 and 4 pertain to triode A, operated with the same filament-potential as that used in the tests graphed in figure 5.

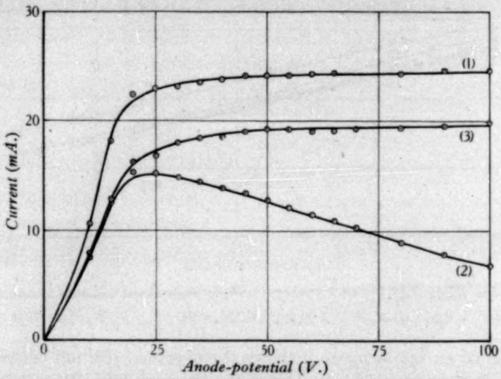

Figure 5. Curves for valve A relating emission current (1), anode current (2) and primary anode current (3)*, with V_a when V_g/V_a is maintained constant and equal to 2.

Figure 6 shows the corresponding curves for triode B. In figure 7 is plotted the emission ratio $I_s/{}_pI_a$ as a function of V_a' for both triodes. Considerable difficulty was encountered in taking the necessary temperature readings in the case of triode B, owing to a slight fault in the arrangement of the thermojunction leads. As a result the readings had to be taken very quickly and it was impossible to maintain a constant total emission. Some more triodes, in which this fault will be remedied, are being constructed.

Results obtained by Barber(2) show that the secondary-emission ratio is affected by temperature, an increase in temperature of the emitting surface causing a decrease in the emission ratio. In the foregoing experiments, where comparatively low voltages and currents were used, the rise in temperature of the anode during a set of readings was small, being less than 25 per cent of that due to radiation from the cathode. For this reason the effect of temperature on secondary emission has been ignored.

---

* See the appendix, page 278.

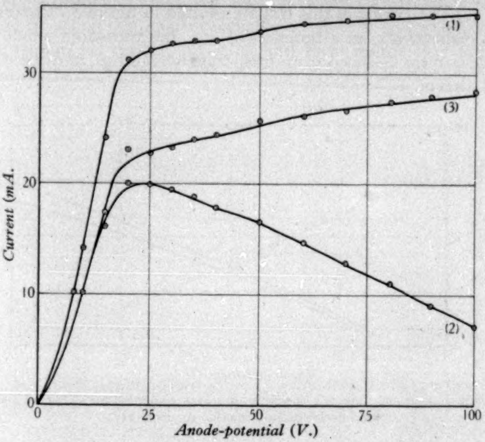

Figure 6. Curves for valve *B* corresponding to figure 5.

§ 11. THE ACCURACY OF THE MEASUREMENTS

As an experimental check on the accuracy of the procedure a similar set of readings was taken, triode A being used under the condition that $V_g = V_a$. In this case there is no appreciable flow of secondary electrons between the anode and grid, and so the total power input to the anode may be evaluated from a knowledge of the measured currents. The table gives comparative results as calculated from the current readings and from the temperature readings.

V_a (and V_g)	I_a	I_g	D	Anode power, from current readings (W.)	Anode power, from temperature readings (W.)
20	12·35	3·25	22	0·33	0·32
40	22·3	5·15	67	1·06	1·04
60	23·2	5·15	96·5	1·58	1·55
80	23·6	5·2	123	2·07	2·07
90	23·9	5·2	136·5	2·32	2·34
100	23·9	5·2	148	2·55	2·59
110	24·1	5·25	162	2·85	2·86

These results indicate that the maximum error is of the order of 2 per cent except when small deflections are to be measured.

§ 12. THE CHARACTERISTIC OF THE DYNATRON

A set of readings was also obtained in the condition pertaining to a dynatron characteristic, i.e. but V_g' is constant. In this case triode A was used, with V_g' equal to 100 V. The results of this test are plotted in figure 8. Curves (1), (2) and (3) represent respectively, as a function of V_a', the measured anode current, the primary anode current deduced from temperature readings, and the corresponding primary grid current.

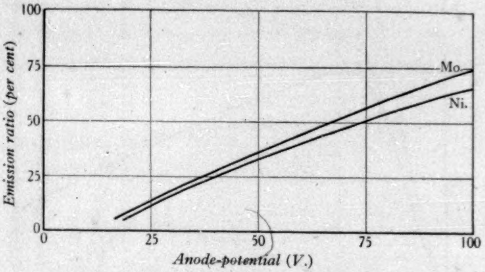

Figure 7. Secondary-emission ratio as a function of anode-potential for valves *A* and *B* with nicke and molybdenum anodes respectively.

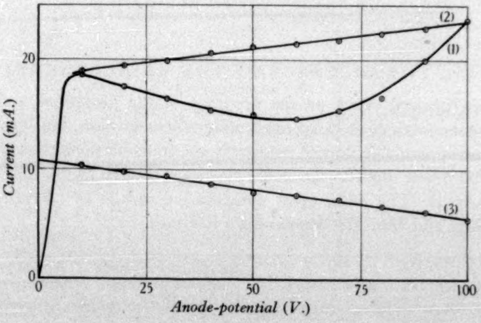

Figure 8. Dynatron characteristic of valve *A* when $V_g = 100$ V. (1) measured anode current; (2) deduced primary anode current; (3) primary grid current.

The difference between curves (1) and (2) gives the secondary current passing to the grid. In figure 9 the secondary current is plotted as a function of V_a', and in the same figure is a curve, deduced from figure 7 and curve (2) of figure 8, showing the secondary current emitted from the anode. It can be seen that when V_a' exceeds 50 V. some of the secondary electrons are returned to the anode, an effect which had been anticipated (see § 9).

§ 13. SECONDARY EMISSION FROM THE GRID

The theory can be extended to the case where the anode collects secondary electrons emitted by the grid. In this case much greater accuracy of measurement and stability of conditions are required, and no satisfactory readings have yet been taken. In order to obtain results of reasonable accuracy it will be necessary to use a more efficient system for cooling the grid, and so to reduce the factor p without diminishing the ratio of primary grid current to primary anode current.

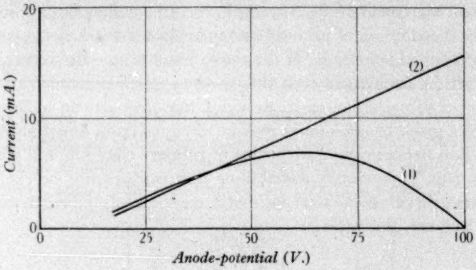

Figure 9. Secondary anode current (1) and secondary anode emission (2) as a function of V_a when $V_g = 100$ V.

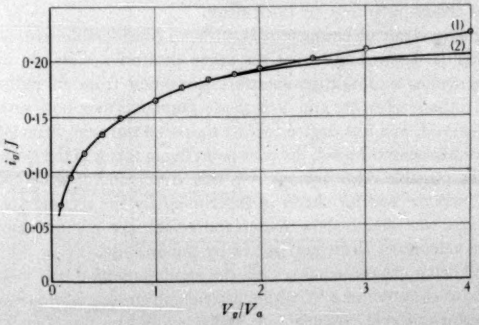

Figure 10. Curve obtained when the anode-potential is insufficient to permit secondary emission: $V_a = 4$ V.

§ 14. MEASUREMENTS IN THE ABSENCE OF SECONDARY CURRENT

A method has been described in the previous sections for examining the distribution of primary current between the anode and grid of a temperature-saturated triode, by making certain assumptions whose validity has been checked experimentally. The problem can be examined by a more direct method if it is assumed that the distribution of primary electrons depends only on the ratio of the potentials applied to the grid and the anode, and not on their absolute values. The results shown in figures 5, 6 etc. justify this assumption.(1) It is also necessary to assume that the emission of secondary electrons from the anode and grid will not affect the distribution of primary electrons.

It is known that, except from specially treated surfaces, secondary emission due to bombardment by electrons having an energy of less than 4 or 5 V. is negligible. If, therefore, the potential of either the grid or the anode is less than 4 or 5 V. there can be no flow of secondary current whatever the value of the other potential. Hence direct measurement of the currents in the grid and anode circuits is sufficient to indicate the distribution of primary current between those electrodes for a given ratio V_g/V_a of applied potentials. If the above assumptions are correct, the primary distribution will be unchanged even though the applied potentials are sufficient to cause the flow of secondary current, provided that they remain in the same ratio.

Hence, for a given triode, curves may be obtained from direct measurements to show the relation between the distribution of primary electrons and the ratio of the applied potentials. The primary distribution may conveniently be expressed as the ratio of primary grid current to total emitted current, i.e. ${}_pI_g/J$. When there is no flow of secondary current, this ratio

$$\frac{{}_pI_g}{J}=\frac{I_g}{J}.$$

Such an investigation must be carried out using very low emission from the cathode, this is necessary in order that temperature saturation may be obtained when the grid- and anode-potentials are both small.

If the cathode is not an equipotential surface a considerable error is introduced, since the potential applied to one of the other electrodes is always small. It was found impracticable to obtain temperature saturation from an indirectly heated oxide-coated cathode when the grid- and anode-potentials were both small. The same effect was observed, to a less degree, with a thoriated tungsten filament. Finally, a plain tungsten filament was used, the mid-point being taken as the zero of potential. In view of the possible error arising from this arrangement, a method, to be described later, was devised for checking experimentally the accuracy of the results. The same means was used to show that no appreciable error is introduced by ignoring the initial velocity of electrons emitted by the cathode.

In the following experimental results the anode-potential was maintained at a constant value of the order of 4 V., while the grid and anode currents were measured for various values of grid-potential. A similar procedure was then followed at a constant grid-potential.

A typical curve obtained in this way is shown in figure 10, curve (1), which relates to the triode A used in the temperature measurements.

In all the triodes examined, the curve was found to follow a relationship of the form

$$\frac{{}_pI_g}{J}=K\sqrt{\frac{V_g}{V_g+aV_a}},$$

within the range

$$0<\frac{V_g}{V_a}<1\cdot 5 \text{ or } 2.$$

Such an empirical curve is shown at (2) in figure 10. When V_g/V_a exceeds 2 V.

the empirical curve falls below the experimental, since it becomes asymptotic to the line ${}_{p}I_{g}/J=K$.

So far it has not been possible to relate the constants K and a with the various dimensions of the triode. However, it has been found that with a given form of grid the ratio ${}_{p}I_{g}/J$ is independent of anode-radius when $V_a=V_g$. Thus it appears that $K^2/(1+a)$ is independent of the anode-radius.

No modification has yet been found for the above equation to make it applicable over the complete range $0<V_g/V_a<\infty$. An approximate theoretical treatment has been attempted, but the differential equations deduced have proved insoluble except by means of tedious numerical approximations.

§ 15. EXPERIMENTAL CHECK

The error due to potential-drop in the cathode and initial energy of emission from it will be negligible if the potentials applied to the anode and grid are much greater than these quantities. The above experiment was therefore repeated with much higher potentials. The resulting curves clearly indicate the existence of a secondary current. Figure 11 shows the results of a test on a certain triode over the range where $V_a>V_g$; for curve (1) the grid-potential was 4 V. and for curves (2) and (3) it was 30 V. and 60 V. respectively. The curves differ according to the existence and magnitude of the secondary current, but all pass through the same point when $V_g/V_a=1$.

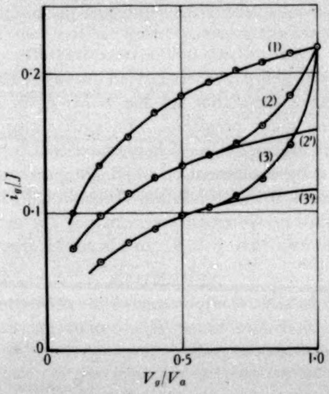

Figure 11. Secondary emission from grid: (1) $V_g=4$ V., (2) $V_g=30$ V., (3) $V_g=6$ V.

As V_g/V_a varies from 0 to 1, a point is reached in curves (2) and (3), where the anode fails to collect all secondary electrons emitted by the grid. This point is indicated approximately by a change in the direction of curvature. If each curve is extrapolated from this point, as shown in the figure, the new curves (2′) and (3′) indicate what the ratio I_g/J would be if all secondary electrons emitted by the grid were collected by the anode. Denote the ordinates of the extrapolated curve, in any particular case, by I_g'/J. Then clearly,

$$\frac{I_g'}{J}=\frac{{}_pI_g}{J}-\frac{I_s'}{J},$$

where I_s' is the maximum secondary current which can possibly be collected from the grid at the relevant potential. At a given potential, I_s'/I_g is a constant whatever the value of I_g, and is equal to the secondary emission ratio q of the surface. Hence

$$\frac{{}_pI_g}{J}=\frac{I_g}{J}\cdot\frac{1}{1-q}.$$

Thus the primary distribution curve can be obtained from the extrapolated curve by increasing the ordinates of the latter in the constant ratio $1:(1-q)$. One point on the primary distribution curve is known, namely the point where $V_g/V_a=1$; the corresponding point on the extrapolated curve is also known, and hence the required dividing factor $(1-q)$ can be determined.

If curves (2′) and (3′) are multiplied by their respective factors determined in this way, the resultant curves are sensibly coincident with curve (1). This has been found to apply for a wide range both of applied potentials and of emitted current. This agreement in the results verifies the validity of the assumptions in the previous method.

§ 16. ACKNOWLEDGEMENTS

The work described in this paper was carried out in the Engineering Laboratory, Oxford, and the thanks of the author are due to Mr E. B. Moullin, M.A., for his criticism and advice on many occasions. The author also wishes to express his indebtedness to Messrs Metropolitan-Vickers Electrical Co., Ltd., for the supply of the high-vacuum pumping equipment on which the preliminary experiments were performed, and to Messrs British Thomson-Houston Co., Ltd., who supplied the triodes on which the final measurements were made. The gratitude of the author is also due to Prof. E. V. Appleton, F.R.S., for his advice from time to time.

APPENDIX

Examples showing the relative importance of the corrections for points on curve (3) of figure 5. The correction factor $R_a=0·086$ (for filament-cooling), while $p=0·175$ (for radiation from the grid).

V_a	V_a'	V_g	V_g'	I_a	I_g	J	R_a	R_0*	R_a-R_0	Filament-cooling correction	D	${}_pI_a$	I_s	W_s
13·5	10	24·0	20	7·7	2·9	10·6	752	744·5	7·5	1	8·5	7·9	0·2	0·114
29·5	25	54·5	50	15·2	7·7	22·9	778	744	34	2	36	16·8	1·6	0·489
49·5	45	94·5	90	13·4	10·8	24·2	805	741	64	2	66	19·0	5·6	0·917
69·5	65	134·5	130	10·9	13·5	24·4	829·5	739	90·5	2	92·5	19·1	8·2	1·29
104·5	100	204·5	200	6·75	18·0	24·75	877	736	141	2	143	19·9	13·15	2·02

* The change in the zero temperature reading (i.e. when $V_a=V_g=0$) is due to a slight fault in construction of the valve, whereby the connexions between the thermocouple wires and the respective leading-in wires are not quite at the same temperature when power is absorbed by the grid.

REFERENCES

(1) Appleton, E. V. *Thermionic Vacuum Tubes*, p. 50 (Methuen, 1931).
(2) Barber, I. G. *Phys. Rev.*, March 1921, p. 335.

STRUCTURAL CHANGES DURING THE GROWTH OF METAL FILMS

By A. G. QUARRELL, Applied Physical Chemistry Laboratories, Imperial College of Science and Technology

Received 22 *January* 1937. *Read* 26 *February* 1937

ABSTRACT. Electron-diffraction patterns afforded by thin films of face-centred cubic metals prepared by evaporation, electrodeposition, chemical deposition and chemical displacement often show extra rings and bands which may be regarded as typical of the face-centred cubic structure rather than of the metal itself. It is shown that the extra rings are due to the fact that the first deposited layers crystallize in close-packed hexagonal crystals having an axial ratio c/a equal to 1·63, the effective atomic radius being the same as in the normal face-centred cubic form. Further, a gradual transition from close-packed hexagonal to face-centred cubic is postulated, and the prominent band is attributed to the progressive contraction of the (100) hexagonal spacing to the (200) cubic spacing during this transition. Certain very thin evaporated films yield structures intermediate between the hexagonal and cubic modifications, and from this it is inferred that the transition occurs gradually as deposition proceeds, and is not due to an atomic rearrangement occurring when a certain critical film-thickness is reached. These views are supported by the discovery of (i) an electrodeposited silver film consisting solely of close-packed hexagonal crystals, (ii) a similar gold specimen yielding a pattern in which the hexagonal and cubic diffractions are equally pronounced, and (iii) evaporated cobalt films consisting mainly of the hexagonal modification, together with a certain amount of the face-centred cubic form.

§ 1. INTRODUCTION

From time to time electron-diffraction effects have been observed which have not been explicable in terms of normal diffraction by the structure under examination, and the development of electron-diffraction as an established method for the investigation of thin films and surfaces has rendered imperative the elucidation of such diffraction effects.

Finch, Quarrell and Wilman⁽¹⁾ observed extra rings and bands in the transmission patterns afforded by metal films which had been heated in contact with oxygen. It was found that in all cases the spacings were dependent upon the structure of the metal, and that the extra diffractions could be removed by heating the specimen *in vacuo*, or more rapidly by heating in hydrogen. It was therefore suggested that they were caused by an interstitial solution of the gas in the metal lattice; the bands, in particular, being regarded as evidence of a gradual change in lattice-dimensions.

Further, Mark, Motz and Trillat⁽²⁾ found that traces of grease could yield sharp extra rings whose corresponding spacings were independent of the nature of the metal substrate, but were characteristic of the types of greases likely to be found as adventitious impurities in the laboratory. Such grease-ring systems are therefore easily recognized, as the pattern rings can be divided into those due to the metal and those characteristic of the grease.

More recently it was shown (3, 4) that amalgamation could give rise to extra-ring systems which, unlike the grease rings, had spacings dependent upon the metal and were therefore more easily confused with those due to gas-absorption. Aylmer, Finch and Fordham (5) examined a comprehensive series of amalgamated metal films, but whilst they were able to analyse three of the resulting structures they found that in general the amalgam ring systems were of such complexity as to render their identification uncertain; they therefore emphasized the importance of preparing and examining specimens prone to amalgamation in mercury-free apparatus.

Finally, Finch and Wilman (6, 7) observed extra rings, and also diffractions which were forbidden by normal structure-factor considerations, from thin single crystals and polycrystalline specimens of graphite and molybdenite. They showed that these new extra diffractions were not due to impurities, but were connected with the thinness of the specimens. They concluded that these extra and forbidden diffractions were due to the fact that whilst the crystals were virtually infinite in the cleavage-plane directions, the number of atom rows in the third dimension was so small that consecutive planes of a parallel group did not contain the same number of lattice points.

During the past two years further search has been made in this laboratory for possible sources of anomalous diffractions other than those outlined above. In addition to these, certain metal films have been found to give rise to sharply defined bands which are characterized by the fact that one head of each band coincides with a ring of the normal metal pattern, whilst the other consists of an extra ring. Such bands and their extra-ring heads cannot be explained on any of the views already discussed. Thus, since the spacings vary from metal to metal, these extra diffractions cannot be due to grease, whilst the possibility of gas-absorption or amalgamation being their true origin is ruled out because bands have been observed in the patterns obtained from specimens which were prepared and examined in the mercury-free high vacuum of a diffraction camera evacuated by oil-diffusion pumps. Nor can these bands be explained in terms of the limited-space-lattice theory put forward for graphite and other layer lattices by Finch and Wilman (6, 7), and we are forced to look for some other explanation. The object of this work was to elucidate this new source of extra diffractions.

§ 2. EXPERIMENTAL DETAILS

The diffraction camera employed was similar in its main design to those previously described (8, 9, 10). In view of the importance of eliminating the possibility of amalgamation of the specimens in the camera, the pumping-equipment consisted in the main of an oil-vapour diffusion pump backed by a two-stage mercury-vapour pump. Prolonged tests with gold-leaf specimens showed that the diffraction chamber was free from mercury.

The filament-heating attachment for preparing metal films by flashing in the evacuated electron-diffraction camera consisted of two long-reach gunmetal sparking-plugs soldered into a brass disc with a standard ground surface, figure 1, the necessary high-vacuum joints being ensured by sealing in the electrodes with picein. Terminals connected to the central electrodes of the plugs received the filament, which was therefore easily replaceable.

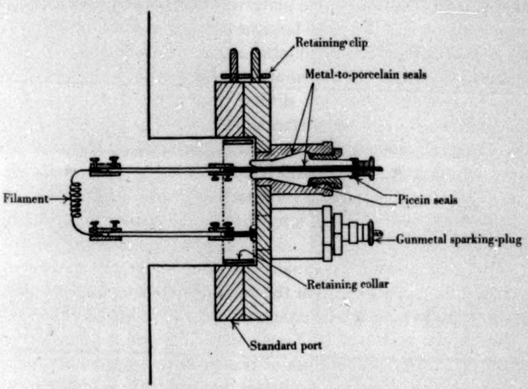

Figure 1. Evaporating assembly.

In view of the importance of avoiding amalgamation, gas-absorption and alloy-formation, specimens were initially prepared by evaporation in the evacuated electron-diffraction camera and the investigation was then extended to films prepared by electrodeposition, chemical displacement and chemical deposition. All transmission specimens were mounted on nickel gauze used as such or thickly electroplated with a deposit of the specimen metal, whilst the filaments used in preparing evaporated films either consisted of the pure metal to be deposited, or else of a tungsten wire so thickly electroplated with the metal that it was still completely coated after flashing. Owing to the slow rate of evaporation employed, the growth of the metal film and the corresponding changes in structure could be followed on the screen. Furthermore, the evaporation could be stopped at any desired stage, and a photographic record made of the diffraction pattern.

§ 3. RESULTS

Evaporated specimens. Specimens of cobalt, nickel, copper, platinum, palladium, gold and silver evaporated on to cellulosic substrates were examined, and in every case a well-defined band was observed extending from the 200 ring of the normal face-centred cubic structure of the metal to an extra ring just within the 111† diffraction. With nickel, copper, platinum, palladium, gold and silver the effect of gradual deposition of metal atoms by slow evaporation, as observed on the fluorescent screen, was as follows. The cellulose haloes gradually weakened and, just as they were becoming indistinguishable from the general background, a single very broad diffuse ring appeared in approximately the position of the normal 111 and 200 face-centred cubic diffractions. With further deposition this ring appeared to develop into a band on which were superimposed the 111 and 200 rings. Gradually the full face-centred cubic pattern, together with certain extra rings and the band, was built up and the rings became sharper and the background relatively less intense. Patterns recorded at suitable stages during deposition confirmed the visual observations, except that even in the early stages the first broad ring to appear was resolved into two very diffuse and almost overlapping rings. This apparent discrepancy is quite understandable in view of the poor resolving-power of the relatively coarse-grained fluorescent screen compared with that of the photographic plate. Not only was the typical band afforded by specimens which were so thin that they could only be seen in reflected light, but also it was obtained when evaporation had been carried on so long that the electrons could hardly penetrate the resulting thick film.

Cobalt. Whilst behaving in essentially the same manner as the rest of the metals examined, cobalt was peculiar in that the fully developed pattern included diffractions due to both the close-packed hexagonal and face-centred cubic modifications. Kersten(11) has shown by means of X-rays that electrodeposition at low *p*H values gives a deposit consisting of a mixture of the hexagonal and cubic forms, whilst at high *p*H values only the hexagonal β cobalt is deposited. It is our general experience with thin electrodeposited films of cobalt, prepared in a manner already described,(12) that the face-centred cubic structure most frequently occurs. Cobalt is interesting because in the hexagonal form, which is regarded as the stable form at low temperatures, the effective atomic radius is the same as in the face-centred cubic variety. Hence many spacings are common to both hexagonal and cubic structures as is shown in table 1, columns I, II and III, in which the spacings are expressed in terms of a, the side of unit cube of the face-centred cubic modification. The average ratios, d_{hkl}/a, obtained from four patterns, figure 2, of different cobalt specimens, the observed intensities, and the number of plates which afforded each diffraction are given in columns IV, V and VI respectively. It will be seen that the (100) hexagonal spacing coincides exactly with the observed inner band-head. Three rings of spacings $0{\cdot}707a$ (M. diff.),* $0{\cdot}524a$ (V.F.)* and $0{\cdot}340a$ (V.V.F.)* are yet to be explained, but it will be convenient to defer their discussion until later.

The observed intensities would suggest that the orientations are (110) and (001) for the cubic and hexagonal crystals respectively, i.e. the cube-face diagonals and hexagonal major axes fall within a cone of small angle about the normal to the

---

† *Notation.* In accordance with the convention explained by W. H. and W. L. Bragg on page 20 of *The Crystalline State* (Bell, 1933), indices (*hkl*) enclosed in brackets are Millerian indices denoting a plane, while indices *hkl* without brackets are Laue indices defining a diffraction. Thus if $h=nH$, $k=nK$, $l=nL$, *hkl* defines the diffraction of order *n* from the crystal plane (*HKL*).

Figure 2. Cobalt evaporated in vacuo.

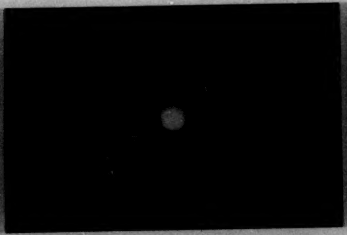

Figure 3. Silver evaporated in vacuo.

Figure 4. Evaporated copper (Rhombohedral).

Figure 5. Electrodeposited silver.

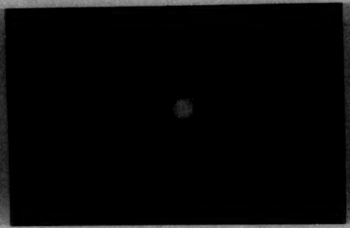

Figure 6. Electrodeposited gold.

Figure 7. Electrodeposited silver (close-packed hexagonal).

To face page 282

I

Clo
pac
hexa
c/a=

1
0
1

1
1

1
2
1
2
2
0
2
1

2
1

the
rat

V.

specimen plane. Owing to the superposition of the two patterns it is not possible to arrive at an estimate of the degree of imperfection of these orientations.

Other face-centred cubic metals. The average spacings and intensities for the diffractions observed in typical patterns, figure 3, yielded by three nickel, one copper, one platinum, one palladium, one gold and two silver specimens are given in columns VII and VIII of table 1. For convenience in comparing the results for metals of differing lattice constants, the spacings are expressed as before in terms of the side of unit cube. It will be seen that the patterns consisted of the normal face-centred cubic diffractions together with an extra ring coinciding with the inner band-head, and another between the 200 and 220 face-centred cubic diffractions. The spacings corresponding to these extra rings agree exactly with those of the 100 and 102 diffractions to be expected from a close-packed hexagonal structure of axial ratio c/a equal to 1·63, in which the effective atomic radius is the same as for the normal face-centred cubic metal. The orientation of the face-centred cubic crystals was strongly pronounced (110). With the thinnest films the crystal size was very small, and increased with increasing film-thickness.

Whilst the majority of the patterns yielded by evaporated films of face-centred

Table 1

Diffractions *hkl*		Theoretical d_{hkl}/a	Cobalt			Average values for other face-centred cubic metals	
Close-packed hexagonal $c/a=1·63$	Face-centred cubic		Mean d_{hkl}/a*	Observed intensity‡	Number of observations	Mean d_{hkl}/a*	Observed intensity‡
—	—	—	0·707	M.	2	—	—
100	—	0·613	[0·613	[M.S. †	4	[0·613	[M. †
002	111	0·577	0·575	V.S.	4	0·577	V.V.S.
101	—	0·541	0·539	S.	4	—	—
—	—	—	0·524	V.F.	1	—	—
—	200	0·500	0·500]	M.]	1	0·500]	M.S.]
102	—	0·420	0·422	F.M.Diff.	4	0·421	M.
110	220	0·353	0·354	S.	4	0·353	S.
—	—	—	0·340	V.V.F.	3	—	—
103	—	0·326	0·322	F.M.Diff.	4	—	—
200	—	0·306	—	—	—	—	—
112	311	0·301	0·302	V.S.	4	0·302	M.S.
201	—	0·296	0·296	V.V.F.	2	—	—
004	222	0·289	0·289	V.V.F.Diff.	1	0·288	M.
202	—	0·270	0·270	V.V.F.Diff.	3	—	—
104	—	0·261	—	—	—	—	—
—	400	0·250	—	—	—	0·249	F.M.
203	—	0·239	0·242	V.V.F.Diff.	4	—	—
120	—	0·231	—	—	—	—	—
—	331	0·229	0·229	M.	1	0·228	M.S.
121	—	0·227	0·226	M.S.	4	—	—
114	420	0·223	0·223	M.	1	0·223	F.M.
105	—	0·216	—	—	—	—	—

* The spacings for cobalt were referred to the most prominent face-centred cubic diffraction, and those for the other metals to the 200 face-centred cubic ring. The maximum divergence of individual values of spacing-ratios from the averages given in this and following tables was ±0·002.

† Square brackets denote the existence of a band.

‡ Throughout this paper the observed intensities are expressed in order of decreasing intensity as follows: V.V.S., V.S., S., M.S., M., F.M., F., V.F., and V.V.F., whilst "Diff." indicates that the diffraction was diffuse.

cubic metals afforded the spacing-ratios tabulated in column VII, the patterns from two platinum, one copper, one lead and two nickel specimens were found to correspond to a rhombohedral structure with interaxial angle rather larger than that of the fundamental unit cell of the face-centred cubic lattice. Thus the spacings obtained from the copper pattern, figure 4, differ considerably from those for a face-centred cubic structure, but agree closely with those to be expected from a rhombohedral structure with α equal to 62° 24′, as is shown in table 2. Since the pattern is not face-centred cubic, the spacings are not expressed in terms of the side of unit cube, but as fractions of the spacing corresponding to the first ring. It will be seen that the pattern, figure 4, bears a very marked resemblance to the normal pattern, figure 3, obtained from evaporated films, and includes the characteristic band between what at first sight would appear to be the 200 face-centred cubic ring and an extra ring at a spacing ratio of 1·069. If it be assumed that this inner band-head is due to the 100 hexagonal diffraction as before, then the lattice constants of the rhombohedral structure are $a_r = 2{\cdot}458$ A., $\alpha = 62°\ 24'$, whilst those for the rhombohedral unit cell corresponding to the copper face-centred cubic lattice are $a_r = 2{\cdot}545$ A., $\alpha = 60°$. Referred to hexagonal axes, the corresponding constants are $a_h = 2{\cdot}547$ A., $c/a = 2{\cdot}32$ and $a_h = 2{\cdot}545$ A., $c/a = 2{\cdot}45$, respectively, as compared with $a_h = 2{\cdot}545$ A., $c/a = 1{\cdot}63$ for a truly close-packed hexagonal arrangement of copper atoms. Similar agreement was found with the other rhombohedral structures, the axial ratios being $c/a = 2{\cdot}24$, 2·30 and 2·42, equivalent to interaxial angles $\alpha = 64°$, 62° 48′ and 60° 34′ respectively.

Table 2

Face-centred cubic indices	Theoretical spacing-ratios for face-centred cube	Observed spacing-ratios	Spacing-ratios for rhombohedral structure, $\alpha = 62°\ 24'$	Rhombohedral indices
111	1·000	1·000	1·000	100
200	0·866	0·855	0·855	110
220	0·612	0·590	0·594	$21\bar{3}$
311	0·522	0·499	0·500	200
222	0·500	0·476	0·476	222

Atmospheric oxidation of evaporated films. The specimens discussed above were exposed to air at normal temperature for about two minutes whilst the photographic plate was being changed, and examined once more immediately afterwards. In general, even with very thin films, no oxide rings were observed in the resulting diffraction patterns. Lead and copper, however, gave two or three very faint oxide rings which were too diffuse to be accurately identified.

Reflection specimens of evaporated silver. Silver was evaporated on to a freshly cleaved rocksalt face which was maintained at room-temperature. The reflection patterns obtained from such specimens invariably consisted of diffuse continuous face-centred cubic rings, and no bands were observed. When the rocksalt was dissolved in water and the silver film mounted as a transmission specimen on thickly silver-plated nickel gauze, however, the resulting pattern consisted of a well-defined face-centred cubic pattern together with the typical band and inner band-head. Although every precaution was taken to prevent contamination of the silver films by mercury whilst they were being removed from the rocksalt, one or two afforded patterns which included typical silver amalgam diffractions as described by Aylmer, Finch and Fordham.(5)

Electrodeposited specimens. Transmission specimens of cobalt, silver, nickel, gold and platinum were prepared by the method described by Finch and Sun.(12)

The patterns afforded by electrodeposited specimens were, in general, similar to those observed with evaporated films except that the electrodeposited cobalt films consisted mainly of the face-centred cubic form. In all cases the patterns exhibited the normal face-centred cubic diffractions of the metal together with the characteristic band and certain other rings which could be attributed as before to a hexagonal modification. The spacing-ratios referred to the side of unit cube agreed well, and were independent of the nature of the metal. The average results obtained from twenty electrodeposited specimens of the above metals are given in table 3.

Table 3

hkl hexagonal	*hkl* face-centred cubic	Theoretical d_{hkl}/a	Observed d_{hkl}/a	Percentage of patterns giving diffraction
100	—	0·613	0·612	100
002	111	0·577	0·576	100
101	—	0·541	0·544	45
—	200	0·500	0·500	100
102	—	0·420	0·421	20
110	220	0·353	0·352	100
103	—	0·326	0·326	10
200	—	0·306	—	—
112	311	0·301	0·301	95
201	—	0·296	0·295	10
004	222	0·289	0·288	100

As will be seen from column V, table 3, not all of the electrodeposited specimens gave rise to all the extra diffractions. Furthermore, in general the extra diffractions were weaker than the true face-centred cubic rings. The orientation of the face-centred cubic crystals was always (110). Occasionally the specimens gave extra rings due to contamination by grease or mercury before insertion in the camera. The available data on such extra diffractions were sufficient to enable them to be identified easily, and they are accordingly omitted from table 3. With most electrodeposited specimens the crystal size was considerably larger than in the corresponding evaporated film; in some cases so much so that the diffraction rings were broken up into spots more or less evenly distributed round the circumference. Whenever the face-centred cubic rings were broken up in this manner, the extra rings included in table 3 also consisted of a series of spots, whilst any extra rings due to grease or mercury were continuous and of uniform circumferencial intensity, figure 5. The same type of pattern was observed whether the specimen was mounted on nickel gauze or on nickel gauze thickly plated with the specimen metal.

An abnormal rhombohedral structure could not be assigned to any of the electrodeposited specimens, but two patterns are worthy of special mention in that they did not conform to the general description given above. Thus, in the pattern, figure 6, afforded by an electrolytic gold specimen, all the spacings corresponding to the hexagonal diffractions were present, and were much more intense than usual. Further, one silver specimen yielded a close-packed hexagonal pattern, figure 7, of axial ratio $c/a = 1{\cdot}63$, without face-centred cubic diffractions or band. The analysis of this pattern is given in table 4, and, since the actual spacings are liable to the 2 per cent experimental error involved in the voltage-measurement, the spacing-ratios are also given, referred to the 100 diffraction as 0·613.

Table 4

Diffraction *hkl*	Theoretical spacings for close-packed hexagonal structure $a_h = 2{\cdot}92$ A., $c/a = 1{\cdot}63$	Observed spacings d_{hkl} (A.)	Observed intensity	Observed d_{hkl}/d_{100} ($d_{100} = 0{\cdot}613$)	Theoretical d_{hkl}/d_{100} ($d_{100} = 0{\cdot}613$)
100	2·532	2·557	M.S.	0·613	0·613
002	2·383	2·373	M.S.	0·569	0·577
101	2·235	2·249	M.S.	0·539	0·541
102	1·735	1·751	M.	0·420	0·420
110	1·458	1·482	M.	0·355	0·353
103	1·347	1·355	M.	0·325	0·326
112	1·244	1·254	M.Diff.	0·301	0·301
201	1·223	1·236	M.Diff.	0·296	0·296
202	1·119	1·125	V.V.F.	0·269	0·271
104	1·077	1·080	V.V.F.	0·259	0·261
203	0·987	0·996	V.F.	0·238	0·239
121	0·938	0·948	F.	0·227	0·227
114	0·927	0·928	F.	0·223	0·223
105	0·892	0·894	V.F.	0·214	0·216

Thinned electrolytic specimens. A number of electrodeposited silver specimens, of thickness approaching the penetrating power of the electrons employed, were examined and shown to give the usual face-centred cubic pattern together with the band and extra rings. The specimens were then gradually thinned on a dilute potassium cyanide solution, and examined at various stages. With progressive thinning the band became more and more faint, until finally it could only be detected when viewed against a suitable background. Furthermore, the extra rings, including the inner band-head, virtually disappeared, although the face-centred cubic diffractions were of undiminished intensity.

Chemically deposited silver. A standard silvering solution for the preparation of mirrors(14) was mixed in a porcelain dish. After about 15 min. the surface of the solution became covered with a film of silver sufficiently thick to be picked up on gauze. Three silver specimens prepared in this manner were washed and examined. In each case the pattern consisted of the face-centred cubic diffractions together with a band between the 200 face-centred cubic ring and an extra ring of spacing 0·611*a*, but no other extra diffractions were observed. As with the evaporated and electrodeposited specimens, the orientation of the face-centred cubic crystals was (110), whilst the crystal-size was midway between that observed in evaporated and electrolytic films. The average spacing ratios for the chemically deposited films are given in table 5.

Table 5

hkl hexagonal	*hkl* face-centred cubic	Theoretical d_{hkl}/a	Observed d_{hkl}/a	Observed intensity
100	—	0·613	0·611	M.
002	111	0·577	0·576	V.S.
—	200	0·500	0·500	M.S.
110	220	0·353	0·353	S.
112	311	0·301	0·301	S.
004	222	0·289	0·288	F.

Chemically-displaced silver. A stainless-steel disc was electroplated with cadmium and, after careful washing, immersed in a solution of silver cyanide (36 g./litre). After about one minute the disc was withdrawn from the solution and washed and the composite cadmium-silver film was removed. The cadmium was then dissolved in saturated ammonium-nitrate solution, and the resulting film of chemically displaced silver was mounted as a transmission specimen and examined.

The patterns obtained from the nine specimens prepared in this manner were similar to those afforded by chemically deposited silver films. No extra rings other than the inner band-head were observed, and the normal-pattern rings were true face-centred cubic diffractions, as will be seen from table 6.

Table 6

hkl hexagonal	*hkl* face-centred cubic	Theoretical d_{hkl}/a	Observed d_{hkl}/a	Observed intensity
100	—	0·613	0·610	M
002	111	0·577	0·577	V.S.
—	200	0·500	0·500	S.
110	220	0·353	0·353	S.
112	311	0·301	0·301	V.S.
004	222	0·289	0·289	F.M.

The face-centred cubic crystals were in (110) orientation, and the crystal-size was comparable with that observed in electrodeposited specimens.

§4. DISCUSSION

From the results set forth above it will be seen that the patterns afforded by evaporated, electrodeposited, chemically deposited and chemically displaced face-centred cubic metal films invariably include a typical band extending from the 200 ring to an extra ring just within the 111 diffraction. Further, the spacing corresponding to the inner band-head is always a constant fraction of the side of unit cube, and this fraction is the same for all the face-centred cubic metals examined and independent of specimen thickness and crystal size. Other extra rings have been observed and these, like the inner band-head, may be regarded as characteristic of the face-centred cubic structure, since the spacing-ratios referred to the side of unit cube were the same for all the metals examined. The band and extra rings under discussion were never observed with specimens prepared by thinning beaten leaf, and the effect of thinning electrodeposited specimens was to decrease the intensity of the extra rings and bands. Specimens prepared by evaporation from a filament of the pure metal on to a cellulosic film in the evacuated electron diffraction camera afforded the characteristic band and extra rings. Under such conditions the possibility of contamination by grease or mercury, gas-absorption or alloy formation, is completely eliminated; nor can these extra diffractions be explained in terms of the Finch-Wilman limited-lattice theory because, unlike with graphite and molybdenite, they did not disappear with increasing film-thickness, but could, on the contrary, be eliminated by etching. Again, the results obtained with silver films evaporated on to rocksalt cleavage faces show that with sufficient film thickness the ultimate structure is face-centred cubic yielding no extra rings or bands. Finally, whenever the face-centred cubic rings consisted of a series of spots, the extra rings were broken up in a similar manner. It seems reasonable to suppose, therefore, that these extra diffractions have their origin in some structural abnormalities occurring in the first few atom-layers when a film of a face-centred cubic metal is built up gradually by atomic deposition.

In the case of the evaporated cobalt films, the patterns did not conform to the general description given above, but consisted of a mixture of the diffractions due to the face-centred cubic and close-packed hexagonal modifications(11) of the metal, in which the face-centred cubic rings might justifiably be regarded as extra diffractions. The effective atomic radius is the same in both forms of cobalt, and since a band was observed extending from the 200 face-centred cubic ring to the 100 hexagonal diffraction, the possibility of the other face-centred cubic metals possessing a truly close-packed hexagonal modification was considered.

As will be seen from the tables, all the extra diffractions observed with metals other than cobalt could be quantitatively explained on the supposition that some part of the metal was in the form of close-packed hexagonal crystals in which the atoms retained their normal effective radius. The hypothesis is further strengthened by the discovery of an electrolytic silver specimen which consisted solely of the close-packed hexagonal modification, and an electrodeposited gold specimen which afforded all the hexagonal diffractions in addition to the face-centred cubic rings.

It has already been pointed out by Finch, Quarrell and Wilman(1) that a band may be regarded as evidence of a gradual expansion or contraction of the crystal lattice, and the possibility that the band observed in this work may be due to the transition from a close-packed hexagonal to the face-centred cubic modification immediately suggests itself.

In all cases the face-centred cubic crystals were in approximate (110) orientation, whilst the hexagonal crystals showed a tendency towards (001) orientation. Owing to the fact that many of the hexagonal and cubic rings were superimposed, the degree of imperfection of these orientations could not be estimated, but it will suffice for our purpose if we assume that the orientations were accurately (110) and (001) respectively, and attempt to find some mechanism by which a gradual transition from (001) hexagonal to (110) face-centred cubic can be explained.

Theoretically the normal lattice forces which result in metal atoms taking up positions on a specific crystal lattice only exist between those atoms which are so completely surrounded by other similar atoms, i.e. so remote from the crystal boundaries, as to be unaffected by edge effects. Indeed, in X-ray crystallographic work, which has been so largely responsible for our conception of the crystal lattice, it is usually tacitly assumed that the crystals examined consist of infinite space lattices; the possibility of edge effects being thus precluded. In electron-diffraction, on the other hand, it has long been recognized that the crystals must be limited in the direction of penetration of the electron beam and can no longer be considered as consisting of infinite lattices. In general it is permissible to assume that the lattice has infinite dimensions in directions at right-angles to the beam, and, owing to the cross-grating nature of the observed diffractions, this results in the method affording the same lattice constants as X-rays for a given substance. Recently, however, Finch and Wilman(6, 7) have shown that the effect of lattice-limitation in the direction of the beam sometimes not only is such as to cause the relaxation of the third Laue condition which results in cross-grating diffraction, but may even give rise to new and forbidden diffractions. Whilst they had no reason for believing that the atoms near the crystal boundaries were taking up abnormal positions, nevertheless their results showed that the possibility of edge effects cannot be ignored in electron-diffraction.

When a metal is deposited atom by atom, as in the experiments described above, it is hardly likely that the normal lattice forces will at once come into play. Thus it is to be expected that in the first place, at least locally, a single layer of atoms will be formed, and the interatomic forces will cause the atoms in this first layer to take up relative positions of maximum stability. In a two-dimensional lattice this will clearly result in the atoms being placed at the corners of equilateral triangles whose sides are equal to the atomic diameter. Similarly one might expect the next layer of atoms to be formed in such a manner that each atom is resting in the hollow between three adjacent atoms in the first layer. If now the third layer of atoms is deposited so that each atom is touching three atoms in the second layer and is immediately above an atom in the first layer, figure 8*a*, then the film will consist of a number of coplanar unit cells of a close-packed hexagonal lattice. If, however, the atoms of the third layer take up positions in which they are immediately above a gap between three atoms in the first layer, whilst still touching three atoms in the second layer, figure 8*b*, then the structure will be rhombohedral with interaxial angle α equal to 60°, i.e. face-centred cubic. Thus the structure is close-packed hexagonal in (001) orientation, or face-centred cubic in (111) orientation, according to the positions adopted by every third layer of atoms, and it may well be that in a very thin film the resultant forces between the atoms favour the formation of a hexagonal structure.

The intensities of the hexagonal pattern varied considerably from specimen to specimen. Thus the chemically deposited silver specimens afforded only the 100 hexagonal ring in addition to the normal face-centred cubic pattern, whilst one electrodeposited silver specimen yielded the full hexagonal pattern without face-centred cubic rings. Hence it would seem that the thickness of the hexagonal layer is determined to some extent by the conditions of preparation of the specimen. The results do not enable the thickness for which the hexagonal structure persists in any specimen to be deduced, but it is clear that as the film-thickness increases, and conditions more nearly resemble those in the infinite space lattice, the structure tends towards the normal face-centred cubic in (110) orientation. In an attempt to explain the transition from the hexagonal to face-centred cubic modifications, it will be assumed that the atoms behave as solid spheres of definite radius. This assumption would appear to be justified by the fact that the experimental spacings of the extra rings can be quantitatively explained if the metal atoms in the first layers of an atomically deposited film crystallize in a close-packed hexagonal form in which the normal effective atomic radius observed in the face-centred cubic crystals is preserved.

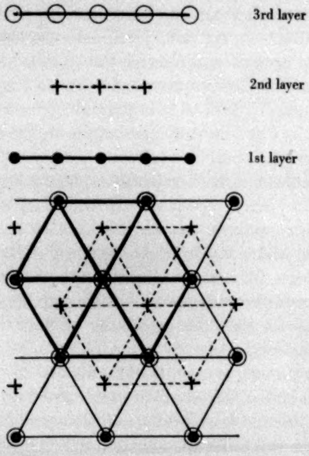

Figure 8*a*. (001) close-packed hexagonal.

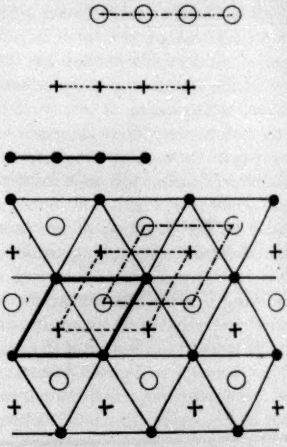

Figure 8*b*. (111) face-centred cubic.

The atomic arrangements in (001) hexagonal and (110) face-centred cubic crystals are shown in figures 9*a* and 9*b*, respectively. Consider the rectangles *ABCDEF* of figure 9*a* and *RSTUVW* of figure 9*b*. It will be seen that whilst

$AC=RV$, $AF>RS$, and furthermore the atoms G and H are coplanar with the atoms $ABCDEF$, whereas in the face-centred cubic form the atoms Y and Z are above the plane $RSTUVW$ by an amount $0{\cdot}353a$. Suppose, therefore, that as the specimen becomes thicker, the hexagonal network puckers in such a manner that, whilst A, B, C, D, E and F remain in the same plane, the atoms of type G and H are lifted out of that plane, thus allowing the atom-row ABC to approach FED. When $AF=RS=a$, the atoms G and H will be in relatively the same positions as Y and Z of figure 9*b*, and the atomic arrangement will be face-centred cubic in (110) orientation. Further, the effective spacing for the planes parallel to ABC was initially such that $AF/2=0{\cdot}613a$, i.e. it was the hexagonal (100) spacing, and this changed during the transition to an effective spacing $a/2$, corresponding to the 200 face-centred cubic diffraction. Thus, if the transition be assumed to take place gradually, extending over a number of atomic layers, a band will be swept out containing all possible spacings within the range $0{\cdot}613a$ to $0{\cdot}500a$.

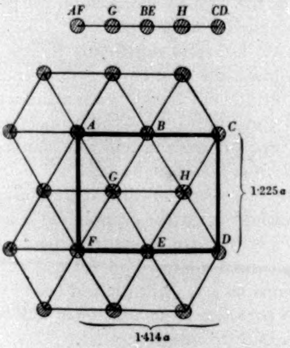

Figure 9*a*. Basal plane of hexagonal lattice.

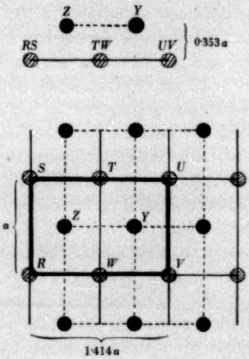

Figure 9*b*. (110) plane of face-centred cubic lattice.

At first sight it might be supposed that if this were the true mechanism entailed in the transition from the hexagonal to the face-centred cubic form, more bands would be observed extending from face-centred cubic rings to the corresponding hexagonal diffraction. Reference to figure 9*a*, however, will show that the (100) hexagonal planes are the only ones which become planes of the face-centred cubic lattice merely by moving closer together, and these are the only conditions under which a band is to be expected. In addition to the very prominent band which is satisfactorily explained by the above theory, a very much weaker band approximately situated between the 400 and 311 cubic rings was observed. The intensity of this band was such that accurate measurements of its limits were not possible, and accordingly its presence has not been noted in the tables. It seems probable, however, that this band is the second order of the one discussed above.

The fundamental unit cell of the face-centred cubic lattice is a rhombohedron with interaxial angle α equal to 60°, and any rhombohedral lattice may be conveniently referred to hexagonal axes. Thus the transition from close-packed hexagonal to face-centred cubic may be regarded, as far as spacing ratios are concerned, as a change in the axial ratio c/a from 1·63 to 2·45, the value of a_h remaining unchanged. A number of specimens were found to give spacings which were definitely not those of a face-centred cubic lattice, but could be fitted to the Hull and Davey (13) chart for a rhombohedral lattice, referred to hexagonal axes, at axial ratios between 2·24 and 2·42. These specimens were exceedingly thin films of the metal evaporated on to the cellulosic substrates in the evacuated electron diffraction camera, and in each case the plate was exposed as soon as the pattern observed on the fluorescent screen appeared to be of the normal face-centred cubic type.

Now, when an electron beam falls upon a crystal sufficiently thin to transmit electrons without giving rise to Kikuchi lines, the first cross-grating encountered by the beam is most effective in causing diffraction. Hence if a transition from one lattice to another occurs within the crystal, those diffractions will be most prominent which correspond to the structure in the layers nearest the electron source, and the stronger rhombohedral patterns observed must therefore be regarded as due to the layers last deposited. In effect, therefore, the rhombohedral structures show the stage in the transition which had been reached when the evaporation ceased. It is rather surprising at first sight that the intermediate structures should be at all stable, yet the rhombohedral copper specimen analysed in table 2 still gave a rhombohedral pattern of axial ratio c/a equal to 2·32, when it had been exposed to air and slightly oxidized as shown by the presence of an additional diffuse ring in approximately the position of the 111 Cu_2O diffraction.

The rhombohedral structures observed enable the conclusion to be drawn that the transition from hexagonal to cubic structure occurs gradually as deposition proceeds, and that the band is not the result of an atomic rearrangement after the metal film has reached a certain critical thickness.

Such intermediate structures were not observed with specimens prepared by any method other than evaporation, but this is easily understood, since the evaporated films were so thin that they could not have been handled had they not been supported on cellulose.

The source of those rings observed in the patterns afforded by certain cobalt specimens, which could not be explained in terms of the hexagonal and cubic diffractions, has not yet been satisfactorily determined. The fact that the strongest of these rings corresponded exactly to the 110 face-centred cubic spacing, however, suggests that perhaps the Finch-Wilman effect is coming into play in those layers which are approximating to the face-centred cubic structure, and allowing forbidden and other extra diffractions to occur.

§5. CONCLUSION

The application of electron-diffraction to the study of surfaces has made it clear that the structure of a thin film may be different from that of the material in bulk. Thus, in the phenomenon of basal-plane pseudomorphism(15), it was found, for example, that the first few layers of aluminium evaporated in vacuo on to a platinum substrate had face-centred tetragonal lattice, whilst thicker films adopted the normal face-centred cubic structure. Similarly, Aylmer, Finch and Fordham(5) found that the structure of amalgam films depends upon film-thickness. In the present work it has been shown that an abnormal structure exists in the first deposited layers of all the face-centred cubic metals examined, and for each of the methods of atomic deposition employed. Even with cobalt, the tendency to change from hexagonal to cubic structure with increasing film thickness was marked, although one would hardly expect it since the hexagonal modification is usually regarded as the stable form at low temperatures. It seems likely, therefore, that abnormal structures will be found in sufficiently thin films of all face-centred cubic metals prepared by atomic deposition.

In view of these facts, the assumption that thin films possess the structure of the bulk metal can no longer be made, and it may well be that many of the properties peculiar to thin films have their origin in the abnormal structures occurring in the first few deposited layers.

§6. ACKNOWLEDGMENTS

I wish to thank Prof. G. I. Finch for his unfailing help and interest in this work, and for the valuable advice he has given me. I also wish to thank the Department of Scientific and Industrial Research for a grant which enabled me to devote my whole time to this research.

REFERENCES

(1) Finch, Quarrell and Wilman, *Trans. Faraday Soc.* **31**, 1085 (1935).
(2) Mark, Motz and Trillat. *Naturwissenschaften*, **20**, 319 (1935).
(3) Finch and Quarrell. *Nature*, Lond., **136**, 720 (1935).
(4) Preston and Bircumshaw. *Phil. Mag.* **21**, 713 (1936).
(5) Aylmer, Finch and Fordham. *Trans. Faraday Soc.* **32**, 864 (1936).
(6) Finch and Wilman. *Proc. roy. Soc.* A, **155**, 345 (1936).
(7) Finch and Wilman. *Trans. Faraday Soc.* **32**, 1539 (1936).
(8) Finch and Quarrell. *Proc. phys. Soc.* **46**, 148 (1934).
(9) Finch, Quarrell and Wilman. *Trans. Faraday Soc.* **31**, 1065 (1935).
(10) Finch and Fordham. *Proc. phys. Soc.* **48**, 85 (1936).
(11) Kersten. *Physics*, **2**, 274 (1932).
(12) Finch and Sun. *Trans. Faraday Soc.* **32**, 852 (1936).
(13) Hull and Davey. *Phys. Rev.* **17**, 549 (1921).
(14) Watson. *A Text-book of Practical Physics*, p. 598 (Longmans, Green and Co., Ltd., 1926).
(15) Finch and Quarrell. *Proc. roy. Soc.* A, **141**, 398 (1933).

INTENSITIES OF X-RAY REFLECTIONS FROM SINGLE CRYSTALS OF SODIUM BETWEEN 120 AND 370° K.

By RALPH H. V. M. DAWTON, B.Sc., Davy Faraday Laboratory of The Royal Institution, London

Received 23 *December* 1936. *Read* 26 *February* 1937

ABSTRACT. Single crystals of sodium are examined by X rays in a temperature range of 120—370° K. Strong hysteresis in the reflecting-power is observed, but this vanishes when the crystals are chilled with liquid air. The normal temperature effect is measured with the chilled crystals and the characteristic temperature is calculated from the Debye-Waller formula.

---

§ 1. INTRODUCTION

The object of this paper is the study, with the aid of X rays, of the changes in structure of single crystals of sodium subjected to heating and cooling over a wide range of temperatures, including a close approach to the melting point. The work was suggested by Dr A. Müller.

§ 2. EXPERIMENTAL DETAILS

The X-ray plant and the recording apparatus are described in a previous paper.(1) The characteristic radiation of molybdenum filtered by zirconium is used. The electric heater required for the heating of the crystal above room-temperature is shown in figure 1. It consists of a copper tube with apertures to let the incident and reflected beams pass through. The heating-coil is wound on the outside of this tube. 10 ft. of $\frac{3}{32}$-in. copper pipe are soldered to the inside wall and air is passed through this spiral to ensure thermal equilibrium. The liquid-air cooler is shown in figure 2. *A* is a solid copper rod, which has a $\frac{1}{4}$-in. hole bored longitudinally as shown. The incident and reflected beams pass through *B* and *C* respectively. Thermocouples *D* and *E* can be kept steady to within 3°. The temperature variations are within $\frac{1}{2}$° during an X-ray measurement. At the lowest temperature *D* is 115° K., *E* is 121° K., and the crystal is taken to be at 117° K.

Two methods of mounting the crystals are used: (1) A glass tube is mounted as shown in figure 3*a*. Soda glass is used because it does not react with the sodium. A test tube, figure 3*b*, contains sodium under oil, and is fitted with an exhausting-tube and a sliding rod *A*, to which the glass tube is attached. The procedure is to evacuate the test tube and melt the sodium. Rod *A* is lowered until the open end of the small tube is in the sodium, and air is admitted into the test tube until sufficient

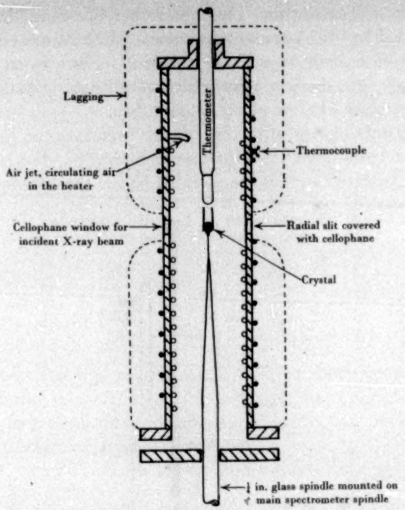
Lagging
Thermometer
Thermocouple
Air jet, circulating air in the heater
Cellophane window for incident X-ray beam
Radial slit covered with cellophane
Crystal
$\frac{1}{4}$ in. glass spindle mounted on main spectrometer spindle

Figure 1.

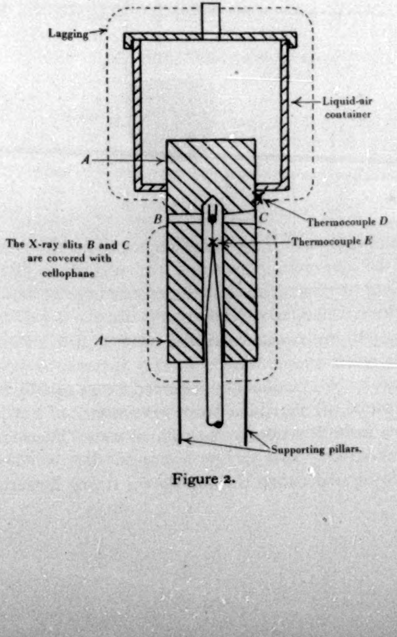
Lagging
Liquid-air container
A
B
C
Thermocouple D
Thermocouple E
The X-ray slits B and C are covered with cellophane
A
Supporting pillars.

Figure 2.

sodium has entered the small tube. The tube is then lifted until its open end is in the oil, tap *T* is opened and the apparatus is cooled. With rare exceptions the sodium solidifies in form of a single crystal. (2) Molten sodium in an evacuated flask is broken, by shaking, into small spheres which give single crystals. The crystals are mounted by being placed in one of the small tubes.

By trial and error the axes of the crystal are found on the X-ray spectrometer, the platinum wire being bent for adjustment, figure 3*c*. For liquid-air work the lower end of the platinum wire is spot-welded to the thermocouple *E*, figure 2.

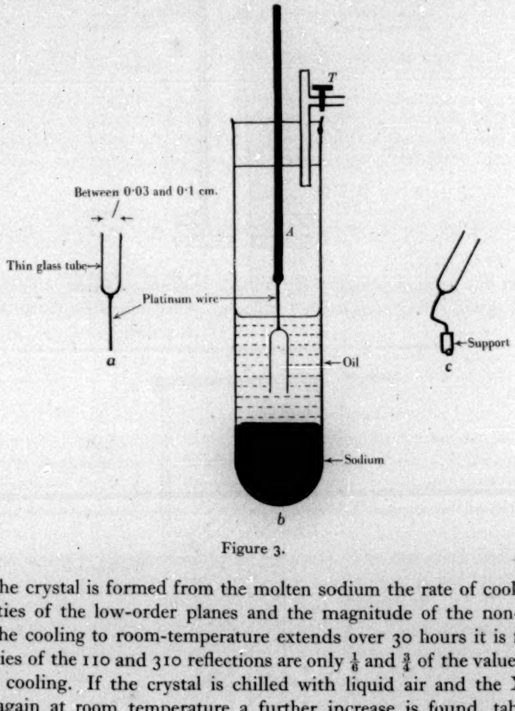

Figure 3.

When the crystal is formed from the molten sodium the rate of cooling affects the intensities of the low-order planes and the magnitude of the non-reversible effect. If the cooling to room-temperature extends over 30 hours it is found that the intensities of the 110 and 310 reflections are only $\frac{1}{6}$ and $\frac{3}{4}$ of the values observed after rapid cooling. If the crystal is chilled with liquid air and the X rays are measured again at room temperature a further increase is found, table 1. The increase in the intensity of a plane is accompanied by an equally marked decrease in the magnitude of the non-reversible effect. No amount of heating and cooling of the crystal can now make it return to its original state. The increases of intensity seem to be permanent.

Reflections of lower order than the 400 show a strong hysteresis which makes a determination of the reversible temperature effect impossible unless a crystal is chilled with liquid air. The high-order reflections, having little or no hysteresis enable a reversible temperature effect for the 330, 400 and 440 reflections to be found without liquid-air treatment. The results are not altered if the crystal is treated.

Table 1

Indices	Intensity at room-temperature before chilling. Crystal formed and cooled during 2 hours to 20° C.	Intensity at room-temperature after chilling with an air blast 80° below crystal-temperature	Intensity at room-temperature after liquid-air chilling
110	500	3600	4100
200	270	1200	1450
220	140	260	300
310	90	144	150
400	23	23	23

Measurements on the 330 reflection are difficult, because overlapping of 110 and 220 reflections due to wave-lengths other than that of the characteristic target radiation occurs. In general this reflection is not measured. Its temperature effect is about 2 per cent greater than that of the 400.

The general accuracy for work above room-temperature may be judged from table 2, where

$$\frac{\text{Change of intensity over the range 292–370° K.}}{\text{Intensity at 292° K.}}$$

is given for various crystals. The variations are caused by variations between individual crystals; the errors of observation are smaller. With crystals of moderate size the 440 reflection is so feeble that it can only be measured below 150° K.

Table 2

Reflection 110		Reflection 200	Reflection 220	Reflection 310	Reflection 400
0·168	0·104	0·294	0·432	0·545	0·712
0·130	0·130	0·287	0·431	0·570	0·707
0·128	0·100	0·266	0·485	0·597	0·738
0·155	0·122	—	0·474	0·510	0·743
0·110	0·143	—	0·415	—	0·723
0·130	—	—	—	—	—
Mean 0·129		—	—	—	—

The discrepancies of the reversible temperature effect below room-temperature, as observed with individual crystals, are much less than those above room-temperature. The 440 reflections give values agreeing within the experimental error of 7 per cent. The 400, 310 and 220 reflections gave values agreeing within the experimental error of 4, 4, 5 per cent respectively. If the 200 and 110 reflections disagree by more than 10 per cent a hysteresis loop is present.

Ordinary commercial sodium and a special supply from Kahlbaum give the same result.

§ 3. RESULTS

Hysteresis. Hysteresis occurs above and below room-temperature, but detailed measurements have been made only above room-temperature. When the temperature is raised to 370° K., the 110 intensity sometimes decreases 60 per cent or increases 20 per cent according to the crystal. Increases of intensity are rare. Big changes of the 110 require ¾ hour before being within 10 per cent of the apparent steady value obtained after 3 hours heating, figure 4. Higher-order planes have less hysteresis even though the intensity changes are greater. The hysteresis observed with the 310 reflection is about ⅕ of that observed with the 110 reflection. The intensity when the crystal is cooled to room-temperature depends on the rate of cooling, figure 5.

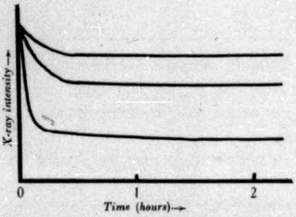

Figure 4. Curves showing 110 intensity for 3 crystals maintained at 370° K. for 2½ hours.

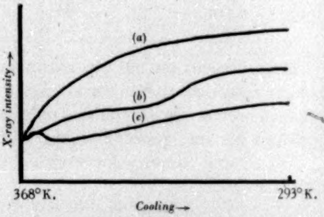

Figure 5. Curves showing, for the same crystal, 110 reflection-intensities during cooling from 368° K. The crystal was cooled (*a*) in 8 minutes; (*b*) in 20 minutes; (*c*) in 50 minutes.

Vibrations seem to change the microstructure of the crystals, particularly at high temperatures. If for instance a crystal is set in vibration by tapping the spectrometer spindle, the intensity measurements before and after the tapping may differ by 30 or even 50 per cent. The effect may be an increase or a decrease, and is sometimes found even at room-temperature. These changes are not in any way connected with accidental mis-settings of the crystal on its support. The intensities are also sensitive to sudden changes of temperature, the effect being larger as the melting point is approached, although no great increase in the effect occurs over the last 10° C. Within this range about one half of the crystals will give a sudden 30 per cent change (almost a jerk on the galvanometer) in the 110 intensity if the temperature, as measured by the thermocouple, changes by 1° C. in a few seconds.

Figures 6 α and 6 β give the 110 and 310 X-ray intensities as the temperature is increased uniformly and then decreased at the same uniform rate. The pairs β, *b* and γ, *c* give the same for two exceptional crystals. None of these crystals are treated with liquid air. It is found that (1) the size of the loop does not seem to depend on the rate of performing the cycle, which varied between 4 and $\frac{4}{9}$° C./min.; (2) generally the curves cross; (3) the dimensions of the crystal do not seem important; (4) crystals mounted by method (1) are not free in the containing tube, but crystals mounted by method (2) are free; in each case hysteresis is present and hence any restriction which the containing tube has on the crystal does not affect the X-ray intensities.

The reversible temperature effect. Except for occasional observations on the 400 and 440 reflections of untreated specimens, the measurements are made on crystals which have been chilled with liquid air. If the crystals are examined, before and after this treatment, in monochromatic radiation of divergence less than $\frac{1}{50}^\circ$, it appears, figures 7*a* and 7*b*, that the crystal splits into small units. Figure 8 shows the crystal of figure 7*b* taken in the more divergent molybdenum characteristic radiation direct from the target. The intensities measured are representable by

$$I_T \propto e^{-(0\cdot04044T+17\cdot08\,.\,10^{-6}T^2)\sin^2\theta},$$

where I_T is the observed intensity at temperature T° K. and 2θ is the angle between incident and reflected beams. In the experiments T ranged from 117 to 368° K.

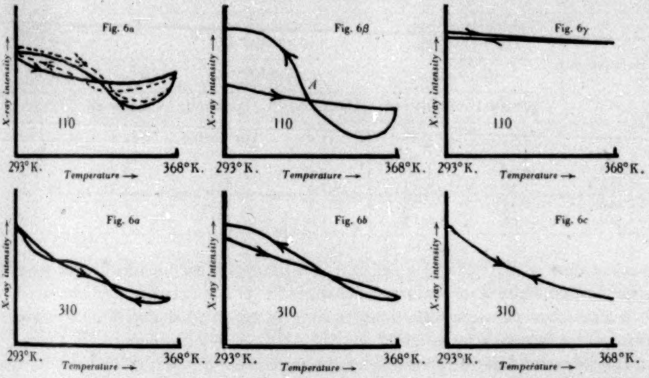

Figure 6. Hysteresis cycles for 3 crystals. The dotted curve of figure 6α is what might be expected if the cycle is repeated. The hysteresis after a large number of repeats is of the same magnitude.

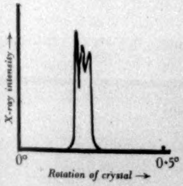

Figure 7*a*. Before chilling.

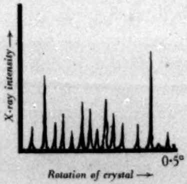

Figure 7*b*. After chilling.

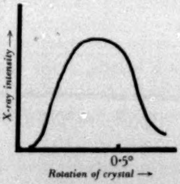

Figure 8.

An indication of the accuracy of the formula is given, for three different temperature ranges, by table 3. The changes of intensity do not seem to be caused by changes in (1) linear absorption of the X-ray beam, (2) the sodium lattice spacing, (3) primary extinction, or (4) secondary extinction, because no change in (1) greater than the experimental error of 3 per cent occurred; the value of (2) given by 2θ does not change more than 1·5 per cent, the limit of error for measurements made in the filtered white X-ray radiation; changes in (3) and (4) affect the strong reflections more than the weak reflections, making it improbable that the experimental temperature factor varies as $\sin^2\theta$.

Table 3

Reflection	Temperature range 117 to 180° K.		Temperature range 117 to 291° K.		Temperature range 117 to 368° K.	
	I_{117}/I_{180}		I_{117}/I_{291}		I_{117}/I_{368}	
	Calculated	Observed	Calculated	Observed	Calculated	Observed
440	3·50	3·26	15·1	Too feeble	81·0	Too feeble
400	1·92	1·96	8·9	8·8	34·6	30·4
310	1·48	1·50	3·7	4·0	8·2	8·3
220	1·37	1·34	2·8	2·9	5·3	5·3
220	1·17	1·23	1·7	2·0	2·3	2·5
110	1·08	1·13	1·3	1·7	1·5	1·9

It is assumed that the reversible temperature effect found is given by the thermal motion of the atoms. On this assumption the characteristic temperature is calculated by using the Debye-Waller temperature factor e^{-M}, where $F_T^2 = F_0^2 e^{-2M}$ and

$$M = \frac{6h^2}{m_a k\Theta}\left\{\frac{\Phi(x)}{x} + \frac{1}{4}\right\}\frac{\sin^2\theta}{\lambda^2},$$

while Θ is the characteristic temperature, 2θ the angle between incident and reflected beams, λ the wave-length of the X rays, h is Planck's constant, k is Boltzmann's constant, m_a is the mean mass of the atom or vibrating systems in the crystal, $x = \Theta/T$ where T is the absolute temperature, and

$$\Phi(x) = \frac{1}{x}\int_0^x \frac{\xi}{e^{\xi} - 1} . d\xi.$$

It is shown, at the end of this paper, that the crystals are nearly of the mosaic type, and hence F_T^2 is not far from being proportional to the reflecting-power of the crystal at $T°$. The value of Θ is calculated as a mean over a range of 20° C. The 310, 400 and 440 reflections are used for this calculation since the agreement from crystal to crystal for these reflections is much better than for the reflections of lower order. Figure 9 gives the results together with the values of Θ determined by other methods. The dotted curves give the experimental error.

The f_0 curve, or atomic-scattering curve, is calculated by using the Debye-Waller formula to extrapolate the X-ray intensities measured at 117° K. Some assumptions as to the value of Θ must be made. Throughout the range of extrapolation an average value is used. Since it is not perfectly legitimate to base this average value on the values of Θ determined by methods other than X-ray data, it was decided to use figure 9. This gives an average X-ray value: $\Theta = 130 \rightarrow 141$, in the range $T = 0 \rightarrow 120^\circ$ K. The f_0 curves calculated for each of these extreme limits are compared with the theoretical Hartree curve in figure 10*a*, in which no zero-point energy is assumed and in figure 10*b* in which zero-point energy *is* assumed. The experimental points given by the smaller values of $\sin\theta/\lambda$ (i.e. the strong planes) fall below the theoretical curve. This can be caused by (1) primary extinction, (2) secondary extinction, and (3) the crystal not being a perfect mosaic. All three of these affect the strong planes more than the weak planes, and further all three, except possibly (1), which occurs within very small internal blocks of the crystal, are affected by the chilling. Since chilling gives no increase in the 400 intensity, it is believed that the f_0 value of the 400, and consequently the higher-ordered 440 reflection, has no important extinction. (1) and (3) give an extinction error which is independent of the size of the crystal, unless this is extremely small, and can only be eliminated by having the crystal in powder form. The breaking up of the crystal by liquid air is an approach to this state. (2) depends on the size of the crystal, and is investigated by taking some small crystals (about $\frac{1}{8}$ the size of those used for determining the f_0 curves) and disintegrating them as far as possible with liquid air. The average ratios of the intensities given by these crystals are given in table 4, column 1. One crystal gave the values given in column 2. Column 3 gives

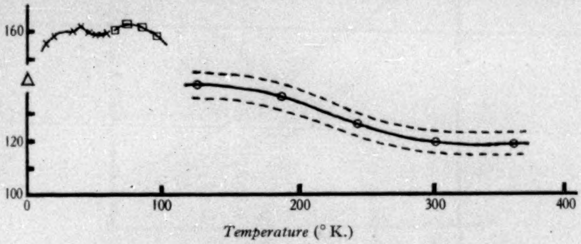

Figure 9. ○ Author's X-ray points; □ specific-heat points; × results by Fuchs$^{(4)}$; △ results by Fuchs$^{(5)}$.

Table 4

Reflection	Intensities, proportional to F^2		
	Column 1	Column 2	Column 3
110	204·0	218·0	162·0
200	78·0	81·0	65·0
220	15·7	16·5	14·5
310	7·6	7·8	7·2
400	1·0	1·0	1·0
440	Too feeble	Too feeble	Too feeble

the average values for the crystals used for determining the f_0 curves. It is evident that these crystals show extinction. Figures 11 *a* and 11 *b* show the curves of figures 10*a* and 10*b* corrected for the extinction indicated by columns 1 and 3 of table 4. On the assumption that the crystal is mosaic we should correct for extinction by using columns 2 and 3, because the mosaic crystal reflects the maximum possible.

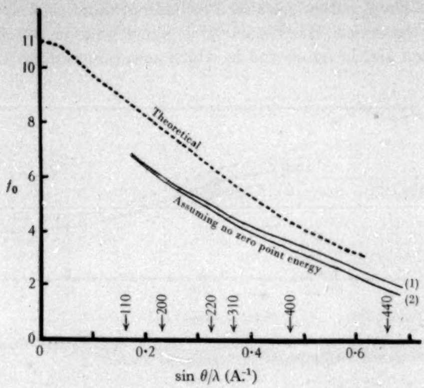

Figure 10*a*. Curve (1), Θ between 0 and 117° K. taken as 130.
Curve (2), Θ between 0 and 117° K. taken as 141.

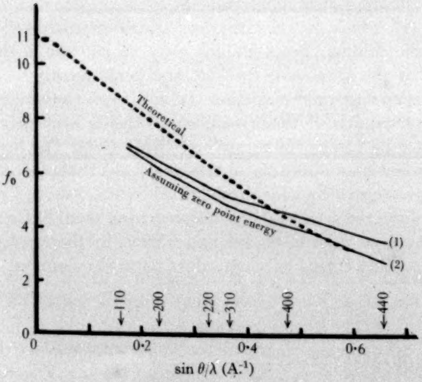

Figure 10*b*. Curve (1), Θ between 0 and 117° K. taken as 130.
Curve (2), Θ between 0 and 117° K. taken as 141.

If the results are based on the one crystal giving column 2, the chain curve shown in figures 11*a* and 11*b* results.

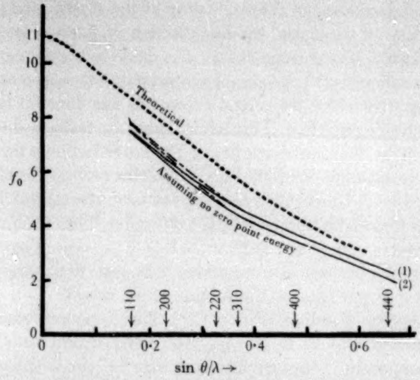

Figure 11*a*. Curve (1), Θ between 0 and 117° K. taken as 130.
Curve (2), Θ between 0 and 117° K. taken as 141.

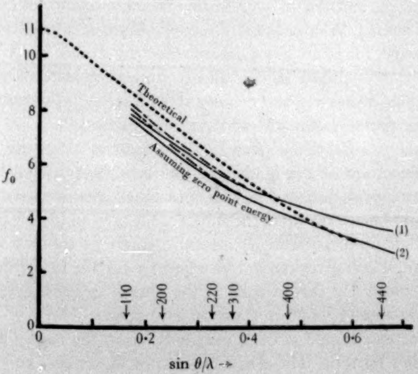

Figure 11*b*. Curve (1), Θ between 0 and 117° K. taken as 130.
Curve (2), Θ between 0 and 117° K. taken as 141.

§ 4. THE ABSOLUTE SCATTERING-POWER OF THE CRYSTALS

The absolute scale of figures 10 and 11 is obtained by determining the scattering-power of the crystal at room-temperature and applying the temperature factor as already explained. Only the more important details of the measurement are given. The error caused by unwanted radiation in the nearly monochromatic

X-ray beam is determined as described in a previous paper.[2] Corrections for the extinctions (*a*) the absorption from photo-electric emission and non-coherent scattering, which is independent of the orientation of the crystal, and (*b*) the shielding of the interior parts of the crystal by the reflection of X rays from the parts lying above them are made. The correction for (*a*) is made to 1·2 per cent by measuring the absorption coefficient and the size of the crystal. (*b*) is lessened by increasing the angular range over which the crystal reflects, as was done for figure 7, and also by measuring a feeble reflection. This latter cannot be realized directly because of lack of intensity in the monochromatic beam. The 110 reflection is therefore measured in monochromatic radiation. With the same crystal the ratio of this plane to the (400) is then measured in the direct filtered radiation from the target. This enables the absolute measurement to be based on the 400 reflection. The maximum experimental error will not affect figures 10 and 11 by more than 6 per cent. The error is probably less than 4 per cent. The crystals are assumed to be near to the mosaic type because the intensities are proportional to the volume of the crystal.

The melting-point of sodium is 97·5° C.[3] The X-ray reflections from sodium behave in a normal manner up to 98·5 ± 0·5° C., when within 0·2° C. the reflections vanish. For comparison *s*-triphenylbenzene may be cited, the melting-point of which is increased by 2° C. if it is enclosed in a small capillary tube. It is therefore possible that a similar effect may occur with sodium. On account of the non-transparency and the softness of sodium this increase could not be observed.

Summary of results. When a small piece of sodium is crystallized from the melt it is, on the average, found to give a lower reflecting-power for X rays than would be expected if it crystallized in the ideally imperfect state. The crystals when subjected to a cycle of heating and cooling show a strong hysteresis effect, as given in figure 6. This applies essentially to the strong planes.

If the crystal is suddenly chilled by liquid air it alters its behaviour. The hysteresis becomes almost negligible and the reflection curves before and after treatment are as shown in figure 7. The intensities increase as shown in table 1. From this it might be assumed that the substance is now an ideally imperfect crystal, but it is found that when the experimental f_0 curve is compared with Hartree's theoretical curve, it still gives too low an intensity for the low-order planes. From this it must be concluded that in spite of the drastic treatment the crystals do not break into blocks small enough to show no extinction.

The characteristic temperature is calculated from the X-ray data by means of the Debye-Waller formula. The result is given in figure 9. The value is based on the weaker planes whose temperature factor is large and whose extinction errors are small. The difference of 20 per cent between the X-ray value and that obtained from specific heats is not excessive, considering the approximate nature of the theory.

§ 5. ACKNOWLEDGMENTS

I wish to express my thanks to the Managers of the Royal Institution and to Sir William Bragg for permission to carry out this work. I am indebted to Dr A. Müller and to Dr R. Eisenschitz for their help in interpreting the experimental results, and also to Dr A. Müller for his interest and advice in the experimental work.

REFERENCES

(1) Robinson, B. W. *Proc. roy. Soc.* A, **142**, 422 (1933).
(2) Robinson, B. W. *Proc. roy. Soc.* A, **147**, 467 (1934).
(3) *International Critical Tables.*
(4) Fuchs, K. *Proc. roy. Soc.* A, **153**, 637 (1936).
(5) Fuchs, K. *Proc. roy. Soc.* A, **157**, 445 (1936).

DISCUSSION

Sir William Bragg. The curious conclusion of these experiments is that the crystal chilled in liquid air arrives at a state which appears to be stable; before the chilling the state is variable. The experiments show that it is stable when the crystal is broken up into a mosaic structure, and the point to be explained is why the material prefers when cold to crystallize as if there were a great number of nuclei, while when prepared from the melt it behaves as if there were a much smaller number of nuclei.

Dr A. Müller. I wish to emphasize one important point in the author's work, namely the fact that the crystal ceases to show hysteresis when it is suddenly chilled and not, as one might expect, when slowly annealed. The results also show that it is very difficult to make certain that a metal shall be in equilibrium.

Mr R. M. Archer. I have made many attempts to produce a gas-free film of sodium on the walls of a soda-glass mercury trap, and was interested to see that the author's method of filling a capsule is almost the same as one which I devised last year. If the author or any other Fellow can help me I shall be grateful, as I have had many difficulties in handling this vicious element. The technique of Hughes and Poindexter is inapplicable to my soda-glass evacuation system because the glass evolves so much water when heated strongly, and hydration follows. My method of filling is the same as the author's, except that all the vessels are of metal, and oil is not used because hydrocarbons would be out of place in valve work. The filled capsule is plugged lightly to exclude air and moisture, and put into a metal test tube wound outside with nichrome strip and insulated with asbestos. This little furnace is mounted concentrically inside the vertical glass tube which forms the trap, the whole being evacuated subsequently. The furnace is purposely made longer than the capsule and its upper end is closed by four or five perforated baffles to prevent the molten sodium from creeping over the rim and severing the nichrome or clinging to the asbestos and puncturing it afterwards. The furnace must be lagged to prevent its overheating or cracking the narrow trap. A difficulty is that the film condenses on a narrow zone of the glass and usually cracks it, presumably because the latent heat is set free in a small area. Moreover the hot glass gives off water and most of the film is spoilt. If the glass tube is very wide the film is better spread and gives little trouble, but a wide trap is probably ineffective. A long perforated delivery tube properly graded might give a longer film, but only a few tests have been made so far. Could an ionic drift of the vapour be effected by applying a suitable field? Another difficulty is that if the furnace is left inside the trap, outgassing of the cold asbestos and metal would be difficult, and further heating of the furnace would disperse the film. Removal after the admission of dry air would involve adsorption of gas by the film, which cannot be safely heated again. Removal in vacuo would be practicable but would involve some complication.

THE AUTHOR said that to his regret he was unable to suggest any solution of Mr Archer's problem.

AN X-RAY INVESTIGATION OF PURE IRON-NICKEL ALLOYS. PART 3: THE THERMAL EXPANSION OF ALLOYS RICH IN IRON

By E. A. OWEN, M.A., D.Sc., F.Inst.P., and E. L. YATES,
M.Sc., Ph.D., A.Inst.P., University College of North Wales, Bangor

Received 6 *January* 1937. *Read in title* 12 *February* 1937

ABSTRACT. This part of the paper deals with the measurement of the parameters of pure iron and iron-nickel alloys in the α phase at different temperatures ranging from room-temperature to 600° C. From these measurements the coefficients of thermal expansion of the alloys were determined. The thermal expansion of iron, 99·97-per-cent pure, was obtained at temperatures between 0 and 500° C. The lattice-parameter of iron of this purity at 15° C. was found to be $2{\cdot}8605_0$ A. and the coefficient of thermal expansion at this temperature to be $10{\cdot}7 \times 10^{-6}$ per ° C. At all temperatures the addition of nickel to iron at first lowered and afterwards increased the value of the thermal coefficient.

---

§ 1. INTRODUCTION

The iron-nickel alloys rich in iron present more difficulty than the other alloys in the system because they behave irreversibly when alternately heated and cooled. Different workers disagree also as to the extent of the pure α phase and the range of temperature over which irreversibility exists.

The investigations of Hanson and Hanson(1), Hanson and Freeman(2), Honda and Miura(3), Chevenard(4) and others lead to the equilibrium diagram shown in figure 1(5). According to this diagram alloys containing between 0 and about 30 per cent of nickel remain in the α condition until raised up to temperatures exceeding about 450° C.; the temperature at which the transformation to $(\alpha+\gamma)$ takes place rises from about 450° C. for an alloy containing 30 per cent nickel to 900° C. for pure iron. The temperature range over which the $(\alpha+\gamma)$ region exists is limited; the transformation to pure γ for a 30-per-cent-nickel alloy takes place at about 550° C., so that the range for this alloy is about 100° C. This range decreases as the nickel-content diminishes and it vanishes for pure iron at about 900° C. This state of affairs exists if the alloys are in the pure α condition initially. To get them into this state alloys having a nickel-content greater than about 15 per cent have to be specially heat-treated and have to be taken to low temperatures before finally being allowed to return to room-temperature.

If, on the other hand, an alloy in this region is raised initially to a high temperature, say of 1000° C., is allowed to reach a state of equilibrium at that temperature, and is then cooled slowly, the transformation from γ to $(\alpha+\gamma)$ does not take place until a temperature is reached which is much lower than the one at which the transformation $(\alpha+\gamma)$ to γ took place on heating. The difference between the transformation temperature on heating and that on cooling increases as the nickel-content of the alloys increases.

If, then, the alloys are in the α condition at ordinary temperatures, they can be raised to temperatures between 450 and 900° C., according to their composition, before they enter the $(\alpha+\gamma)$ region. It is advisable therefore to keep the annealing temperatures of the powders, before X-ray photographs are taken with them, below those corresponding with the boundary α, $(\alpha+\gamma)$ on heating. A good deal of work was done on these alloys before this was realized, for the equilibrium table available at the time was that published in the *International Critical Tables*. Our own investigation of the heat treatments of the alloys led us to adopt the course mentioned above before our attention had been drawn to the later diagram. A description of the heat treatments to which the alloys were submitted is given below.

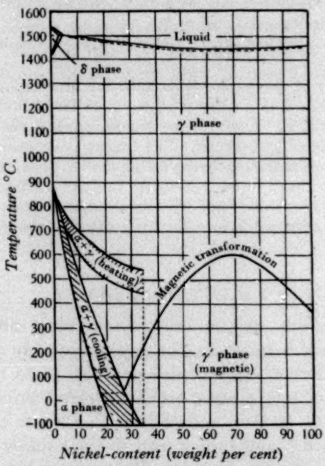

Figure 1. Equilibrium diagram of iron-nickel alloys.

In the present part of this paper an account is given of the work done on three alloys of composition ranging between 3 and 16 per cent of nickel. Pure iron also is considered. It is felt that much more work than has already been done is necessary on alloys at this end of the equilibrium diagram. The present contribution is therefore to be regarded as preliminary to a fuller investigation which is now in progress.

§ 2. COMPOSITION OF THE ALLOYS

Three alloys were investigated. They were kindly supplied by the Mond Nickel Company Limited and were prepared from pure materials. Their compositions are given in table 1.

Table 1. Composition of the alloys

Alloy	Nickel-content	
	Weight %	Atoms %
3	3·1	3·1
9	9·0	8·8
16	16·7	16·4

Iron, the purity of which was 99·966 per cent, was available. Its lattice-parameter at 18° C. had already been carefully measured in the laboratory(6), and it was now decided to investigate its thermal expansion up to 600° C., about the highest temperature attainable with the high-temperature camera which has been employed hitherto for all measurements above room-temperature.

§ 3. HEAT TREATMENT

A good deal of preliminary work had been carried out before this investigation on the heat treatment of these alloys by Mr C. W. Thompson, M.Sc.(7) of this laboratory. It was found that when a powdered alloy containing 3 per cent nickel was annealed for 3 hours at 600° C. in vacuo and cooled slowly to room-temperature in about 12 hours, well-defined lines were obtained at the greatest glancing angles, and accurate values of the lattice-parameters could be calculated from the measurements of the lines. It should be stated that all the alloys had been lump-annealed at 800° C. for periods ranging between 11 and 21 days and cooled over periods ranging between 6 and 16 days, and it had been found that further lump-annealing did not alter the lattice-parameters.

When powders of alloys containing 9 and 16 per cent of nickel were treated similarly to alloy 3, the lines at great glancing angles were badly defined and could not be measured with the necessary degree of precision. Annealing at 600° C. for 12 hours instead of 3 hours did not improve the definition. After this a detailed investigation of the heat treatment of alloy 16 was carried out, but the annealing temperature in the first instance was never less than 600° C. The powder was annealed at the high temperature for periods ranging from 24 to 192 hours and cooled down to room-temperature over periods ranging from 12 to 144 hours, but in every case the precision lines were unsatisfactory, being broad, faint and ill defined. When the annealing temperature was reduced to 500° C., lines were obtained which could be measured with tolerable accuracy. All the alloys described here were therefore annealed in powder form at 500° C. for 3 hours. In the hope of improving the lines obtained with alloy 16 the powder was further annealed at 300° C. for 24 hours, but little if any improvement was effected by this additional heat treatment. The precision lines in all cases were however measurable, but the accuracy of measurement with alloy 16 was not as great as with the other alloys. Spectrum photographs taken with the alloys at room-temperature showed them to possess body-centred cubic structure only. These results are in conformity with the equilibrium diagram of the alloy system shown in figure 1.

Powder was prepared from the sample of pure iron by two methods, (1) by filing, and (2) by rubbing on coarse glass paper and extracting the iron. By alternately passing the resulting powder through a 250-mesh sieve and extracting the iron with a magnet, iron powder free from contamination was prepared by the second method. Exposures taken with this specimen at 611° C. showed that the lattice-parameter was identical with that of specimens prepared by filing.

When photographs were taken with iron the procedure adopted was to heat the filings in an evacuated glass tube at 500° C. for 50 min. Excellent spectral lines were obtained after this heat treatment.

The usual procedure(8) was adopted in taking the X-ray photographs. The powders were raised to the required temperature in the evacuated chamber enclosing the camera, and the temperature was maintained for at least half an hour before the exposure was started.

Cobalt radiation* was used, reflections being obtained from the (310) planes of the body-centred cubic lattice of the α phase.

The thermocouple used to measure the temperature of the specimen exposed to X rays was carefully calibrated, and a check was frequently made on the calibration by taking exposures with silver raised to different temperatures. With the exception of the exposure made at 640° C. with iron, the accuracy of the temperature-measurement is considered to be within ± 1 per cent.

§ 4. RESULTS

Iron. Two different cameras were employed, one serving as a check on the other. The filings showed a tendency at the highest temperatures to become dark in colour and to lose their metallic lustre. When this occurred new filings were taken, but no change in the lattice-parameter was observed in consequence of the discoloration. The observed values of the lattice parameter at the temperatures stated are collected in table 2. Each value has been corrected for refractivity, as were all other values of lattice-parameters recorded in this paper.

The lattice-parameter values were plotted against the corresponding temperatures and a smooth curve was drawn through the points. The parameter-values given in table 3 were taken from this curve, and the coefficients of thermal expansion were calculated from tangents drawn to it.

The values of the coefficient of expansion are estimated to have an accuracy of ± 5 per cent. The same values of the coefficient of thermal expansion were obtained with a specimen of iron of 99·989-per-cent purity. There is good agreement between the values at the lower temperatures, and the recently published⁽⁹⁾ values of the coefficient of expansion of very pure iron at those temperatures.

---

* The wave-lengths taken were: $\mathrm{CoK}\alpha_1 = 1{\cdot}78529$ A., $\mathrm{CoK}\alpha_2 = 1{\cdot}78919$ A.

Table 2. Lattice-parameter of pure iron at various temperatures

Film number	Temperature (° C.)	Lattice-parameter (A.)	Film number	Temperature (° C.)	Lattice-parameter (A.)
E 632	14	$2{\cdot}8604_8$	E 631	261	$2{\cdot}8697_0$
E 641	15	$2{\cdot}8605_6$	E 179	294	$2{\cdot}8707_4$
E 177	16	$2{\cdot}8604_4$	E 636	315	$2{\cdot}8719_5$
E 176	18	$2{\cdot}8605_2$	E 627	366	$2{\cdot}8740_0$
E 185	22	$2{\cdot}8607_0$	E 182	391	$2{\cdot}8751_4$
E 181	36	$2{\cdot}8610_9$	E 634	417	$2{\cdot}8764_3$
E 178	98	$2{\cdot}8632_3$	E 630	476	$2{\cdot}8791_7$
E 633	147	$2{\cdot}8651_0$	E 180	488	$2{\cdot}8798_9$
E 183	195	$2{\cdot}8669_5$	E 642	530	$2{\cdot}8817_2$
E 635 E 638	208	$2{\cdot}8674_0$	E 628	576	$2{\cdot}8842_7$
			E 640	640	$2{\cdot}8883_5$

Table 3. Coefficient of thermal expansion of pure iron

Temperature (° C.)	Lattice-parameter (A.)	True coefficient of expansion × 10⁶
0	$2{\cdot}8600_3$	10·5
15	$2{\cdot}8605_0$	10·7
100	$2{\cdot}8633_3$	12·0
200	$2{\cdot}8671_5$	13·5
300	$2{\cdot}8711_8$	14·7
400	$2{\cdot}8755_5$	15·8
500	$2{\cdot}8803_6$	16·9
600	$2{\cdot}8854_4$	18·0*

* Extrapolated.

Alloy 3. This alloy according to all the equilibrium diagrams is well within the region of the α phase at all temperatures up to about 600° C. A powder photograph of the sample taken at room-temperature showed that its structure was body-centred cubic, which is the structure of the α-phase alloys.

The crystal lattice was measured over a range of temperature extending from room-temperature to about 600° C. The fact that a smooth curve was obtained when the parameter-values were plotted against temperature indicates that the alloy remained in the α region throughout this range of temperature. It was impracticable to measure the lattice-dimensions at temperatures higher than 600° C. with the camera employed, and so the change taking place at the α, $(\alpha+\gamma)$ boundary for this alloy could not be investigated. Well-defined spectral lines were obtained over the whole range of temperature, those at high temperatures being of weaker intensity owing to the heat motion of the atoms but still quite strong enough for accurate measurement. X-ray exposures of 15 min. were found to be ample.

Table 4. Lattice-parameters of α iron-nickel alloys at various temperatures

Alloy	3			9			16	
Nickel-content (per cent by weight)	3·1			9·0			16·7	
Film number	Temperature (° C.)	Lattice-parameter (A.)	Film number	Temperature (° C.)	Lattice-parameter (A.)	Film number	Temperature (° C.)	Lattice-parameter (A.)
E 186	16	$2{\cdot}8620_6$	E 224	15	$2{\cdot}8634_2$	E 243	13	$2{\cdot}8628_1$
E 190 E 197	17	$2{\cdot}8621_9$	E 206 E 207	16	$2{\cdot}8634_1$	E 248	14	$2{\cdot}8629_3$
E 194	18	$2{\cdot}8622_7$	E 198	17	$2{\cdot}8634_8$	E 241	15	$2{\cdot}8630_9$
E 191	101	$2{\cdot}8650_1$	E 203 E 217	18	$2{\cdot}8633_9$	E 225 E 240	16	$2{\cdot}8628_7$
E 187	199	$2{\cdot}8683_8$	E 200 E 208	20	$2{\cdot}8635_2$	E 231 E 232	17	$2{\cdot}8630_8$
E 193	301	$2{\cdot}8723_1$	E 202	100	$2{\cdot}8663_1$	E 227 E 229	18	$2{\cdot}8631_0$
E 219	360	$2{\cdot}8748_6$	E 199	203	$2{\cdot}8696_2$	E 234	100	$2{\cdot}8655_4$
E 188	393	$2{\cdot}8761_9$	E 210	294	$2{\cdot}8728_1$	E 235	200	$2{\cdot}8687_4$
E 195	444	$2{\cdot}8786_7$	E 209	295	$2{\cdot}8727_4$	E 233	304	$2{\cdot}8724_3$
E 218	457	$2{\cdot}8785_6$	E 201	296	$2{\cdot}8729_5$	E 226 E 228 E 230	306	$2{\cdot}8728_4$
E 192	489	$2{\cdot}8808_2$	E 220	340	$2{\cdot}8741_2$	E 246	340	$2{\cdot}8741_1$
E 196	522	$2{\cdot}8822_6$	E 200 E 223	394	$2{\cdot}8765_1$	E 247	345	$2{\cdot}8741_7$
E 189	575	$2{\cdot}8840_7$	E 203	416	$2{\cdot}8774_5$	E 245	350	$2{\cdot}8744_1$
			E 222	470	$2{\cdot}8793_4$	E 244	380	$2{\cdot}8757_4$
			E 204 E 205	502	$2{\cdot}8807_9$	E 238	418	$2{\cdot}8771_4$
			E 213	556	$2{\cdot}8827_7$	E 242	456	$2{\cdot}8787_6$
			E 212	600	$2{\cdot}8845_0$	E 239	501	$2{\cdot}8803_4$
						E 236	598	$2{\cdot}8840_1$

Table 5. Coefficient of thermal expansion of α iron-nickel alloys at various temperatures.

Temperature	Alloy 3		Alloy 9		Alloy 16	
	Lattice-parameter	Coefficient of expansion × 10⁶	Lattice-parameter	Coefficient of expansion × 10⁶	Lattice-parameter	Coefficient of expansion × 10⁶
0	$2{\cdot}8616_2$	10·9	$2{\cdot}8629_0$	10·9	$2{\cdot}8625_0$	10·3
15	$2{\cdot}8621_2$	11·0	$2{\cdot}8633_8$	11·0	$2{\cdot}8629_6$	10·4
100	$2{\cdot}8649_4$	11·7	$2{\cdot}8661_7$	11·5	$2{\cdot}8655_2$	11·2
200	$2{\cdot}8684_5$	12·8	$2{\cdot}8695_2$	12·1	$2{\cdot}8689_3$	11·9
300	$2{\cdot}8722_7$	13·7	$2{\cdot}8730_3$	$12{\cdot}7_5$	$2{\cdot}8725_0$	12·7
400	$2{\cdot}8763_9$	14·8	$2{\cdot}8767_9$	13·3	$2{\cdot}8763_8$	13·5
500	$2{\cdot}8809_2$	16·0	$2{\cdot}8806_2$	13·7	$2{\cdot}8803_7$	14·2
600	$2{\cdot}8857_0$	17·0	$2{\cdot}8845_4$	14·2	$2{\cdot}8845_0$	14·9

Alloy 9. According to the equilibrium diagram reproduced in figure 1 this alloy is in the region of the α phase, and when it is heated it remains in the α phase up to a temperature of about 600° C. A spectrum photograph taken with this alloy showed that at room-temperature its structure was body-centred cubic, and in all the photographs taken at higher temperatures no indication of the presence of the γ phase was observed, the lines registered in the photographs being accounted for by the body-centred α phase. Well-defined lines were obtained from the (310) planes with cobalt radiation.

Alloy 16. This alloy also is in the α-phase region. It was observed that the α structure existed at all temperatures up to the highest temperature at which the alloy was examined. This is in agreement with the equilibrium diagram in figure 1 but in disagreement with the phase diagram published in the *International Critical Tables*, according to which the alloy should be in the mixed $(\alpha+\gamma')$ region at ordinary temperatures, transforming to $(\alpha+\gamma)$ at 345° C. and into pure γ at a temperature of about 440° C. No change in phase was detected in the present investigation as the alloy was heated to higher temperatures. It is worthy of note that Chevenard also gives for a 17·2-per-cent iron-nickel alloy a thermal-expansion curve which is smooth up to 550° C.; this shows that the α structure existing at room-temperature probably is not transformed to another phase below this temperature.

It was noted that after the exposure at 598° C. the crystal lattice was much too distorted to yield spectral lines after the material had cooled to room-temperature. This fact suggests that the alloy was already undergoing some structural change at 598° C. and that the change was not complete when the specimen started cooling in the camera enclosure. It should be stated that all the specimens after exposure to X rays at high temperatures were allowed to cool to room-temperature in the camera enclosure in which a vacuum was maintained. When this procedure was adopted the material did not become oxidized and could be used for several exposures.

Poor spectral lines were obtained with alloy 16 at all temperatures, and the measurement of the films was rendered somewhat difficult in consequence. The first seven exposures (E 225 to E 231 inclusive) were made with powder which had been annealed at 500° C. for 3 hours.

The observed lattice-parameters of the alloys at various temperatures are given in table 4, and the coefficients of thermal expansion calculated from them in table 5. It will be observed that the parameter of alloy 16 at room-temperature is less than that of alloy 9, but that the coefficient of thermal expansion increases more rapidly with temperature for alloy 16 than for alloy 9.

These preliminary measurements of the lattice-parameters of the α iron-nickel alloys show that if the material is in the α condition at room-temperature it remains in this condition at all temperatures up to 600° C. in alloys which contain up to about 17 per cent of nickel. This is in accordance with the equilibrium diagram, figure 1. More readings on alloys which have been subjected to varied heat treatments are necessary before it will be possible to make any very definite statements regarding the behaviour of these α alloys and the exact disposition of the phases existing in this part of the equilibrium diagram. The few observations recorded here do, however, confirm, though not as adequately as could be desired, certain features of the equilibrium diagram shown in figure 1. Further work on these alloys is now in progress.

§ 5. ACKNOWLEDGEMENTS

See page 324 of this volume.

REFERENCES

(1) Hanson and Hanson. *J. Iron Steel Inst.* **102**, 39 (1920).
(2) Hanson and Freeman. *J. Iron Steel Inst.* **107**, 301 (1923).
(3) Honda and Miura. *Trans. Amer. Soc. Steel Treat.* **13**, 270 (1928).
(4) Chevenard. *Rev. de Mét.* **11**, 841 (1914); **14**, 618 (1917); *C.R. Acad. Sci.*, Paris, **159**, 53 (1914); **170**, 1499 (1920); **171**, 93 (1920); **172**, 594 (1921); **174**, 109 (1922).
(5) Merica. *National Metals Handbook*, p. 607 (1930).
(6) Owen and Yates. *Phil. Mag.* **15**, 472 (1933).
(7) Thompson. Thesis submitted for the degree of M.Sc. of the University of Wales.
(8) Owen and Yates. *Proc. phys. Soc.* **49**, 17 (1937).
(9) Adcock and Bristow. *Proc. roy. Soc.* A, **153**, 172 (1935).

AN X-RAY INVESTIGATION OF PURE IRON-NICKEL ALLOYS. PART 4: THE VARIATION OF LATTICE-PARAMETER WITH COMPOSITION

By E. A. OWEN, M.A., Sc.D., D.Sc., F.Inst.P., E. L. YATES, M.Sc., Ph.D., A.Inst.P. and A. H. SULLY, M.Sc.

Received 6 *January* 1937. *Read in title* 12 *February* 1937

ABSTRACT. In this part of the paper the variations of lattice-parameter with the composition of the alloys is considered. Twenty alloys in the γ phase ranging in composition from 23 to 97 atomic per cent of nickel, and four alloys in the α phase ranging in composition from 3 to 16 atomic per cent of nickel were studied at different temperatures. At room-temperature, when iron is added to nickel the nickel lattice expands almost linearly with the atomic composition until the lattice-parameter reaches a maximum value of 3·5895 A. for an alloy the composition of which is 39 atomic per cent of nickel. On further addition of iron the lattice contracts. The variation of the parameter of the γ alloys with composition was examined at temperatures ranging up to 600° C. From the values of the lattice parameters the densities of pure iron-nickel alloys over the whole range of composition from pure iron to pure nickel were calculated.

§ 1. VARIATION OF THE LATTICE-PARAMETER WITH COMPOSITION OF γ-PHASE ALLOYS AT ROOM-TEMPERATURE

Twenty alloys ranging in composition from 23 to 97 atomic per cent of nickel were examined with the precision and spectrum cameras at room-temperature. Particular attention was paid to alloys of composition in the neighbourhood of 36 per cent of nickel. The alloys were all given initially a heat treatment in lump form—some were maintained at 1150° C. for 20 hours in a nitrogen atmosphere, others at the same temperature for 8 hours in vacuo, and others at 800° C. for some days in vacuo. The standard treatment adopted with the filings taken from the ingots was to heat them for 14 hours at 600° C. After this heat treatment some of the samples were quenched in iced water and others cooled to room temperature in 120 hours before their parameters were measured. It was found that with all the alloys containing more than about 28 per cent of nickel the same lattice-parameter values were obtained whether the alloys were quenched or slowly cooled. This behaviour is characteristic of unsaturated solid solutions. The γ phase exists alone, therefore, in all alloys containing more nickel than about 28 per cent.

The results of the measurements are collected in table 1. Each parameter-value included in the table is the mean of several determinations obtained with quenched and slowly cooled specimens.

The lattice-parameters are plotted against the compositions of the alloys in figure 1. The lattice-parameter of nickel increases when iron is added. This is in

Table 1. Lattice-parameters of γ-phase iron-nickel alloys at 15° C.

Nickel-content of alloy		Lattice-parameter of γ phase at 15° C.	Nickel-content of alloy		Lattice-parameter of γ phase at 15° C.
Weight per cent	Atoms per cent		Weight per cent	Atoms per cent	
100	100	3·5171$_3$	42·71	41·75	3·5882$_7$
96·75	96·6	3·5206$_6$	40·66	39·7	3·5894$_0$
93·95	93·8	3·5241	38·42	37·5	3·5895$_4$
91·04	90·8	3·5278	37·17	36·3	3·5884$_0$
82·86	82·2	3·5378	35·10	34·3	3·5858$_6$
74·00	72·8	3·5494	33·59	32·65	3·5833$_4$
63·82	62·6	3·5626	32·20	31·4	3·5807$_5$
58·41	57·0	3·5691	31·67	30·9	3·5796$_5$
52·15	50·75	3·5779	30·30	29·7	3·5768$_9$
48·00	46·7	3·5828$_4$	28·12	27·5	3·5743$_1$
45·50	44·3	3·5858$_6$	24·22	23·4	3·5732$_8$

accordance with expectation, as solution takes place by substitution and the atomic volume of iron is greater than that of nickel. The lattice-parameter increases almost linearly with composition for alloys between pure nickel and 40 per cent of nickel. There seems however to be a slight departure from strict linearity, the alloys showing a small contraction the maximum value of which occurs in an alloy containing about 78 atomic per cent of nickel.

The lattice-parameter at 15° C. reaches a maximum value of 3·5895 A. for an alloy containing 39 atomic per cent of nickel. It then diminishes at almost the same rate as that at which it previously increased with increase of iron-content, and reaches a minimum value of 3·5732 A. The composition corresponding to the intersection of the horizontal line through the γ lattice-parameter of the alloy containing 24·2 per cent of nickel, which also contained the α constituent in the specimen as prepared, and the line representing the slope of the left-hand limb of the {parameter, composition} curve is 28 atomic per cent of nickel. It is interesting to note that the boundary $(\alpha+\gamma)$, γ in figure 1 of part 3 (p. 308 of this volume) corresponds to a composition of 28 per cent of nickel at about 20° C. for an alloy which is cooled from above about 550° C. down to room-temperature.

The above results are in approximate agreement with the work of Phragmén(1) on nickel steels of low thermal expansion and ranging in composition from 29 to 50 per cent of nickel. Phragmén finds that the maximum occurs at 38 per cent of nickel by weight, and that the value of the parameter at the maximum is 3·5883 A. at 10° C. Jette and Foote(2) find that the maximum occurs at about 39 atomic per cent nickel and that the value of the parameter at the maximum is 3·5884 at 25° C. These results are all in satisfactory agreement, although the lattice-parameter at the maximum is a little higher according to the present measurements, and whereas Jette and Foote find a strictly linear relation between parameter and composition in atomic per cent of nickel from pure nickel to the maximum, a slight contraction is now observed. The values of the parameters at various compositions are however on the whole in good agreement when reduced to the same temperature.

It is noteworthy that the lattice-parameter of taenite, the γ structure found in meteorites composed of iron and nickel alone, is about 3·59 A.(3), the parameter corresponding to the maximum of the {parameter, composition} curve and an alloy containing 40 per cent of nickel by weight. This would point to the stability of alloy 40, which has an open structure and is able to take into solution either iron or nickel, both metals on solution decreasing the dimensions of the lattice.

The conclusions reached from this part of the investigation carried out on alloys at 15° C. are that: (1) when iron is added to nickel, the nickel lattice which is face-centred cubic expands almost linearly with the atomic composition of the alloy; (2) the lattice-parameter reaches a maximum value of 3·5895 A. for an alloy, the composition of which is 39 atomic per cent of nickel; (3) on further addition of iron, the lattice contracts again almost linearly with composition, reaching a minimum value of 3·5732 A.

§ 2. VARIATION OF LATTICE-PARAMETER OF α-PHASE ALLOYS AT ROOM-TEMPERATURE WITH COMPOSITION

A preliminary study of the variation of the lattice-parameters of the α-phase alloys at room-temperature was made with five alloys ranging in composition from 3 to 24 per cent of nickel. According to the equilibrium diagram in figure 1 of part 3 (p. 308 of this volume) all the alloys except alloy 24 were in the region of the α phase at room-temperature. The behaviour of alloy 24 was considered in part 2, when it was found that both the α and γ phases were present. The expansion of each phase was examined, the α phase disappearing at about 350° C. and leaving only the γ phase. The other alloys remained in the α phase from room-temperature up to 600° C., the lattice-parameters at the higher temperatures are given in part 3, except for alloy 6 which was examined at room-temperature only. Table 2 contains a summary of the lattice-parameters at 15° C. of the α alloys so far examined,

Table 2. Lattice-parameters of α-phase iron-nickel alloys at 15° C.

Alloy	Nickel-content of alloy		Lattice-parameter of α phase at 15° C.
	Weight per cent	Atoms per cent	
24	24·2	23·5	2·8630
16	16·7	16·4	$2{\cdot}8629_6$
9	9·0	8·8	$2{\cdot}8633_8$
6	6·0	5·9	2·8629
3	3·1	3·1	$2{\cdot}8621_2$
Fe	0·0	0·0	$2{\cdot}8605_0$

and it will be seen that, contrary to expectation, the iron lattice expands when nickel is added, and the increase in parameter does not bear even an approximately linear relation to the composition of the alloys. In addition the parameter reaches a maximum value and then decreases to a steady value for alloys 16 and 24.

The heat treatment given to the alloys has already been described. It will be necessary, as has already been stated, to vary and extend the heat treatment in order to arrive at more definite information concerning these α alloys.

§ 3. VARIATION OF THE LATTICE-PARAMETER OF γ-PHASE ALLOYS AT VARIOUS TEMPERATURES UP TO 600° C. WITH COMPOSITION

The values of the lattice-parameters of the γ phase in alloys of different compositions at temperatures ranging from 15° to 600° C. are collected in table 3.

Table 3. Parameters of iron-nickel alloys at different temperatures

Alloy	Nickel-content	Parameter (A.)						
	Atoms per cent	15° C.	100° C.	200° C.	300° C.	400° C.	500° C.	600° C.
				γ phase				
Ni	100	3·5171$_3$	3·5212$_8$	3·5263$_7$	3·5317$_7$	3·5384$_2$	3·5446$_2$	3·5508$_7$
97	96·6	3·5206$_5$	3·5246$_1$	3·5294$_0$	3·5347$_0$	3·5409$_2$	3·5467$_9$	3·5526$_8$
94	93·8	3·5240$_5$	3·5280$_0$	3·5328$_3$	3·5381$_8$	3·5443$_5$	3·5504$_0$	3·5561$_8$
91	90·8	3·5277$_5$	3·5316$_7$	3·5365$_8$	3·5418$_0$	3·5478$_0$	3·5543$_8$	3·5601$_7$
83	82·2	3·5378$_0$	3·5417$_0$	3·5466$_2$	3·5518$_0$	3·5572$_0$	3·5630$_0$	3·5691$_0$
74	72·8	3·5491$_6$	3·5529$_8$	3·5576$_4$	3·5625$_6$	3·5676$_1$	3·5730$_2$	3·5787$_3$
58	57·0	3·5690$_8$	3·5728	3·5771$_7$	3·5816$_0$	3·5861$_2$	3·5905$_2$	3·5950
45	44·3	3·5855$_7$	3·5879$_0$	3·5905$_7$	3·5928$_7$	3·5954$_6$	3·5993$_0$	3·6061$_3$
43	41·75	3·5882$_7$	3·5893$_3$	3·5910$_0$	3·5927$_2$	3·5956$_0$	3·6009$_2$	3·6067$_3$
35	34·3	3·5855$_6$	3·5863$_0$	3·5875$_5$	3·5914$_8$	3·5974$_7$	3·6036$_9$	3·6099$_9$
32	31·2	3·5812$_5$	3·5825$_7$	3·5860$_7$	3·5916$_8$	3·5979$_0$	3·6042$_0$	3·6105$_6$
24	23·4	3·5733	3·5809	3·5872	3·5934	3·5997	3·6059$_4$	3·6122
				α phase				
24	23·4	2·8630	2·8655	2·8686	2·8721	—	—	—
16	16·4	2·8629$_6$	2·8655$_2$	2·8689$_3$	2·8725$_0$	2·8763$_8$	2·8803$_7$	2·8844$_0$
9	8·8	2·8633$_8$	2·8661$_7$	2·8695$_2$	2·8730$_3$	2·8767$_9$	2·8806$_2$	2·8845$_4$
3	3·1	2·8621$_2$	2·8649$_4$	2·8684$_5$	2·8722$_7$	2·8763$_9$	2·8809$_3$	2·8857$_0$
Fe	0·0	2·8605$_0$	2·8633$_9$	2·8671$_8$	2·8712$_3$	2·8756$_0$	2·8803$_3$	2·8855$_4$

When the results are plotted, figure 1, it is observed that the maximum becomes less pronounced as the temperature is raised, and with increase of temperature it is displaced in the direction of lower nickel-content. At 600° C. the maximum has disappeared, but at this temperature the rate of increase of the lattice-parameter with decrease in nickel-content is much less below about 40 per cent of nickel than it is for higher percentages of nickel. It was impossible with the camera used in the investigation to reach temperatures higher than about 600° C., but it is desirable to extend this work to higher temperatures.

The parameters and the compositions corresponding to the maxima at various temperatures are included in table 4.

Table 4

Temperature (°C.)	Lattice-parameter at maximum	Nickel-content (atoms per cent) at maximum
15	3·5895	39·0
100	3·5898	40·5
200	3·5912	42·0
300	3·5930	43·5
400	3·5952	45·0

The rate at which the lattice-parameter increases with decrease of nickel-content is about the same at all the temperatures investigated up to the maximum, but the rate varies considerably for different temperatures after this.

It is important to note that all the alloys containing more than about 30 atomic per cent of nickel give the same parameter at room-temperature whether they are quenched or slowly cooled. This fact shows that the alloys are unsaturated and are therefore in the pure phase, so that an explanation of the maximum on the supposition that supersaturation occurs is untenable.

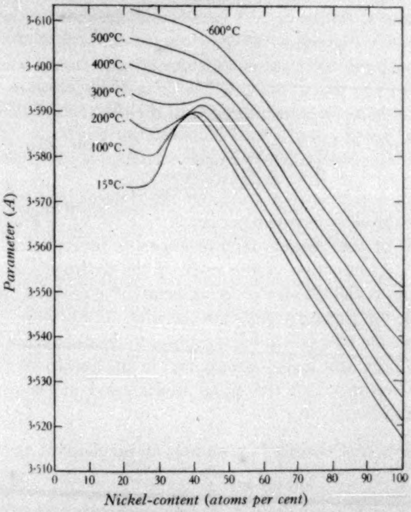

Figure 1. Parameters of γ alloys at different temperatures.

§4. VARIATION OF THE LATTICE-PARAMETER OF α-PHASE ALLOYS AT VARIOUS TEMPERATURES UP TO 600° C. WITH COMPOSITION

The values of the α-phase parameters for the alloys examined are included in table 3. The form of the curves at the higher temperatures is the same as that at room-temperature; a maximum value of the parameter is reached and then there is a drop to a steady value. The position of the maximum moves in the direction of lower nickel-content as the temperature is increased; at 15° C. it occurs for an alloy containing about 11·5 atomic per cent of nickel, while at 500° C. the composition corresponding to the maximum is 5 atomic per cent of nickel. The maximum with the α alloys therefore moves towards higher iron-content and that with the γ alloys towards higher nickel-content as the temperature is increased. The ascending limb of the curve for the α alloys is not a straight line over any portion of its length. The descending part of this curve changes its direction at points corresponding to progressively lower nickel-content as the temperature rises. This point of discontinuity in the curve may prove to be the position of the boundary between α and (α+γ) phases, but further observations on more alloys are necessary before any definite statement can be made.

§ 5. DENSITIES OF PURE IRON-NICKEL ALLOYS

The accurate values of lattice-parameters provide data for the calculation of the densities of the alloys. In the density calculations the mass of the hydrogen atom was taken to be $(1{\cdot}662 \pm 0{\cdot}002) \times 10^{-24}$ g. If the atomic weight of hydrogen is taken to be 1·0078 ($O = 16{\cdot}00$), the mass of an atom of unit atomic weight m is $(1{\cdot}649_1 \pm 0{\cdot}002) \times 10^{-24}$ g. The atomic weights⁽⁴⁾ of iron and nickel are 55·84 and 58·69 respectively. The density was calculated with the aid of the following formula:

$$\rho = \frac{n}{a^3}\{58{\cdot}69x + (100 - x)\,55{\cdot}84\}\frac{m}{100},$$

where a is the lattice-parameter, n is the number of atoms per unit cube and x is the nickel-content of the alloy in atoms per cent.

The accuracy of the density-determinations is limited considerably by the accuracy of the determination of the mass of the hydrogen atom. An error of $\pm 0{\cdot}0003$ A. in the lattice-parameter or an error of $\pm 0{\cdot}05$ in the atomic weight introduces an error of $\pm 0{\cdot}005$ g./cm.³ in the density. The error of $\pm 0{\cdot}002 \times 10^{-24}$ g. in the mass of the atom with unit atomic weight introduces an error of $\pm 0{\cdot}009$ g./cm.³ in the density of pure iron and $\pm 0{\cdot}011$ g./cm.³ in the density of pure nickel. The values of the densities of all the alloys investigated at room-temperature are included in table 5.

Table 5. Densities of pure iron-nickel alloys at 15° C.

Nickel-content (atoms per cent)	Density at 15° C. (g./cm.³)	Nickel-content (atoms per cent)	Density at 15° C. (g./cm.³)
	γ phase		
100	$8{\cdot}89_8$	41·75	$8{\cdot}14_3$
96·6	$8{\cdot}85_7$	39·7	$8{\cdot}12_7$
93·8	$8{\cdot}81_9$	37·5	$8{\cdot}11_7$
90·8	$8{\cdot}77_8$	36·3	$8{\cdot}12_0$
82·2	$8{\cdot}66_8$	34·3	$8{\cdot}12_9$
72·8	$8{\cdot}54_4$	32·6₅	$8{\cdot}13_9$
62·6	$8{\cdot}40_7$	31·4	$8{\cdot}15_2$
57·0	$8{\cdot}33_8$	30·9	$8{\cdot}15_7$
50·75	$8{\cdot}25_1$	29·7	$8{\cdot}17_1$
46·7	$8{\cdot}20_0$	27·5	$8{\cdot}18_0$
44·3	$8{\cdot}16_9$	23·4	$8{\cdot}17_0$
	α phase		
23·4	$7{\cdot}94_2$	5·9	$7{\cdot}87_8$
16·4	$7{\cdot}91_4$	3·1	$7{\cdot}86_8$
8·8	$7{\cdot}88_2$	α-Iron	$7{\cdot}86_9$

As the nickel-content decreases the density of the γ alloys decreases and reaches a minimum value of about 8·12 g./cm.^{3} when the nickel-content is 37·5 atomic per cent. When the nickel-content is lowered still further, the density increases and reaches a maximum value of 8·18 g./cm.^{3} at a composition of about 27·5 atomic per cent of nickel. The density of the α alloys increases gradually as the nickel-content increases.

The characteristics of the density curve are similar to those of the curve determined by Chevenard(5), but in the present work the curve of the α alloys is not a straight line. The density curve of the γ alloys is however very similar to that determined by Chevenard and by Jette and Foote(2); there is very close agreement between the values of the densities determined by Jette and Foote and the present values for the γ alloys.

In table 6 are included the values of the densities of the iron-nickel alloys at 200, 400 and 600° C. calculated from the parameter-values at these temperatures appearing in table 3. When the results at 600° C. are plotted, the density of the γ alloys shows a continuous fall as the nickel-content decreases; this differs from the curve of densities at 15° C., which shows a minimum value. The α alloys show at 600° C. as at 15° C. a steady increase in density with increase of nickel-content.

Table 6. Densities of pure iron-nickel alloys at various temperatures

Nickel-content (atoms per cent)	Density (g./cm.^{3})		
	At 200° C.	At 400° C.	At 600° C.
	γ alloys		
100 (Ni)	$8{\cdot}82_9$	$8{\cdot}73_9$	$8{\cdot}64_7$
96·6	$8{\cdot}79_1$	$8{\cdot}70_6$	$8{\cdot}62_0$
93·8	$8{\cdot}75_4$	$8{\cdot}66_9$	$8{\cdot}58_3$
90·8	$8{\cdot}71_4$	$8{\cdot}63_1$	$8{\cdot}54_1$
82·2	$8{\cdot}60_3$	$8{\cdot}52_7$	$8{\cdot}44_2$
72·8	$8{\cdot}48_4$	$8{\cdot}41_3$	$8{\cdot}33_5$
57·0	$8{\cdot}28_1$	$8{\cdot}21_9$	$8{\cdot}15_9$
44·3	$8{\cdot}13_7$	$8{\cdot}10_4$	$8{\cdot}03_2$
$41{\cdot}7_5$	$8{\cdot}12_4$	$8{\cdot}09_3$	$8{\cdot}01_8$
34·3	$8{\cdot}11_7$	$8{\cdot}05_0$	$7{\cdot}96_7$
31·4	$8{\cdot}11_6$	$8{\cdot}03_6$	$7{\cdot}95_1$
23·4	$8{\cdot}07_5$	$7{\cdot}99_1$	$7{\cdot}90_9$
	α alloys		
23·4	$7{\cdot}89_5$	—	—
16·4	$7{\cdot}86_5$	$7{\cdot}80_4$	$7{\cdot}73_9$
8·8	$7{\cdot}83_0$	$7{\cdot}77_1$	$7{\cdot}70_8$
3·1	$7{\cdot}81_5$	$7{\cdot}75_1$	$7{\cdot}67_6$
0·0 (Fe)	$7{\cdot}81_4$	$7{\cdot}74_5$	$7{\cdot}66_6$

§ 6. ACKNOWLEDGEMENTS

See p. 325 of this volume.

REFERENCES

(1) Phragmén. *J. Iron Steel Inst.* **123**, 465 (1931).
(2) Jette and Foote. *Metals Technology*, **3** (1936), Tech. Publ. No. 670.
(3) Young. *Proc. roy. Soc.* A, **112**, 630 (1926).
(4) Guillaume. *Proc. phys. Soc.* **32**, 374 (1920).
(5) Chevenard. *Rev. de Mét.* **11**, 841 (1914); **14**, 618 (1917); *C.R. Acad. Sci.*, Paris, **159**, 53 (1914); **170**, 1499 (1920); **171**, 93 (1920); **172**, 594 (1921); **174**, 109 (1922).

AN X-RAY INVESTIGATION OF PURE IRON-NICKEL ALLOYS. PART 5: THE VARIATION OF THERMAL EXPANSION WITH COMPOSITION

By E. A. OWEN, M.A., D.Sc., F.Inst.P., E. L. YATES, M.Sc., Ph.D., A.Inst.P. and A. H. SULLY, M.Sc.

Received 6 *January* 1937. *Read in title* 12 *February* 1937

ABSTRACT. The variation of the thermal coefficient of expansion with composition of the γ alloys, as deduced from measurements of crystal parameters, agrees in the main with that found by Guillaume and by Chevenard, who made measurements on rods of the materials. Certain divergences, which may be due to differences in the purities of the alloys employed in the different investigations, have been observed.

---

§ 1. VARIATION OF THE THERMAL COEFFICIENT OF EXPANSION OF IRON-NICKEL ALLOYS AT ROOM-TEMPERATURE WITH COMPOSITION

The measurements already made on the lattice-parameters of the iron-nickel alloys in the course of the present investigation provide sufficient data to follow the variation of the coefficient of expansion of the alloys when the composition is altered. We shall consider first the coefficients of expansion of the various alloys at room-temperature, which are shown in figure 1. The portion *ADBE* of the curve refers to the γ alloys and has been thoroughly investigated by Guillaume(1) and by Chevenard(2). The curve now determined shows the same characteristics as the curves determined by these authors. The coefficient of expansion shows at first a gradual decrease with decrease in nickel content; at about 50 per cent of nickel the value of the coefficient drops rapidly, reaching a minimum value for a composition of about 36 atomic per cent of nickel; it then rises rapidly as the nickel-content is further decreased. In the present instance the curve is shown rising to a value $18{\cdot}2 \times 10^{-6}$ at 28 atomic per cent of nickel. The assumption is made that the boundary γ, $(\gamma+\alpha)$ is situated at 28 atomic per cent of nickel for alloys which have been cooled slowly or quenched from temperatures above 600° C. to room-temperature. Alloy 24 has been found to contain both the α and the γ phases, and the latter if present at room-temperature expands uniformly up to the highest temperature (600° C.) reached in the present investigation. The value of its coefficient of expansion is $18{\cdot}2 \times 10^{-6}$. At 15° C. the region between about 28 and 18·6 atomic per cent of nickel is a duplex region, the latter figure being the composition which contains the saturated α phase. It was found that the coefficient of expansion at 15° C. of the α phase in alloy 24 was $10{\cdot}1 \times 10^{-6}$, which is therefore the coefficient of expansion of the saturated α phase at 15° C. Hence between *C* and *A* in the expansion curve of figure 1 the alloy expands as a mixture of phases, the coefficient of expansion of the saturated pure γ phase being represented by the point A and that of the saturated pure α phase by the point C. Between C and pure iron, the results obtained with alloys reported in part 3 of this paper are shown.

The absolute values of the coefficient of expansion of the γ-phase alloys do not differ greatly from the values given by Guillaume(1). Some difference between the values in the two investigations is to be anticipated because the purities of the materials differ quite appreciably. In Guillaume's work the iron-nickel alloys contained 0·4 per cent of manganese and 0·1 per cent of carbon by weight, whereas in the present work the materials used in making the alloys gave on analysis the following figures:

Nickel. Nickel 99·94, copper 0·008, iron 0·028, carbon 0·011, sulphur 0·004 per cent.

Iron. Iron 99·84, carbon 0·034, sulphur 0·012, manganese 0·10, phosphorus 0·014 per cent, silicon a trace.

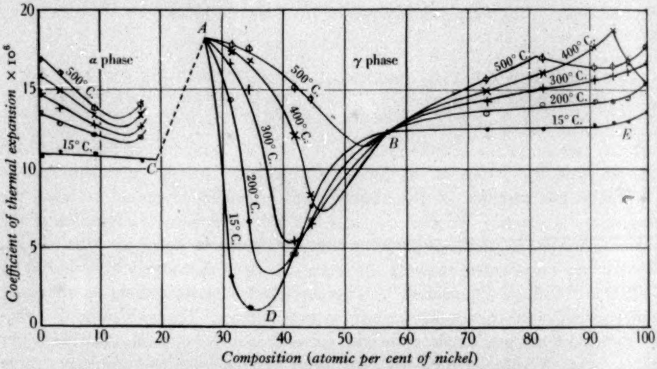

Figure 1. Coefficient of thermal expansion of iron-nickel alloys.

It should be emphasized that the part of the curve representing the coefficient of expansion of the α alloys refers to material which has been brought from high temperature (above about 600° C.) to room-temperature. The shape of the curve might have to be modified, especially in the region AC, if the alloys were quenched to temperatures much below atmospheric temperature and then brought up slowly to room-temperature. This point is now being investigated.

§2. VARIATION OF THE COEFFICIENT OF THERMAL EXPANSION OF IRON-NICKEL ALLOYS AT VARIOUS TEMPERATURES WITH COMPOSITION

The values of the coefficients of thermal expansion of the alloys examined at various temperatures are plotted against composition in figure 1. The curves are similar in form to those published by Chevenard(2), the differences between the two sets of curves being probably due to the difference between the purities of the alloys used in the two investigations. Since alloy 58 shows a uniform coefficient of expansion over the whole range of temperature investigated, all the curves pass through the point *B*. They all pass also through the point *A*, since the alloy in question expands uniformly over the whole temperature range.

The α alloys also are included in the curves shown in figure 1. These curves might need modification if a different heat treatment were given to the alloys. As the nickel-content increases the coefficient of expansion of the α alloys diminishes, and it reaches a minimum value at a composition which corresponds to a lower percentage of nickel the higher the temperature. When still more nickel is added the value of the coefficient of thermal expansion increases. At 15° C. it increases to $18{\cdot}2 \times 10^{-6}$, the value corresponding to the point *A*. How the other curves converge to this point will be decided when further measurements on alloys in the region *CA* have been carried out. Pure iron-nickel alloys containing respectively 20 and 25 per cent of nickel should have at 15° C. coefficients of thermal expansion of about $11{\cdot}5 \times 10^{-6}$ and 16×10^{-6} when measurements are made on rods of the materials in the usual way. But as has already been stated the material has to be submitted to suitable heat treatment in order that the two phases may be obtained in equilibrium at room-temperature before measurements are made at higher temperatures.

§ 3. CONCLUSION

The agreement of the results obtained by Guillaume and by Chevenard with those recorded in this paper is closer than had been expected in view of the fact that the alloys used by them contained more manganese and carbon than was contained in the alloys considered in this paper.

§ 4. ACKNOWLEDGEMENTS

The authors are glad of this opportunity to record their indebtedness to the Research and Development Department of the Mond Nickel Company for their assistance in supplying material to carry out the investigation, and particularly to Dr L. B. Pfeil for his interest throughout the investigation and his readiness at all times to supply information concerning the method of preparation and the heat treatment of the alloys. They also wish to thank the National Physical Laboratory for a sample of pure iron.

REFERENCES

(1) GUILLAUME. *Proc. phys. Soc.* **32**, 374 (1920).
(2) CHEVENARD. See reference (5) on p. 322 of this volume.

REVIEWS OF BOOKS

Radioactivité, by MADAME PIERRE CURIE. Pp. 563, 168 figs. (Paris: Hermann et Cie., 1935.) Price 150 fr.

This voluminous and comprehensive volume on radioactivity was begun by Mme Curie a few years before her death. The book had indeed reached the proof stage, and it has clearly been a labour of love for her distinguished daughter and son-in-law, Irene Joliot-Curie and her husband Frederic Joliot, to complete the work and so pay their tribute to a great woman whom the scientific world had delighted to honour.

That world will be well content too to accept such a book written under such auspices, and we need only mention that there are some 29 chapters dealing authoritatively with, among other matters, ionization, cathode rays, positive rays, X rays, alpha rays, beta rays, gamma rays, artificial radioactivity, and much besides. In accordance with the French custom there is no index, a major omission in a book covering so much ground. There are two excellent portraits of Mme Curie and her husband Prof. Pierre Curie, who predeceased her by many years as the result of a lamentable traffic accident in Paris.

Elements of Nuclear Physics, by F. RASETTI. Pp. xiv + 327. (London: Blackie and Son, Ltd., 1937.) Price 18*s*. 6*d*.

Prof. Rasetti is a master of his subject and an able expositor of it. His introductory chapters on radioactivity and on the physics of the various radiations emitted are models of conciseness and clarity. His chapters on the general properties of nuclei and on the artificial disintegration of the elements are almost equally good. The more theoretical portions of the book, though good in their own way, seem, at any rate to a physicist, to be aimed at a different class of reader. Thus, while the author is at pains to explain the distinction between alpha, beta and gamma rays, references to Bose and Fermi statistics, to Schroedinger waves, and to Dirac's relativistic theory are assumed to need little or no explanation. Though, in general, mathematical results are quoted without proof, in some cases the full analysis is included. The book is thus very uneven in the demands which it makes upon the previous knowledge of the reader.

In spite of this it can be recommended. The author has a clear and interesting style, and marshals his extensive material well. The value of the work is increased by numerous tables and diagrams which together afford an excellent summary of the present state of knowledge in the subject. Readers who find the more mathematical portions of the book beyond their scope, or outside their interest, can exercise the reader's prerogative and skip them.

J. A. C.

A Complete Physics written for London Medical Students and General Use, by W. H. WHITE. Pp. viii + 850. (London: Richard Clay and Sons, Ltd.) Price 15*s*. net.

Firstly, congratulations to Mr White, as publisher, on the production of a 900-page text-book, of excellent format and fount of type, at a very reasonable price.

This book was published rather over a year ago and now, after some considerable experience of its use by medical students and of its help to one of their teachers, the latter can wholeheartedly express his appreciation of the merits of a handbook on Physics in which emphasis is so clearly and definitely laid on the broad and liberal outlook to be gained by those who study Natural philosophy for its own sake. The book amply covers the purposely restricted syllabus laid down for preliminary medical examinations, and not only the medical student (Mr White's first love) but all other students will find great help from the study of the numerous answers to examination questions. However, in a review that will not be read by many students of medicine it is evidently more appropriate to refer to, and to emphasize, the completeness of the treatment of the subject matter for the use of the general reader. For this nought but the highest encomiums can be offered to the author.

Here we have all the rudiments of physics and Mr White asks—"Can these bones live?" The reply must surely be that the spirit of natural philosophy has imbued the author so plenteously that what might have remained mere osseous relics are here made to stand upon their own feet, to live and to be an exceedingly great army—the whole house of physics. The felicitous treatment of such diverse subjects as meteorology and the thick lens, the inclusion of accounts of the Shortt clock and the copper-oxide rectifier, the many novel illustrations, from that of the tiddlers and the bread (Brownian motion) to propeller troubles (electrolytic corrosion) and many more features might be instanced in order to commend a book which should be in the possession of all.

Mr White's valedictory remarks should be read by all who have to take part in examinations, either as examiners or as examinees.

I end this review in which I have tried to express my own personal gratitude to "good fellow" White by adding that, after using this book for some months, one of my older students told me that for the first time in his life he was *enjoying* a textbook of physics which had a real cultural value.

J. H. B.

Magnetochemie, by W. KLEMM. Pp. xv + 262. (Leipzig: Akademische Verlagsgesellschaft, 1936.) Price M. 18.

The importance of magnetic measurements in deciding points of chemical structure has been increasingly realized in recent years, and the appearance of a book dealing with the subject is very opportune. The volume deals with the classical magnetic theory and methods of measurement in the first part. The second part contains an account of the relations between magnetic moment and atomic theory, in which the deductions of the old and new quantum theories are clearly explained. In this section such matters as quantum numbers and term symbols for atoms and ions receive attention. A thorough discussion of various types of chemical compounds follows, in which numerical results are given in preference to mere symbols, a method of treatment which will commend itself to chemists. The third part of the book illustrates the utility of magnetic measurements in chemistry by the consideration of a large number of typical examples, again from the point of view of arithmetic. Short accounts of Pauling's bond theory and metals and alloys are included in this section. The book is an excellent and intelligible survey of the subject, and can be strongly recommended.

J. R. P.

Instrument Transformers, by B. HAGUE. Pp. xxiv + 656. (London: Pitman and Sons, Ltd.) 35*s*. net.

Comparatively few physicists will require to know more about instrument transformers than that they may provide a more convenient and accurate means of extending the ranges of alternating-current ammeters, voltmeters, and the like, than do shunts and series resistors such as must be used with direct-current instruments. Nevertheless there is a vast amount of published literature concerned with the properties of these instruments and the methods of testing them.

This book presents a digest of all the available information on the subject. To those specially interested it is a work of considerable value, for the author has carried out his laborious task with great thoroughness. The book is quite up-to-date and well arranged, and the subject matter is presented with the skill of an experienced teacher. It may be recommended as a work of reference to all who are interested in precision measurements of current, voltage and power.

L. H.